AFCRL-63-596

STUDY DIRECTED TOWARD OPTIMIZATION OF OPERATING
PARAMETERS OF THE EMAC PROBE FOR THE REMOTE
MEASUREMENT OF ATMOSPHERIC PARAMETERS

By

Clayton H. Allen*
and
Stephen D. Weiner*

*BOLT BERANEK AND NEWMAN INC.
50 Moulton Street
Cambridge 38, Massachusetts

FINAL REPORT
Contract No. AF 19(628)2774
Project 6672, Task 667205

September 1963

TABLE OF CONTENTS

LIST OF FIGURES

LIST OF FIGURES (CONT)

LIST OF FIGURES (CONT)

LIST OF FIGURES (CONT)

Bolt Beranek and Newman Inc.

Acknowledgements

ABSTRACT

The concept of utilizing sound waves as reflectors for pulsed
Doppler radar as a means for measuring wind velocity, turbulence,
and air temperature has been examined theoretically. Any
extension of the initial and successful, small scale experiments
performed by Midwest Research Institute to a practical system
for atmospheric probing is shown to require a change in the
operating concept of the acoustic system. This change involves
the abandoning of the concept of coherent reflection reinforce-
ment from a multiple wave train and the substitution of
reflection from a single acoustic shock front with the introduc-
tion of coherent integration of the pulsed Doppler radar signal.

A preliminary experimental approach to a practical system is
proposed.

1. INTRODUCTION

The use of radar to detect meteorological disturbances is now
quite commonplace. Weather fronts can be observed, wind dis-
turbances behind a front carrying humid air off the ocean upward
and mixing with relatively dryer air are clearly visible under
some conditions[1] — the problem of "angels" and clear air turbu-
lence detection by radar are being studied with some success.[2,3,4]
Back scattering from turbulence and precipitation are being used
to study storms and evaluation of vertical winds in storm centers.

In storm centers radar is reflected from the interfaces where
gross difference in refractive index exists between air and water
or ice particles. In the study of weather fronts and turbulence,
use is made of the much smaller index variations caused by changes
in density as between warm and cold air, moving and stationary air
in turbulence or between dry and humid air These variations in
index though small amount to several N-units, i.e., several parts
per million in the index of refraction of air which itself is of
the order of 1.000,320 .

The present study considers the use of a sound wave as a reflecting
surface. Such a surface has the great advantage of being available
upon command and having a relatively large area oriented exactly
or nearly in such a way as to focus the reflected radar beam back
toward the receiver. Unfortunately, a sound wave which can be
tolerated by personnel and buildings in the vicinity of the sound
source can provide a change in index of refraction which is small
compared with the changes associated with normal variations
occurring naturally in the atmosphere. Near the source sound
levels higher than about 160 db would not be tolerable; these
would create index variations of about 10 N-units.

As sound waves propagate away from the source, they decrease in amplitude because of divergence of the sound, normal absorption of sound as heat in the atmosphere, and because of excess absorption caused by finite amplitude losses when large sound waves are used. All of these factors limit the amount of sound which can be propagated any great distance from the source. In order to observe sound waves which travel 2 miles or more from the source it appears necessary that the radar system be able to detect changes in index of refraction which are small compared with an N-unit.

The fact that a sound wave gives a large, substantially coherent surface from which to reflect radar aids in making possible the detection of its small change in index of refraction.

Pioneering theoretical and experimental work on the EMAC probe carried on by Midwest Research Institute has shown the feasibility of this tool for measuring wind velocity. Experiments have checked well with theory.

In summary, the efforts of MRI have been directed toward overcoming the limitations of the small change in index of refraction associated with a sound wave by using a train of many waves and obtaining coherent reinforcement of the reflections from the individual waves by matching the radar and acoustic waves according to the equation

$$\lambda_e = 2\lambda_a \tag{1.1}$$

where λ_e is the electromagnetic wavelength λ_a is the acoustic wavelength.

-2-

With an exact wavelength match, a reflection with zero phase change occurs at each index rise and a reflection with 180° phase change occurs at each index fall along the wave train. Thus, a train of 100 waves gives the effect of 200 mirrors. If coherence is maintained throughout the entire train of n waves the net reflected power will be n^2 times the power from 1 wave or $4n^2$ times the power from 1/2 of a sinusoidal sound wave.

The advantage of coherent reinforcement resulting from a train of waves is indeed inviting, but it has serious limitations in a real atmosphere with wind, turbulence, and other inhomogeneities. It is necessary that the wavelengths of radar and sound match according to Eq. 1.1 to within $1/4 \; \lambda_a$ over the full length of the train in order to obtain the n^2 advantage. Such a match made at any location generally will not remain a match as the sound train passes into a region of different temperature or a region where wind changes the sound ground speed.

Thus, in order to obtain a match at a new location the radar frequency must be altered so that the radar wavelength tracks the sound wavelength at the location of the reflection.

This, at best, involves complicated tracking circuits and requires expenditure of some tracking time for the optimization of the radar frequency. Inherent in the fact that the air is generally turbulent and otherwise inhomogeneous is the concomitant fact that the acoustic wavelength along a wave train will not be constant and in general there will be no one radar frequency which can satisfy the requirement for wave matching over more than a very limited wave train length. The seriousness of this limitation increases with the inhomogeneity of the air being studied.

In order to localize the region of the atmosphere being studied the wave train should not be more than several feet long. In order that such a wave train contain many wavelengths the waves must be short. Midwest Research Institute used an acoustic signal of 22 kc for which the wavelength was approximately 1/2 inch. For such a beam the length of 100 waves is only 50 inches, a very reasonable length permitting fine detail in atmospheric probing. However, sound at this high frequency and small wavelength is rapidly attenuated in air. In their experiments, measurements could not be carried beyond about 93 feet.

Calculations in Section 4.43 show that the experimental system used by MRI was very nearly optimized for the acoustic frequency used, and that no increase in range may be expected by increasing the size or power of the acoustic source. Some gain might be secured from an increase in radar power but at 100 ft the acoustic wave had a sound level of the order of 100 db and decreased so rapidly that within a few feet it would be at the noise level expected in a turbulent atmosphere.

The present study extends the concept explored by MRI, and considers the use of individual shock fronts as the reflector for the radar signal, since such shock fronts can be made to propagate and maintain useful intensity for ranges of several thousand feet. This study indicates the direction which should be taken in developing the EMAC Probe into a practical tool.

1.1 Statement of the Problem

The present study of the parameters governing the operation of
the EMAC Probe has been motivated by the need for the measure-
ment of the atmospheric conditions at distances remote from the
measurement position on the ground. Specifically, this study
is directed towards measurement of wind and temperature in the
atmosphere as an aid in weather observation and as an aid in
aircraft and missile guidance problems where such detailed
information within a range of a mile or two from the source is
needed on a substantially instantaneous and continuous basis.

1.2 Atmospheric Parameters of Interest

In addition to the measurement of wind it is desirable to measure
or at least to obtain qualitative description of the wind shear,
turbulence, humidity, and temperature variation throughout this
field of search. The present study considers the possibility
of observing these parameters with the EMAC Probe.

1.3 Means for Remote Measurement

Conventional techniques for remote measurement of wind velocities,
such as the visual observation of free balloons or clouds, and
radar interception of chaff or naturally occurring inhomogenei-
ties in the atmosphere have serious limitations arising either from
the delayed response or the relatively small and highly unpredict-
able region which may be covered by such measuring techniques. It
is desired to be able to measure the wind velocity at any height
and in any direction from a fixed observation point in a substan-
tially continuous manner in order that the total wind field in
the vicinity of the measuring point can be determined completely.

Several means for indirect probing of the atmosphere are under
consideration by various agencies. A good discussion of these
probing methods has been published.[5/] They include the use of
infra-red radiometry, optical lasers, and radar of several types
including coherent pulse Doppler radar. All of these depend
upon observing particles, inhomogeneities or density irregulari-
ties in the atmosphere. Interpretation of the reflected signal
in many cases can give significant information concerning the
nature of irregularities causing the reflection and about their
motion in the atmosphere. However, since these irregularities
are random in nature and since there is no control over their
position, the detailed measuring of atmospheric parameters
throughout the region surrounding the measuring point is generally
incomplete and therefore the mapping of such parameters necessarily
involves large extrapolation of the observable data. This process
gives insufficient accuracy for many purposes.

Wind velocity and turbulence can be measured by obtaining radar
reflections from density irregularities in the atmosphere or
solid particles such as rain, snow, chaff and fog suspended in
the air. Such measurements approximate the motion of the air
since the particles observed follow the motions of the air
fairly accurately if their size is less than 1 mm in diameter.
In some instances the observed objects are dropping through the
air at speeds which are large compared with the velocity of the
air itself. Chaff, which is light and can fall slowly, has
limited application since it must be carried to a position
above the point of observation and allowed to drift at the mercy
of the elements hopefully into the region of interest.

1.4 EMAC Probe Technique

The electromagnetic acoustic (EMAC) probing method provides a reflecting surface which moves through the atmosphere with the speed of sound altered only by variations in wind speed and air temperature. The reflected signal carries information by which the speed of the sound wave can be determined in the direction of the radar beam. By combining the information gained from reflected signals in various directions it appears possible and practical to calculate, not only the speed of the wave in the direction of the radar but to deduce the actual wind speed and direction, as well as to determine the air temperature and estimate the amount of turbulence existing in various regions within the range of the system.

The use of radar to observe or interrogate vibrating media, surfaces, or objects is not new. Basic patents[6] reading on the art of detecting and measuring the velocity or vibration of air, liquids, or solid objects were issued on disclosures made during World War II.

The application of this art to the specific problem of measuring wind velocity by reflecting radar pulses from intense sound waves as described in reports by Midwest Research Institute[7,8,9,10] demonstrates the feasibility of the process. Comparison of the theory and the experimental results indicates that as yet the theoretical limitations on the useful range of the velocity measuring technique have not been approached. This report provides a theoretical discussion of the parameters influencing the optimization of the range and sensitivity of the EMAC Probe. In particular, theory and experience available regarding acoustic wave propagation in the atmosphere and the more subtle finite

amplitude phenomena associated with the propagation of sound waves of large amplitudes indicates that the range of the EMAC Probe can be greatly extended by proper choice of the acoustic wave parameters.

The electromagnetic acoustic probe as described by Midwest Research Institute has proved successful out to distances approaching 100 ft but the extension of its useful range requires significant changes in its operating parameters. The choice of high frequency sound waves is its greatest limitation. A sufficiently large reduction of the frequency, however, results in such long acoustic wavelengths that it becomes impractical to use a radar wave which is comparable in length with the acoustic wave and still maintain the degree of beam definition which is necessary for fine scanning and analysis of wind and turbulence structure. Thus, the radar wavelength must be kept relatively short compared to the acoustic wavelength.

This change appears at first to imply that the reflection coefficient for the acoustic wave will drop severely, but it is possible to utilize a sawtoothed sound wave which has a steep leading edge. This will have the reflectivity of a pressure discontinuity less than 1 ft in thickness. Such a discontinuity will act as a good reflector for a radar wave of the order of 2 ft in length, i.e., a 400 megacycle frequency.

The use of a long acoustic wave necessitates abandoning the concept of coherence between acoustic wave fronts. This loss, however, is not as serious as may appear from theoretical considerations of ideal wave propagation conditions. Such coherence would be effective only in homogeneous air masses which are of small interest and highly improbable in a real atmosphere

outside of the laboratory. It is more realistic to substitute coherent integration between radar pulses since the radar speed is substantially unaffected by the atmospheric variations of wind turbulence, etc., and within the time interval of 50 radar pulses (repetition rate of 3000 pps) the sound wave will travel only 15 ft and the wind and turbulence velocities will remain substantially constant over all points within the radar beam cross section. By this means, full advantage can be taken of a fifty pulse coherent integration. Such a change in operating technique will more than make up for the loss in potential gain from multiple wave reflection. This mode of operation will also eliminate the need for frequency variation in the radar which was required to match lengths between radar and acoustic waves. The use of a fixed radar frequency will eliminate one search dimension and permit the more rapid accumulation of data and the more thorough search of the dimensions which are of direct interest.

The results of the present analysis show that an EMAC Probe system employing proper sound pulses can provide a substantially continuous sweep scan of the hemispherical atmospheric region around the observation point and provide a relatively complete map of the wind velocity and turbulence in this region out to a distance of about 2 miles. The ultimate range will depend primarily upon the weather conditions, the amplitude of the sound waves permitted at the source as determined by community and personnel considerations, and upon the sensitivity of the radar receiving system.

2. RADAR REFLECTION COEFFICIENTS

2.1 Reflection From a Sharp Dielectric Discontinuity

The simplest case of reflection of electromagnetic waves is by a plane discontinuity in the index of refraction n. A change in n is "sharp" if it takes place over a distance short compared with one quarter of the electromagnetic wavelength. For reflection at normal incidence, the Fresnel formula for reflected power gives

$$\frac{P_r}{P_i} = \left(\frac{n_1 - n_0}{n_1 + n_0} \right)^2 \tag{2.1}$$

where P_i, P_r are incident and reflected radar powers respectively n_1, n_0 indices of refraction on opposite sides of the discontinuity.

In the atmosphere, n is nearly unity and the variation in n obtainable with usable pressure discontinuities is so small compared with unity that Eq. (2.1) can be replaced by the simpler form

$$\frac{P_r}{P_i} = \left(\frac{\delta n}{2} \right)^2 \tag{2.2}$$

where $\delta n = n_1 - n_0$.

2.2 Reflection From Gradual Dielectric Variations

For a gradual change in n, reflection of the radar will occur at all points in the region of variation. Since, as the radar wave progresses, its phase changes from point to point, the

reflected contributions of each point must be added in proper phase to obtain their sum. This requires determination of the reflected electric field in order to determine the reflected power, rather than calculation of the power directly. The reflected wave is found by replacing the continuously varying $n(x)$ [Fig. 2.1a] by a series of steps [Fig. 2.1b].

The Fresnel formula for the electric field amplitude reflected from each step $dn(x)$ is

$$\left| dE_x \right| \simeq \frac{E_1(x)\ dn(x)}{2} \tag{2.3}$$

By allowing the incident electric field amplitude $E_1(x)$ to vary with x, we can take into account effects of different pulse shapes as discussed in Siegert and Goldstein.[11] For an electromagnetic wave have a wavelength λ_e the electric field contribution reflected from point x has a phase of $2(2\pi x/\lambda_e)$ relative to the contribution reflected from $x = 0$. Thus, the amplitude and phase of dE_x is given by

$$dE_x = \frac{E_1(x)\ dn(x)}{2}\ \exp\left[-4\pi i x/\lambda_e\right] \tag{2.4}$$

As $dx \rightarrow 0$, the sum of the reflected contributions from all elements, dx, between x_0 and x_1, can be expressed as the integral

$$E_r = \int_{n_0}^{n_1} \frac{E_i(x)}{2} \exp \left[- \frac{4\pi i x}{\lambda_e} \right] dn(x)$$

$$= \frac{1}{2} \int_{x_0}^{x_1} \frac{dn}{dx} E_i(x) \exp \left[- \frac{4\pi i x}{\lambda_e} \right] dx \tag{2.5}$$

if multiple reflections are neglected. The reflected power is the square of the magnitude of the reflected E field.

There are many combinations of pulse shape and index of refraction variations which are of interest. We will consider a few of these special cases below.

<u>Case A.</u> Radar pulse length infinite (E_i = const). In this case Eq. (2.5) becomes

$$E_r = \frac{E_i}{2} \int_{x_0}^{x_1} \frac{dn}{dx} \exp \left[- \frac{4\pi i x}{\lambda_e} \right] dx \tag{2.6}$$

A sub-case of Case A is that of linear variation of n from n_0 to n_1 over a distance Δ as shown in Fig. 2.2.

In this case

$$E_r = \frac{E_i}{2} \frac{\delta n}{\Delta} \int_{x_0}^{x_0 + \Delta} \exp \left[- \frac{4\pi i x}{\lambda_e} \right] dx$$

$$= \frac{E_i \delta n}{8\pi i} \frac{\lambda_e}{\Delta} \exp \left[- \frac{4\pi i x_0}{\lambda_e} \right] \left[1 - \exp \left(- \frac{4\pi i \Delta}{\lambda_e} \right) \right] \tag{2.7}$$

-12-

or

$$P_r = \frac{P_1 \delta n^2}{4} \left[\frac{\sin (2\pi\Delta/\lambda_e)}{(2\pi\Delta/\lambda_e)} \right]^2 \tag{2.8}$$

The value of $4P_r/[P_1(\delta n)^2]$ is plotted vs. Δ/λ_e in Fig. 2.3. This gives the reflection coefficient relative to that for an infinitely sharp shock. For $\Delta \ll \lambda_e$ this case reduces to that of the sharp discontinuity discussed in Sec. 2.1.

The variation in n shown in Fig. 2.2 and used in calculations above has two "sharp" edges at $x = x_o$ and $x = x_o + \Delta$. The interference between these edges produces maxima and minima in the reflection coefficient as shown in Fig. 2.3 We can also calculate the reflection from shocks with one or zero sharp edges. A shock with one sharp edge at $x = 0$ and the other rounded such that

$$n = n_o \qquad\qquad\qquad\qquad x < 0$$
$$n = n_o + \delta n \, [1 - \exp (-x/\Delta)] \qquad x > 0 \tag{2.9}$$

for which the shock width is defined by Δ. For this variation in n, the power reflection coefficient is

$$\frac{P_r}{P_1} = \left(\frac{\delta n}{2} \right)^2 \frac{1}{1 + 16\pi^2 \, \Delta^2/\lambda_e^2} \tag{2.10}$$

which is also plotted in Fig. 2.3. This curve does not show the maxima and minima of Eq. (2.8) but falls off as $(\lambda_e/\Delta)^2$ as does the average value for wide shocks described by Eq. 2.8.

Friend[12] has calculated the reflection from index of refraction changes with no sharp edges. He considers a change, of "width" Δ, of the form

$$n = n_0 + \delta n \; \frac{\exp \, (4 \, x/\Delta)}{1 + \exp \, (4 \, x \, /\Delta)} \tag{2.11}$$

for which the reflection coefficient is

$$\frac{P_r}{P_1} \approx \left(\frac{\delta n}{2} \right)^2 \; \frac{9\Delta/\lambda_e}{\sinh \, (9\Delta/\lambda_e)} \tag{2.12}$$

which is also plotted in Fig. 2.3. The reflection from this shock falls off much more rapidly with shock thickness than the reflection from the shocks with either one or two "sharp" edges.

This fact may be of practical significance in regard to reflection from acoustic shock waves. The leading edge of the shock front, at which the density begins to rise, appears experimentally to be much sharper than the crest of the wave at large distances from the source. This matter is discussed in more detail in Sec. 4.43.

Case B. Finite radar pulse length

To show the importance of the radar pulse shape, we will consider a linear variation in n extending over all space. Thus $\frac{dn}{dx}$ = constant. In this case Eq. (2.5) becomes

$$E_r = \frac{1}{2} \; \frac{dn}{dx} \int_{-\infty}^{\infty} E_1 \, (x) \; \exp \left[- \frac{4\pi i x}{\lambda_e} \right] \, dx \tag{2.13}$$

Since the radar pulse length is finite, E_1 is zero at the lower and upper limits and we can integrate (2.13) by parts obtaining

$$E_r = \frac{1}{2} \; \frac{dn}{dx} \; \frac{\lambda_e}{4\pi i} \int_{-\infty}^{\infty} \frac{dE_1}{dx} \; \exp \left[- \frac{4\pi i x}{\lambda_e} \right] dx \qquad (2.14)$$

Siegert and Goldstein consider the case of a trapezoidal pulse as shown in Fig. 2.4. For this pulse

$$\frac{dE_1}{dx} = 0 \text{ except for } 0 < x < a \text{ and } b < x < (b + a)$$

so Eq. (2.14) becomes

$$E_r = \frac{1}{2} \frac{dn}{dx} \; \frac{E_o}{a} \frac{\lambda_e}{4\pi i} \left\{ \int_0^a \exp \left[- \frac{4\pi i x}{\lambda_e} \right] dx - \int_b^{b+a} \exp \left[- \frac{4\pi i x}{\lambda_e} \right] dx \right\}$$

$$(2.15)$$

Integrating gives

$$E_r = \frac{1}{2} \frac{dn}{dx} \frac{E_o}{a} \left(\frac{\lambda_e}{4\pi} \right)^2 \left[1 - \exp \left(- \frac{4\pi i a}{\lambda_e} \right) \right] \left[1 - \exp \left(- \frac{4\pi i b}{\lambda_e} \right) \right] \qquad (2.16)$$

which results in a reflected power $P_r = |E_r|^2$ of

$$P_r = \frac{1}{4} \left(\frac{dn}{dx} \right)^2 \left(\frac{E_o}{a} \right)^2 \left(\frac{\lambda_e}{2\pi} \right)^4 \; \sin^2 \left(\frac{2\pi a}{\lambda_e} \right) \sin^2 \left(\frac{2\pi b}{\lambda_e} \right) \qquad (2.17)$$

-15-

Writing this with the notation of Case A gives

$$P_r = \frac{P_1 (\delta n)^2}{4} \left[\frac{\sin (2\pi a/\lambda_e)}{(2\pi a/\lambda_e)} \right]^2 \left[\frac{\lambda_e}{2\pi \Delta} \right]^2 \left[\sin \frac{2\pi b}{\lambda_e} \right]^2 \qquad (2.18)$$

In actual practice, a pulsed radar will probably be used to conserve power, to produce minimum interference with the reflected signal, and permit the measurement of the range of the acoustic wavefront. Then Eq. (2.18) shows that if $\Delta > b > a$, the maximum reflection will occur for a value of a as small as possible and a value of b equal to an odd multiple of $\lambda_e/4$. Siegert and Goldstein also show that for a smooth radar pulse (not a trapezoid), the reflection is greatly decreased if $a \gg \lambda_e$. This is analogous to the difference shown in Fig. 2.3 between sharp and smooth variations in n.

The use of pulsed radar though useful, for reasons sited above, will involve some loss in returned signal. It can be seen from a comparison of Eqs. 2.8 and 2.18 that a radar pulse of any shape gives less return signal intensity than a continuous radar wave from a gradual change of index in which $\Delta \gg \lambda_e$. It can be similarly shown that changing the radar pulse shape cannot enhance the reflection from a "sharp" change in n. For the type of variation of n shown in Fig. 2.2, the reflected E field described by Eq. (2.5) becomes

$$E_r = \frac{1}{2} \frac{dn}{dx} \int_0^\Delta E_1 (x) \exp \left[- \frac{4\pi i x}{\lambda_e} \right] dx \qquad (2.19)$$

In the case of $\Delta \ll \lambda_e$, the exponential in Eq. (2.19) is almost constant and the maximum reflection results for any shape pulse with its largest amplitude between $x = 0$ and $x = \Delta$. Thus, changing the pulse shape will not change the reflection from a sharp variation in n.

-16-

In the following sections we will calculate the reflection from different forms of variation in n. The pulse shape will not affect these results significantly and the radar signal will be taken as an infinite wave train for simplicity of calculation.

2.3 Reflection From a Sinusoidal Wave Train

The normal incidence reflection from a train of plane sine waves has been calculated by means of a transmission line analogy.[13/] A more direct derivation makes use of the methods of Sec. 2.2. With a constant radar pulse amplitude, Eq. (2.5) becomes

$$\frac{E_r}{E_1} = \frac{1}{2} \int_{x_o}^{x_1} \frac{dn}{dx} \exp \left[- \frac{4\pi i x}{\lambda_e} \right] dx \qquad (2.20)$$

For a train of N sine waves of wavelength λ_a, we have

$$\begin{cases} n = n_o + \delta n . \sin 2\pi x/\lambda_a & \text{for} \quad 0 < x < N \lambda_a \\ \\ n = n_o & \text{otherwise} \end{cases} \qquad (2.21)$$

Putting

$$\begin{cases} \frac{dn}{dx} = \frac{2\pi}{\lambda_a} \delta n \cos \frac{2\pi x}{\lambda_a} & \text{for} \quad 0 < x < N \lambda_a \\ \\ \frac{dn}{dx} = 0 & \text{otherwise} \end{cases} \qquad (2.22)$$

-17-

into Eq. (2.20) gives

$$\frac{E_r}{E_1} = \frac{\pi \delta n}{\lambda_a} \int_0^{N\lambda_a} \cos \frac{2\pi x}{\lambda_a} \exp \left(- \frac{4\pi i x}{\lambda_e} \right) dx \qquad (2.23)$$

The power reflection coefficient is the absolute square of this ratio. This reflection coefficient has two different forms depending on whether $\lambda_e = 2 \lambda_a$ or not.

<u>Case 1</u> $\lambda_e = 2 \lambda_a$

In this case the power reflection coefficient is

$$\frac{P_r}{P_1} = \frac{(\delta n)^2 \pi^2}{4} \quad N^2 \qquad (2.24)$$

The power reflected increases as the square of the number of wavelengths in the train. However, it is important to realize that this expression is valid only if the radar and acoustic waves remain in phase throughout the entire length of the train.

Fluctuations in phase and amplitude of the acoustic wave occur because of propagation through inhomogeneities in the atmosphere. The radar wave is affected much less by inhomogeneities than is the acoustic wave and consequently the acoustic and radar waves may get out of phase seriously even within the length of the acoustic wave train.

Case 2 $\lambda_e \neq 2\lambda_a$

In this case the power reflection coefficient is

$$
\frac{P_r}{P_1} = \frac{\pi^2 (\delta n)^2}{4} N^2 \left[\frac{\sin 2\pi N \left(1 - \frac{2\lambda_a}{\lambda_e}\right)}{2\pi N \left(1 - \frac{2\lambda_e}{\lambda_e}\right)} \right]^2 \tag{2.25}
$$

The value[10] of P_r/P_1 for values of λ_e about $2\lambda_a$ are plotted in Fig. 2.5 for two values of N.

It is apparent that the reflection coefficient drops to zero when the phase difference between acoustic and radar waves increases to π over the wave train. Equation (2.25) represents a diffraction pattern whose height increases as N^2 and whose width decreases as $1/N^2$. The height of the secondary maxima in Fig. 2.5 is at least 13 db below that of the principal maximum. The results show the effect of a deviation from $\lambda_e = 2\lambda_a$ but do not show the effect of phase fluctuations in the acoustic wave train.

2.4 Normal Incidence Reflection from a Train of Plane Shock Waves

In this case we take $n(x)$ as shown in Fig. 2.6.

The power reflection from each steep wavefront will be

$$
\frac{P_r}{P_1} = \left(\frac{\delta n}{2}\right)^2 \tag{2.26}
$$

as calculated in Sec. 2.1. The power reflection from each sloping portion of the wave will be

$$\frac{P_r}{P_i} = \frac{\delta n}{2} \left(\frac{\sin 2\pi\lambda_a/\lambda_e}{2\pi\lambda_a/\lambda_e} \right)^2 \tag{2.27}$$

as calculated in Sec. 2.2 and plotted in Fig. 2.3 (Δ takes the place of λ_a in Fig. 2.3). It is apparent that the power reflected from the more gradual slope can be neglected compared with that reflected from the steep leading edge if λ_a is comparable with or larger than $\lambda_e/2$. Therefore in considering a train of shock waves, we need only consider the leading edges of the shocks. From Eq. (2.20) for a train of N shocks, we find

$$\frac{E_r}{E_i} = \frac{\delta n}{2} \sum_{m=0}^{N} \exp \left(-4\pi i m \frac{\lambda_a}{\lambda_e} \right) \tag{2.28}$$

For $N \gg 1$, there will be strong reflection if $2\lambda_a/\lambda_e = s$ where s is any integer. This is to be contrasted with the condition for reflection from a train of sine waves where strong reflection can be obtained only when $2\lambda_a/\lambda_e = 1$.

For the shock waves

$$\frac{P_r}{P_i} = \left(\frac{\delta n}{2} \right)^2 N^2 \tag{2.29}$$

The maximum useful wave train length is still limited to that for which the waves remain in phase. For the train of shock waves, we must have $N\lambda_a = Ns\lambda_e/2$ to within about $\lambda_e/4$. If product Ns is much greater than one, this requirement is very stringent and will probably prevent coherent reinforcement in a wave train. In this case the reflection, on the average, will be approximately equal to that from a single shock front and there will be no enhancement of the power reflection due to multiple shock waves.

2.5 Normal Incidence Reflection From One Plane Shock Wave

We have already seen that $P_r/P_1 = (\delta n)^2/4$ for reflection from one plane shock. It is now necessary to calculate δn as a function of the shock strength. For shocks that are not too strong, density and pressure are related adiabatically

$$\frac{1}{\gamma} \frac{dp}{p} = \frac{d\rho}{\rho} \tag{2.30}$$

where γ = the ratio of specific heats.
The index of refraction n is related to density by

$$\frac{d(n-1)}{n-1} = \frac{d\rho}{\rho} = \frac{1}{\gamma} \frac{dp}{p} \tag{2.31}$$

For weak shocks in air,

$$\delta n \approx (n_o - 1) \frac{1}{\gamma} \frac{\delta p}{p_o} \tag{2.32}$$

Since P_r/P_i depends on $(\delta n)^2$, the reflection coefficient will depend on the square of the shock strength. Since the shock intensity is proportional to $(\delta p)^2$ also, the curve of reflection coefficient vs. shock intensity will be linear. For typical atmospheric conditions of $p_0 = 1000$ millibars, $T = 15^0$ C., and R.H. $= 65\%$, the index of refraction $n_0 = 1.00032$. The curve of reflection coefficient vs. shock intensity is plotted in Fig. 2.7.

When n_0 differs from 1.000320 the reflection losses as given in Fig. 2.7 will change. Such change in n_0 results from changes in absolute humidity and from changes in pressure primarily due to altitude. The gross magnitude of such changes in N units and the corresponding effect upon the radar reflection in db for typical air masses as a function of altitude is shown in Fig. 2.7a.
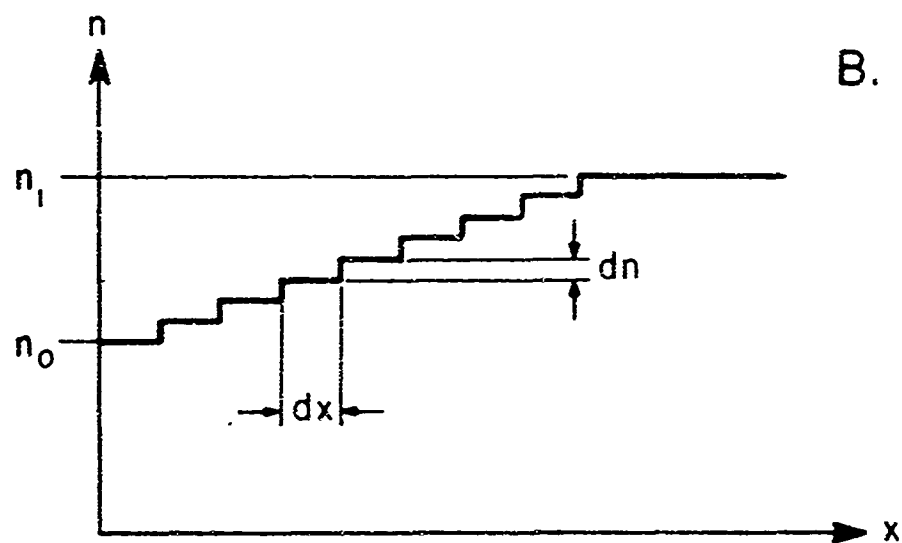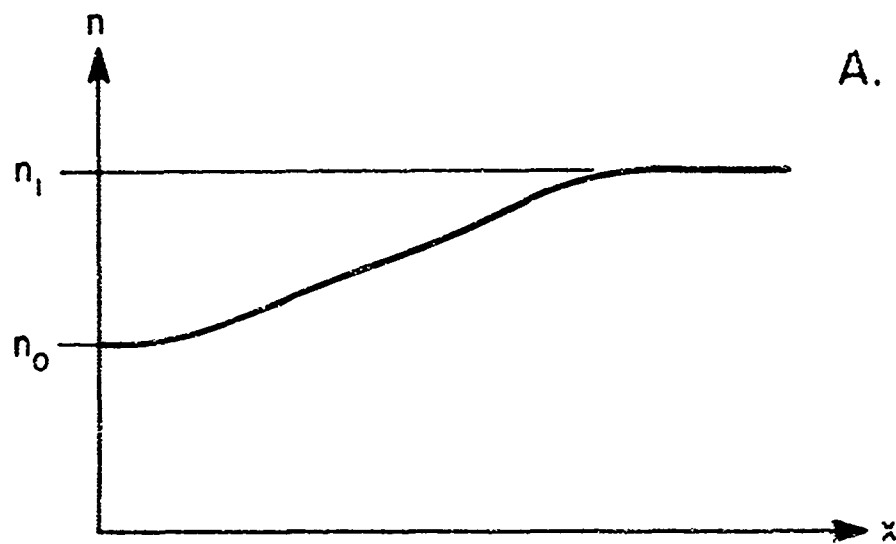
FIG. 2.1   INDEX OF REFRACTION VS. DISTANCE
ARBITRARY VARIATION
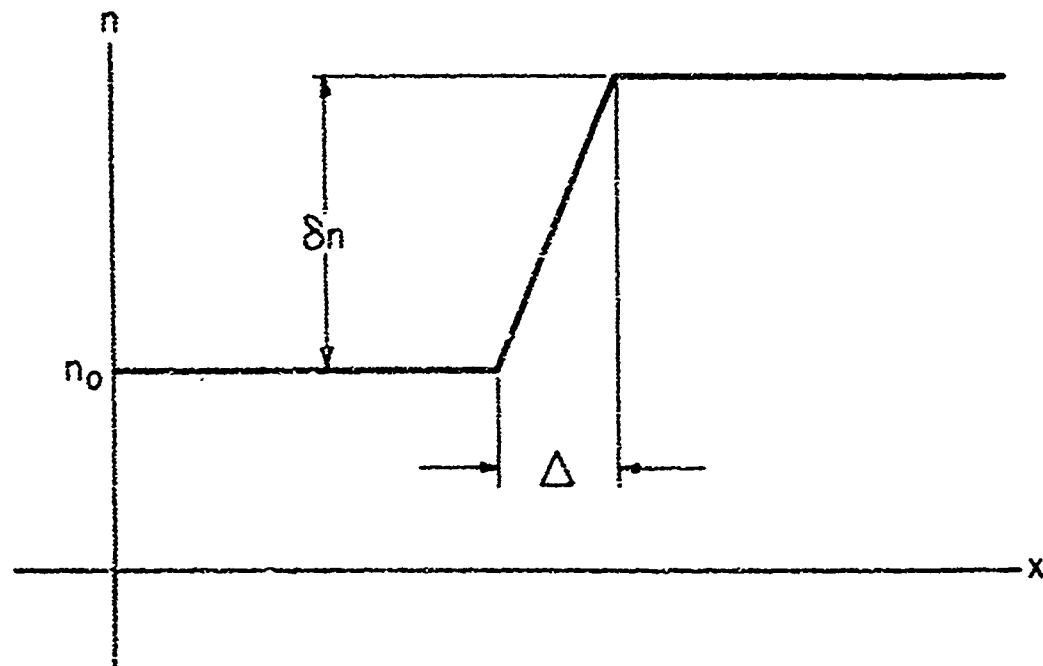
FIG. 2.2 INDEX OF REFRACTION VS. DISTANCE
LINEAR SHOCK
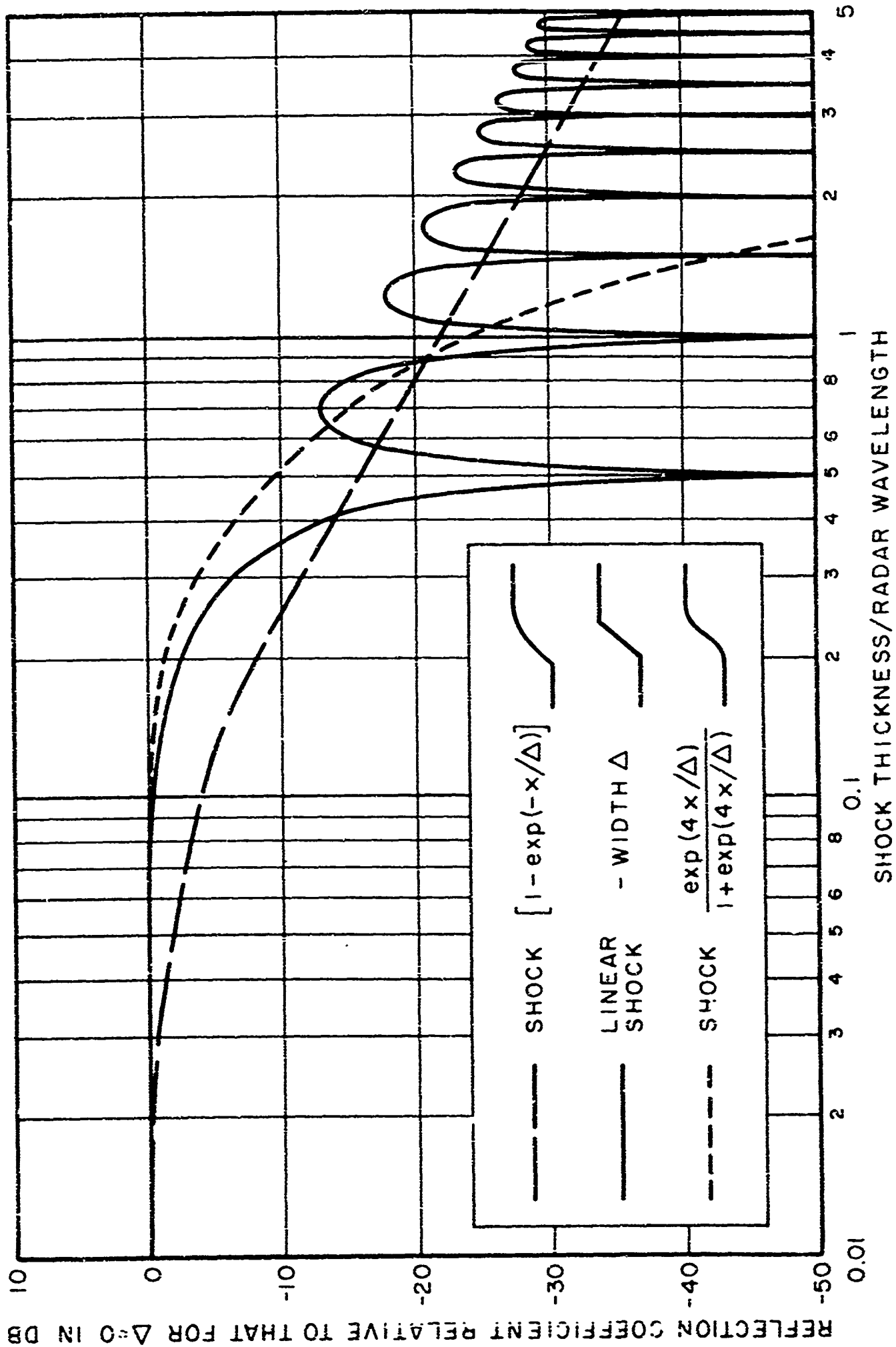
FIG.2.3 RELATIVE REFLECTION COEFFICIENT VS. Δ/λ_e FOR SHOCKS WITH TWO, ONE, AND ZERO SHARP EDGES
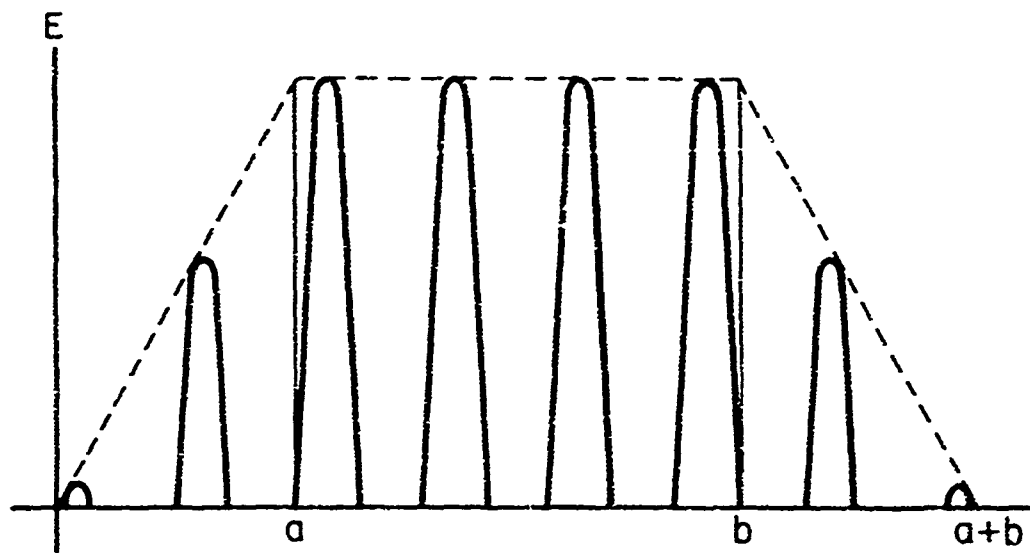
FIG. 2.4   RADAR PULSE SHAPE
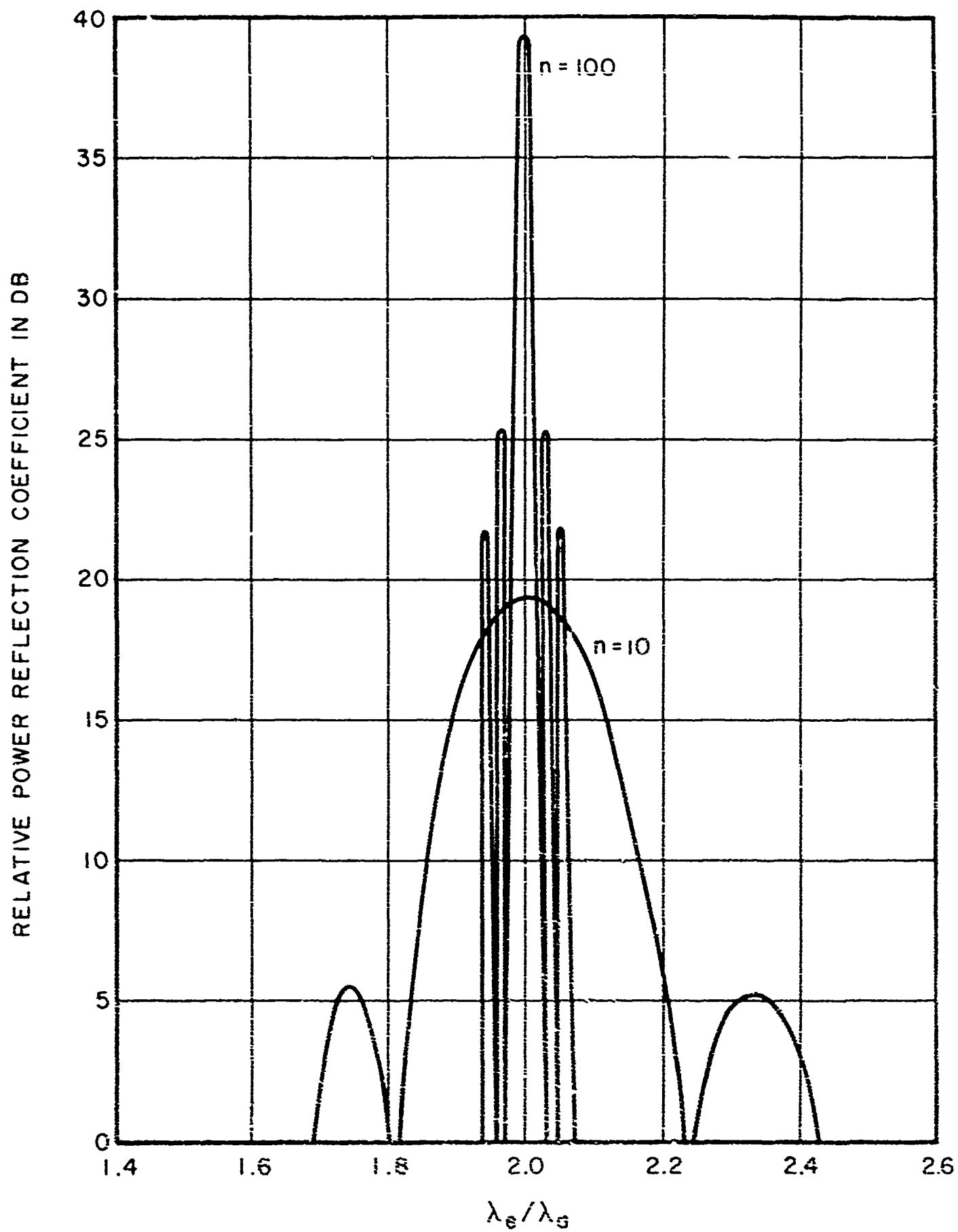
FIG. 2.5   RELATIVE POWER REFLECTION COEFFICIENT
VS. λ_e/λ_0 FOR DIFFERENT n
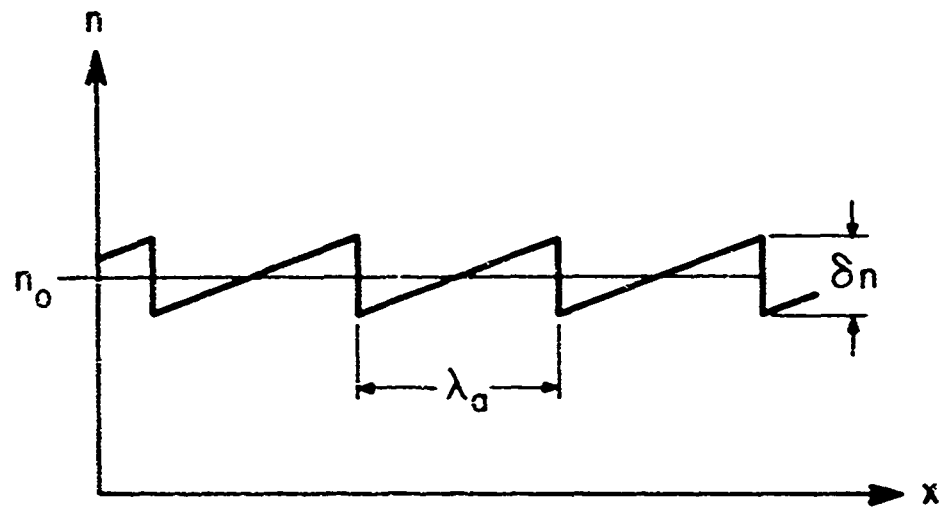
FIG. 2.6   INDEX OF REFRACTION VS. DISTANCE
REPEATED SAWTOOTH
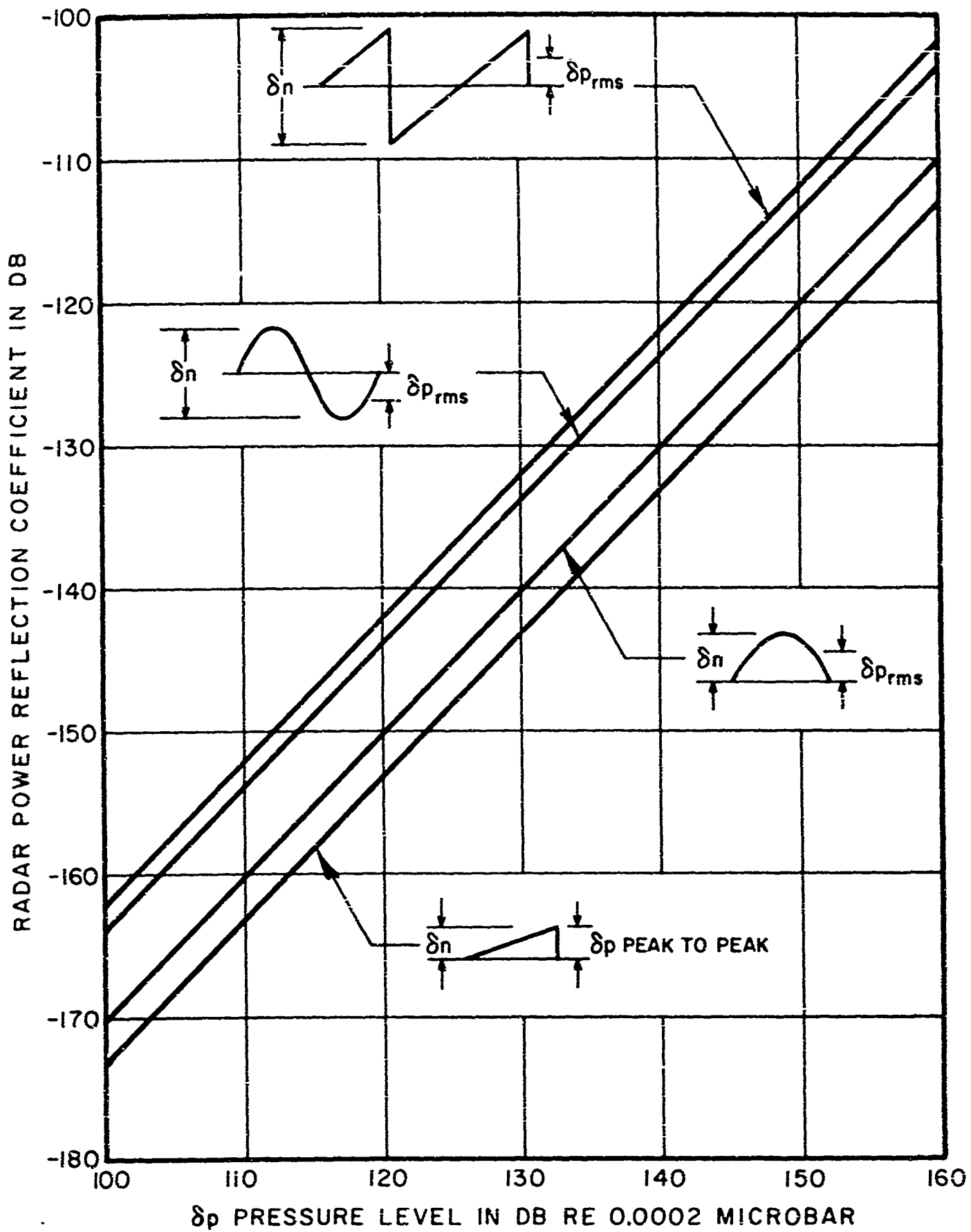
FIG. 2.7 RADAR POWER REFLECTION COEFFICIENTS
VS. SHOCK PRESSURE LEVEL
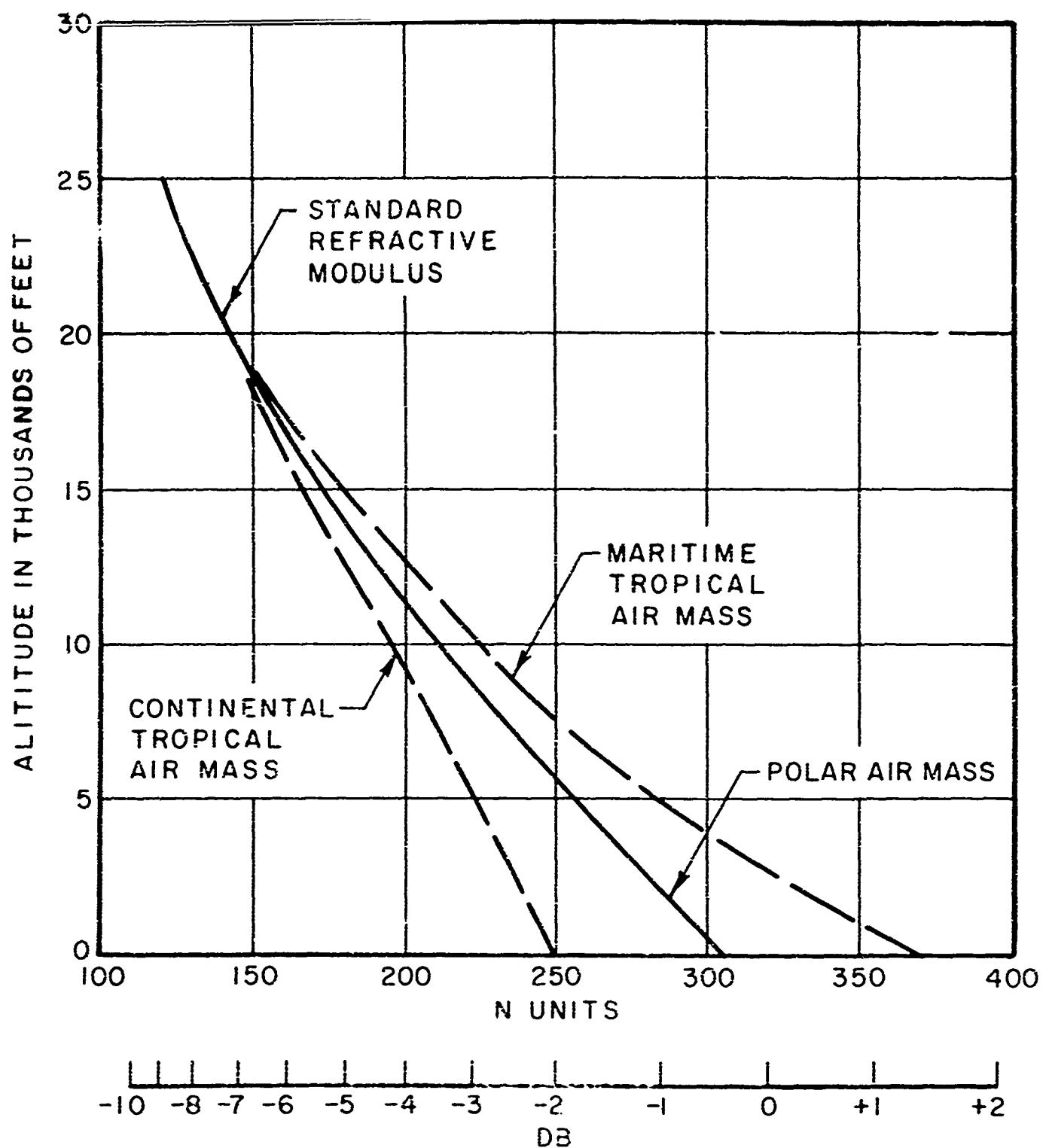
FIG. 2.7a CORRECTION FOR RADAR REFLECTION FROM
PRESSURE DISCONTINUITY AS PLOTTED IN
FIG. 2.7

3. VARIATION IN REFLECTION DUE TO INHOMOGENEITIES

3.1 Wavefront Deformation Due to Atmospheric Inhomogeneities

The distortion of the acoustic wavefront caused by large scale
atmospheric inhomogeneities such as steady wind, wind shear, and
temperature gradients can be calculated using geometric acoustics.[14]
The location of a point on the wavefront is given by

$$\overline{r} = \int_{0}^{t} (\overline{a} + \overline{V}) \, dt \tag{3.1}$$

where $\overline{a}$ = sound velocity

          $\overline{V}$ = wind velocity

3.11 Wind direction and magnitude

If the temperature and wind velocity are constant in the region
considered, then $\overline{a}$ and $\overline{V}$ can be taken outside the integral giving

$$\overline{r} = (\overline{a} + \overline{V}) \, t \tag{3.2}$$

This is shown in Fig. 3.1 B for V/a = .1

The wavefront is a sphere whose center is located a distance Vt
downwind from the source.

3.12 Wind Shear

Consider a wind in the x-direction whose magnitude depends on z.
A sound ray will propagate as shown in Fig. 3.2.

The sound speed $\bar{a}$ is always directed along the ray and the wind speed V is always along the x-axis. Defining θ as the angle the ray makes with the x-axis, and considering only motion in the x-z plane, the equations for the path of the ray are

$$\frac{dz}{dt} = a \sin \theta$$

$$\frac{dx}{dt} = a \cos \theta + V(z)$$

(3.3)

As the wave progresses θ changes.

Equation (3.3) can be solved by successive approximations taking

$$z = z_0 + z_1 \cdots$$

$$x = x_0 + x_1 \cdots$$

$$\theta = \theta_0 + \theta_1 \cdots$$

(3.4)

The zero order equations are

$$\frac{dz_0}{dt} = a \sin \theta_0$$

$$\frac{dx_0}{dt} = a \cos \theta_0$$

(3.5)

with the solution

$$z_o = at \sin \theta_o$$

$$(3.6)$$

$$x_o = at \cos \theta_o$$

corresponding to a ray in the direction θ_o . In the first order equations, we can set $\cos \theta_1 = 1$ and $\sin \theta_1 = \theta_1$ since $V/a \ll 1$ so that

$$\frac{dz_1}{dt} = a \; \theta_1 \cos \theta_o$$

$$(3.7)$$

$$\frac{dx_1}{dt} = - a\theta_1 \sin \theta_o + V (z_o)$$

Equations (3.7) can be solved most easily by first neglecting θ_1 and then correcting for it using

$$\tan \theta \approx \tan (\theta_o + \theta_1) \approx \frac{dz}{dx} \approx \frac{\dfrac{dz_o}{dt} + \dfrac{dz_1}{dt}}{\dfrac{dx_o}{dt} + \dfrac{dx_1}{dt}} \tag{3.8}$$

For the winds $V(z)$ used in this section, the terms involving θ_1 in Eq. (3.7) will be smaller than the term $V(z)$ and will involve only a small correction to x_1 and z_1. This can be made more explicit by considering various types of wind.

Constant Wind Shear

In this case $V_x = Gz$ and the ray equations become

$$\frac{dz_1}{dt} = 0$$

$$\frac{dx_1}{dt} = Gz_o = Gat \sin \theta_o \qquad (3.9)$$

with solution

$$z = z_o = at \sin \theta$$

$$x = x_o + x_1 = at \cos \theta_o + \frac{Gat^2}{2} \sin \theta_o \qquad (3.10)$$

The ray paths are found by eliminating t from (3.10) giving

$$x = z \cot \theta_o + \frac{Gz^2}{z \, a \, \sin \theta_o} \qquad (3.11)$$

The wavefront configuration as a function of time is found by eliminating θ_o from (3.10) giving

$$x = \sqrt{a^2 t^2 - z^2} + \frac{Gtz}{2} \qquad (3.12)$$

Equations (3.12) is plotted for a wind shear of $G = (.2'/\text{sec})/\text{ft}$ in Fig. 3.3. It is apparent that the acoustic wavefronts are no longer spherical but are slightly blunt nosed downwind and increase in deformation with range. The terms involving θ_1 in Eq. (3.7) can now be calculated. Equation (3.8) gives

$$\tan \theta = \frac{a \sin \theta_o}{a \cos \theta_o + Gat \sin \theta_o} = \frac{\tan \theta_o}{1 + Gt \tan \theta_o}$$

(3.13)

$$\tan \theta = \tan (\theta_o + \theta_1) = \frac{\tan \theta_o + \tan \theta_1}{1 - \tan \theta_o \tan \theta_1}$$

which gives

$$\theta_1 = - Gt \sin^2 \theta_o$$

(3.14)

Thus the correction terms in Eq. (3.7) are always less than the term $V(z_o)$. Since the distortion as shown in Fig. 3.3 is not very large, there will not be much error in using Eq. (3.9) instead of Eq. (3.7).

Turning Wind

A turning wind assumed to have a velocity increasing steadily with height will have a sinusoidal variation in velocity with height when projected on the xz plane as

$$V_x = Hz \sin \frac{z}{b}$$

in which H is a constant relating to wind strength and b is a constant relating to the tightness of turning. The wind profile is shown in Fig. 3.4 for one vertical plane. The ray equations becomes

$$\frac{dz_1}{dt} = 0$$

$$\frac{dx_1}{dt} = H \, at \sin \theta_o \sin \frac{at \sin \theta_o}{b}$$

(3.14)

The solution is

$$z = at \sin \theta_o$$

$$x = at \cos \theta_o + Hb \left[-t \cos \frac{at \sin \theta_o}{b} \right.$$

$$\left. + \frac{b}{a \sin \theta_o} \sin \frac{at \sin \theta_o}{b} \right] \tag{3.15}$$

The ray paths are

$$x = z \cot \theta_o + \frac{H b z}{a \sin \theta_o} \left[\sin \frac{z}{b} - \cos \frac{z}{b} \right] \tag{3.16}$$

and the wavefront configuration is given as a function of t by

$$x = \sqrt{a^2 t^2 - z^2} + H b t \left[\frac{b}{z} \sin \frac{z}{b} - \cos \frac{z}{b} \right] \tag{3.17}$$

These results are plotted in Fig. 3.1 for b = 1140'
Hb = .02 a = 23'/sec. The wavefront has some dents but remains
almost spherical.

3.13 Temperature gradients

The sound speed, a, depends on the temperature, T, through the
relation

$$a = \sqrt{\gamma R T} \tag{3.18}$$

where $\gamma = C_p / C_v$, R = gas constant

-28-

If $T = T_0 + \Delta T$, $a = a_0 + \Delta a$ then

$$\frac{\Delta a}{a_0} = \frac{1}{2} \frac{\Delta T}{T_0}$$ (3.19)

Δa is given as a function of ΔT in Table 3.1 for $T_z = 27^{\circ}C$.

ΔT	$1^{\circ}C.$	$2^{\circ}C.$	$5^{\circ}C.$	$10^{\circ}C.$	$20^{\circ}C.$	$50^{\circ}C.$
Δa	1.8'/sec	3.7'/sec	9.2'/sec	18.4'/sec	37'/sec	92'/sec

Table 3.1

To find the ray paths and wavefronts we make use of the analogy with geometric optics.[15] Since the speed of propagation at any point is independent of the direction of propagation, we can define an effective "index of refraction," $\bar{n} = a_0/a \approx 1 - \Delta a/a$. In the atmosphere, temperature varies primarily with height so we can take $\bar{n} = \bar{n}(z)$. As in geometric optics, we can use Snell's law of refraction to obtain the ray path. Consider a ray in the layered atmosphere shown in Fig. 3.5.

At each interface, Snell's law states that

$$\bar{n}_1 \cos \theta_1 = \bar{n}_2 \cos \theta_2 = \bar{n}_3 \cos \theta_3 = \bar{n}_4 \cos \theta_4 \text{ etc.}$$ (3.20)

These relations hold regardless of the number of layers and we have the general equation

$$\bar{n}(z) \cos \theta(z) = \text{constant} = \cos \theta_0$$ (3.21)

The ray paths and wavefront shapes can be found by integrating Equation (3.21) and using the fact that a wavefront is a surface of constant acoustical path length from the source.

Constant Temperature Gradient

For this temperature distribution, we have

$$\Delta T = - Gz \text{ and}$$

$$\bar{n}(z) = 1 + \frac{G}{2T_o} \cdot z \tag{3.22}$$

for temperature decreasing with height.

Since $\bar{n}(z) \geq 1$, the ray will have no turning points for which $\theta = 0^o$ as is seen from Eq. (3.21). The ray paths and wavefront shapes can be found exactly through integration of Eq. (3.21) using

$$\tan \theta = \frac{dz}{dx} \tag{3.23}$$

but since $Gz/2T_o \ll 1$, it will be simpler to solve equations similar to (3.3) approximately. The ray equations are

$$\frac{dz}{dt} = \frac{a_o}{\bar{n}} \sin \theta = \frac{a_o}{\bar{n}^2} \sqrt{\bar{n}^2 - \cos^2 \theta_o}$$

$$\tag{3.24}$$

$$\frac{dx}{dt} = \frac{a_o}{\bar{n}} \cos \theta = \frac{a_o \cos \theta_o}{\bar{n}^2}$$

Taking $\bar{n}(z) = \bar{n}(z_0) = \bar{n}(a_0 t \sin \theta_0)$ in Eq. (3.24) gives

$$\frac{dz}{dt} \approx a_0 \sin \theta_0 - \frac{G a^2 t}{T_0} (\sin^2 \theta_0 - \frac{1}{2})$$

$$\frac{dx}{dt} \approx a_0 \cos \theta_0 - \frac{G a^2 t}{T_0} \sin \theta_0 \cos \theta_0$$

(3.25)

The solution is

$$z = a_0 t \sin \theta_0 - \frac{G a_0^2 t^2}{2 T_0} (\sin^2 \theta_0 - \frac{1}{2})$$

$$x = a_0 t \cos \theta_0 - \frac{G a_0^2 t^2}{2 T_0} \sin \theta_0 \cos \theta_0$$

(3.26)

which is valid for $\frac{G a_0 t}{T_0} \ll \sin \theta_0$. Eliminating t gives the ray paths

$$x = z \cot \theta_0 - \frac{G z^2 \cos \theta_0}{4 T_0 \sin^3 \theta_0}$$

(3.27)

Eliminating θ_0 gives the wavefront configuration as a function of time

$$x = \left[1 - \frac{Gz}{2 T_0} \right] \sqrt{a_0^2 t^2 - z^2 - \frac{Gz}{T_0} z^2 - \frac{1}{2} a_0^2 t^2)}$$

(3.28)

The wavefronts are plotted in Fig. 3.6 for $G = 1^\circ C/400'$.

3.14 Wavefront Roughening by Turbulence

The distorted wavefronts considered in Sec. 3.11-3.13 and plotted in Fig. 3.1, 3.3, 3.4, and 3.6 are all fairly "smooth." The distance over which significant changes occur in the rays or wavefronts is much larger than the acoustic or radar wavelength. It is this property which allowed us to use the geometric acoustics approximation. For propagation in a turbulent atmosphere, however, the temperature and wind speed will vary almost randomly over shorter distances (although still larger than a wavelength). Since turbulence is a random phenomenon, its effect can be predicted only in a statistical manner. Chernov[16] is an excellent reference on wave propagation in turbulence. We will refer to his work frequently in the following sections. Propagation through turbulence will cause the amplitude and phase of a wave to deviate from their values for propagation in a homogeneous medium. Since a wavefront is a surface of constant phase, knowledge of the phase fluctuations will determine the distortion of the wavefront. If the fluctuations are small, the amplitude of the wave will be approximately the same as in a homogeneous medium. Thus, for our purposes, phase fluctuations are much more important than amplitude fluctuations. The phase of the wave, ψ , is defined by writing the wave amplitude (a plane wave in this case) in the form

$$p\,(\overline{r},\ t) = A\,(\overline{r})\ \exp\,[-i(\omega t-kx) + i\psi(\overline{r})] \qquad (3.29)$$

where ω = frequency

$\quad k = 2\pi/\lambda_a$ = wavenumber

$\quad A\,(\overline{r})$ = amplitude

For a homogeneous medium, $\psi = 0$ and for the case of isotropic turbulence $\langle\psi\rangle = 0$ where $\langle\ \rangle$ denotes average value.

The mean local speed of propagation is $\langle a \rangle + \langle V \rangle$ while the instantaneous speed of propagation is $a + V$. We can define a "turbulence strength" μ as

$$\frac{a + V_r}{\langle a \rangle + \langle V \rangle_r} = 1 + \mu \qquad (3.30)$$

where V_r is the component of V in the direction of propagation. From this expression μ is a random function of position with average value zero and is given approximately by

$$\mu = \frac{\Delta V}{a_o} + \frac{1}{2} \frac{\Delta T}{T_o} \qquad (3.31)$$

where ΔV, ΔT are the differences $V_r - \langle V \rangle_r$, $T - \langle T \rangle$. The phase fluctuations in the wave are determined by the space correlation function, $N(\bar{r}_1, \bar{r}_2)$, of the turbulence defined as

$$N(\bar{r}_1, \bar{r}_2) = \langle \mu(\bar{r}_1) \mu(\bar{r}_2) \rangle \qquad (3.32)$$

For homogeneous turbulence $N(\bar{r}_1, \bar{r}_2) = N(\bar{r}_1 - \bar{r}_2)$ and for isotropic turbulence $N(\bar{r}_1 - \bar{r}_2) = N(r)$ where $r = |\bar{r}_1 - \bar{r}_2|$. The functional form of $N(r)$ is not well known, but there usually exists a correlation distance, s, such that $N(r)$ is very small for $r > s$. This correlation distance can be associated with the scale of the turbulence. For many of his calculations, Chernov assumes a Gaussian correlation function for μ so that all possible information is given by the values of $\langle \mu^2 \rangle$ and s. Chernov considers the phase fluctuations for a plane wave but most of his results are equally applicable to the case of a spherical wave.

There are two dimensionless parameters which are important for determining phase fluctuations. The first is ks or $2\pi s/\lambda_a$, the ratio of the turbulence scale to the acoustic wavelength. While the inner scale of turbulence may extend down to centimeters, most of the turbulent intensity is found in larger scale inhomogeneities. Golitsyn, Gurvich, and Tatarskii[17] found that most turbulence has a scale of between 100' and 10,000'. Since the smallest turbulence produces the greatest wavefront distortion, we will choose $s \approx 100'$. For acoustic wavelengths considered (114 cps; $\lambda_a = 10'$) the ratio $2\pi s/\lambda_a \gg 1$. The second dimensionless ratio is called the wave parameter d and is given by

$$d = 4R/ks^2 = \frac{2R\lambda_a}{\pi s^2} \qquad (3.33)$$

where R is the distance of propagation through the turbulent medium. Physically, d is the ratio of the size of the first Fresnel zone to the scale of the turbulence. For $\lambda_a = 10'$, $s = 100'$, we find

$$d = \frac{R}{1500'}$$

so that small R corresponds to $d \ll 1$ while large R corresponds to $d \gg 1$. With a Gaussian correlation function for μ, Chernov finds for the mean square phase fluctuation[18]

$$\langle \psi^2 \rangle = \frac{2\pi^2 \sqrt{\pi} \langle \mu^2 \rangle s R}{\lambda_a^2} \left(1 + \frac{1}{d} \tan^{-1} d\right) \qquad (3.34)$$

For the case $d \ll 1$.

$$\langle \psi^2 \rangle = \frac{4\pi^2 \ \sqrt{\pi} \langle \mu^2 \rangle \ s \ R}{\lambda_a^2} \qquad (3.35)$$

while for $d \gg 1$

$$\langle \psi^2 \rangle = \frac{2\pi^2 \ \sqrt{\pi} \langle \mu^2 \rangle \ s \ R}{\lambda_a^2} \qquad (3.36)$$

In these cases the rms phase fluctuation varies as

$$\psi_{rms} \sim \mu_{rms} \ \frac{\sqrt{sR}}{\lambda_a} \qquad (3.37)$$

The R dependence of ψ_{rms} is the same regardless of the form of the correlation function. In addition to the mean square phase fluctuation $\langle \psi^2 \rangle$, we are interested in the correlation distance of the phase fluctuations along the wavefront. Chernov[19] found that the correlation distance for phase fluctuations is approximately the same as the correlation distance for turbulent fluctuations. In fact, with a Gaussian correlation function for turbulence, the correlation function for phase fluctuations is also Gaussian with exactly the same correlation distance. Thus, the effects of turbulence on the acoustic wavefront are given in Eq. (3.34) - (3.37) together with the fact that for phase fluctuations, the correlation distance along the wavefront is s. To get an order of magnitude estimate of $\langle \psi^2 \rangle$, we can substitute $\lambda_a \approx 10'$, $s \approx 100'$, $\mu_{rms} \approx .01$ giving

$$\psi_{rms} \approx \sqrt{\frac{R}{500}} = \frac{1}{22} \sqrt{R} \quad \text{where range is in ft}$$

For $\mu_{rmw} \approx .001$

$$\psi_{rmw} \approx \sqrt{\frac{R}{50,000}} = \frac{1}{220} \sqrt{R}$$

so ψ_{rms} may be large or small depending on μ_{rms} .

Essentially the same results may be obtained from a highly simpli-
fied model of propagation in turbulence. Consider the propagation
of sound through a turbulent eddy of size s and turbulent wind
strength ΔV. Some parts of the wavefront are speeded up by ΔV
while other parts, within a distance s, are slowed down by ΔV.
This difference in velocities obtains for a time s/a producing a
distortion in the wavefront which may be considered as a phase
fluctuation. The size of the phase fluctuation is

$$\Delta\psi_{rms} \approx \frac{2\pi\Delta x}{\lambda_a} = \frac{2\pi}{\lambda_a} \Delta V \frac{s}{a} = \frac{2\pi s \Delta V}{a\lambda_a} \tag{3.37}$$

where Δx is shown in Figure 3.7.

In traveling a distance R, the wavefront passes through R/s such
eddies. Since the direction of each wavefront distortion is ran-
dom, the problem of finding the total phase fluctuation is a
random walk problem. For a sequence of N fluctuations of $\Delta\psi$ each
in random directions, the rms total deflection is $\Delta\psi \sqrt{N}$. The
final result for $\langle\psi^2\rangle$ is thus

$$\langle \dot{v}^2 \rangle = \frac{4\pi^2 \, s \, R}{\lambda_a^2} \left\langle \left(\frac{\Delta V}{a}\right)^2 \right\rangle = \frac{4\pi^2 \, \langle \mu^2 \rangle \, s \, R}{\lambda_a^2} \tag{3.38}$$

which has the same functional dependence as Eqs. (3.35) and (3.36)
and differs only by a numerical factor between 0.9 and 1.8.

3.2 Reflection From Deformed Wavefronts

3.21 Single Wavefront

The radar beam will be incident on a certain region of the acoustic
wavefront. This region can be characterized by its location, area,
orientation, curvature, and roughness. This section will consider
the conditions affecting the reception of a reflected signal but
will not consider the interpretation of the information carried by
the signal. To study the effects of wind, temperature, turbulence,
and humidity, it is necessary to first look at the reflection from
an acoustic wave propagated in a completely homogeneous, isotropic
atmosphere (no wind, constant temperature, no turbulence). The
wavefront will be a smooth sphere of radius, ta, centered at the
acoustic source which is assumed to be co-located with the radar
antenna. According to either geometric optics or wave theory, the
entire radar signal reflected from the wavefront will return to
the antenna. This follows from ray theory because all rays strike
the wavefront at normal incidence and retrace their paths when
reflected. According to wave theory, the acoustic wavefront is
also a surface of constant phase for the radar signal. The solu-
tion of the wave equation then gives a transmitted diverging
spherical wave and a reflected converging spherical wave. Since
the transmitting antenna has a finite area, the reflected signal
will not focus to a point but will cover an area at least equal
to that of the antenna.

Any deviation from homogeneity or isotropy in the atmosphere will change the wavefront characteristics from those of a smooth sphere centered at the antenna. A steady wind will keep the wavefront smooth and spherical but will cause the center to move. Wind shear will cause the curvature of the wavefront to change as will temperature gradients. Turbulence will cause the wavefront to become rough (because of phase fluctuations). In this section we will consider radar reflection from the types of distorted wavefronts discussed in Sec. 3.1.

Steady Wind

The wavefront in a steady wind V is a sphere of radius ta whose center is a distance Vt downwind from the source. The wavefront still acts like a spherical mirror but the antenna is no longer at the center. This is seen in Fig. 3.8.

ϕ is the angle between the wind and direction of search and

$$\theta_w = \frac{V \sin \phi}{a} \tag{3.39}$$

using the approximation $V \ll a$ which is certainly valid. The reflected beam comes to a focus at a distance 2Vt from the antenna (t = time at which the radar reflects from the wavefront). All rays within the radar beam width will be focused at the image therefore increasing the beamwidth will not increase the image size significantly for such a spherical reflecting surface. The reflection of a finite-width radar beam from a curved wavefront produces essentially the same result as reflection of a single radar ray (no beam width) from a plane wavefront whose normal makes an angle θ_w with the incident ray.

If the diameter of the antenna is D then the diameter of the image will be at least D. Examination of Fig. 3.8 shows that the reflected beam passes within a distance $2Vt \sin \phi$ of the antenna. Thus if $D > 2Vt \sin \phi$, part of the reflected beam will fall on the antenna. Expressing t in terms of the range R, the condition becomes

$$\frac{D}{R} > \frac{2 V \sin \phi}{a} \tag{3.40}$$

If this condition is not satisfied, then no reflected signal (to this approximation) will be received. This condition is too strict, however, since the reflected beam usually has a finite width at its closest approach to the antenna, making the area of the beam at that point much greater than that of the antenna. Also, as we will see in the discussion of reflection from "rough" wavefronts, the reflected signal will cover an even larger area if there is turbulence in the atmosphere.

The same results for the reflected signal obtained above using geometric optics, can be obtained using the wave theory. The wavefront may be regarded as an aperture which is illuminated by the incident radar beam. The pattern of the signal reflected from the wavefront is known for the case $\theta_w = 0$ where the wavefront is a surface of constant phase. When $\theta_w \neq 0$, the relative phase of the radar wave varies linearly with distance along the acoustic wavefront which is acting as a mirror (the linear variation holds approximately if the illuminated portion of the wavefront is not too large). Silver[20] has shown that if the relative phase distribution on an aperature differs by a linear

function of distance from that on an aperture with a known radiation
pattern, then the pattern of the new aperture is identical to that
of the old aperture but rotated through a constant angle. In this
case the reflected beam makes an angle $2\theta_w$ with the incident beam
which agrees with the relation obtained using geometric optics.

Wind Shear, Temperature Gradients

These two conditions affect the wavefront by displacing it, changing
its orientation, and changing its curvature. The results of changes
in location and orientation have been considered above and in this
part we will consider only effects of curvature.

At any point, the wavefront has two principal radii of curvature.
For reasonable values of wind shear and temperature gradient, both
these radii of curvature are approximately equal to the range R.
The beam sent out from the antenna will be focused at a point be-
tween the effective wavefront center and the wavefront if range is
greater than the radius of curvature. If range is less than the
radius of curvature, the beam will be focused further from the wave-
front than the effective wavefront center. These cases are shown
in Fig. 3.9. In both cases shown in Fig. 3.9, the reflected beam
at the antenna is much larger than the size of the antenna (the
size of the image). Figure 3.9 is drawn for rays in one of the
principal planes of the wavefront. If the two principal radii of
curvature differ, the rays in the two principal planes will focus
at different points and there will be no well-defined image of the
antenna. The area of the reflected beam at any point can be found
from knowledge of the radar beam width, the range of the wavefront,
and its two principal radii of curvature.

The fact that the reflected beam covers a larger area for distorted wavefronts can cause a decrease or an increase in the received signal under different conditions. If the beam falls on the antenna satisfying Eq. (3.40) then the received signal will decrease for a distorted wavefront since the power in the reflected beam is spread over a larger area thus giving a smaller intensity in the beam at the antenna. On the other hand, if the beam does not fall on the receiving antenna the beam spreading caused by a distorted wavefront would increase the intensity striking the antenna.

These results also follow qualitatively from the wave theory. Again considering the wavefront as an illuminated aperture, a change in curvature will change the relative phase symmetrically about the center line. This is seen in the fact that the drawings in Fig. 3.9 are symmetric about their center lines. The relative phase will be a quadratic function of distance along the aperture (wavefront). The reflected pattern depends on the shape and illumination of the aperture but some general results can be found. Silver[20] calculates the radiation patterns of several apertures for zero phase differences and for quadratic phase differences. He finds that the reflected pattern is wider for the quadratic phase difference aperture regardless of whether the phase differences were positive or negative. This agrees with the resuls of Fig. 3.9 that the reflected beam is wider regardless of whether the radii of curvature are larger or smaller than the range.

The result that deviations from a spherical wavefront produce a broadening of the reflected beam will be encountered again in the sub-section on turbulence. This will not be unexpected since turbulence is composed of small scale wind and temperature gradients and should produce roughly the same effect.

3.23 Reflection From Roughened Wavefronts

The principal difference between what we call "turbulence" and what we call "wind and temperature gradients" is one of scale. Turbulence has a smaller scale than other inhomogeneities. There are many characteristic lengths of importance for the reflection of radar from acoustic wavefronts. The smallest of these is the radar wavelength λ_e which is of the order of 1 or 2 feet. The acoustic wavelength λ_a is about 10 feet. The diameter of the illuminated portion of the wavefront is BR where B = radar beamwidth angle, R = range, and BR may be as large as 1,000 feet. The largest scale is the range itself which extends to about 10,000 feet. The scales of wind and temperature gradients considered (larger than 1,000 ft) are larger than the illuminated portion of the wavefront while the scale of turbulence considered ($s \approx 100$ ft) is larger than λ_a but may be smaller than BR. A graph of BR vs. R for various beamwidths is shown in Fig. 3.10. If BR < s then the phase fluctuation will vary smoothly over the illuminated portion of the wavefront and the radar reflection will be similar to that considered in the section on wind shear and temperature gradients. However, if BR > s, the illuminated portion of the wavefront will appear rough producing a more diffuse reflection. It is this case (BR > s) which will be considered in this section. Chernov[21] considers the type of image produced when the illumination of a lens has random phase fluctuations of magnitude, ψ_{rms} and characteristic scale length s.

$$I(y) = I_o \exp [-(y/y_o)^2] \tag{3.41}$$

where I(y) = received intensity at a distance y away from the focus in the focal plane

I_o = received intensity at the focus

and

$$y_o = \frac{R\lambda_a}{s} \frac{\psi_{rms}}{\pi} \tag{3.42}$$

I_o depends on y_o since approximately the same total power is reflected, regardless of the area over which it is spread. Using the fact that

$$P_r = \int I(\bar{y}) \, dS = 2\pi I_o \int_0^\infty \exp\left[-(y/y_o)^2\right] y \, dy \tag{3.43}$$

is the total power reflected from the wavefront, we find

$$I_o = \frac{P_r}{\pi y_o^2} \tag{3.44}$$

Equation (3.41), (3.42), and (3.44) thus serve to determine the received intensity at a distance y from the focal point of the reflected beam. Putting in $y = 2Vt \sin \phi = 2RV \sin \phi/a$ as is the case for reflection in a steady wind, and ψ_{rms} from (3.36), we obtain

$$I = \frac{P_r s}{2\pi \sqrt{\pi} \langle\mu^2\rangle R^3} \exp\left[-\frac{V^2 s \sin^2 \phi}{2 \sqrt{\pi} a^2 \langle\mu^2\rangle R}\right] \tag{3.45}$$

or

$$I = P_r \frac{C_1}{R^3} \exp\left[-\frac{C_2}{R}\right] \tag{3.46}$$

with $\qquad C_1 = \dfrac{s}{2\pi \ \sqrt{\pi} \ \langle \mu^2 \rangle}$, $\qquad C_2 = \dfrac{V^2 \ s \ \sin^2 \ \phi}{2 \ \sqrt{\pi} \ a^2 \ \langle \mu^2 \rangle}$ $\qquad$ (3.47)

The same qualitative results may be obtained from the simplified model introduced in Sec. 3.14. The rms phase fluctuation is ψ_{rms} with a correlation distance s. Thus any two points on the wavefront within a distance s from each other may be advanced or retarded with respect to each other in space by a distance:

$$2\Delta x = 2 \ \frac{\psi_{rms}}{2\pi} \ \lambda_a \qquad (3.48)$$

The rms angle that the turbulent wavefront makes with the average (smooth) wavefront is

$$\theta_T = \frac{2\Delta x}{s} = \frac{\psi_{rms}}{\pi} \ \frac{\lambda_a}{s} \qquad (3.49)$$

We can assume that the reflected beam will have a half-width of $2\theta_T$. Since the direction of reflection from a smooth wavefront makes an angle $2\theta_w$ with the incident beam, we have the situation shown in Fig. 3.11.

The angular distribution in the reflected beam is assumed to be Gaussian

$$I'(\theta) = I_o' \ \exp \ \left[- \ (\theta/2\theta_T)^2 \right] \qquad (3.50)$$

-44-

As in Eq. (3.43), $I_o^{'} = \dfrac{P_r}{4\pi \, \theta_T^2} \quad \dfrac{1}{R^2}$ \hfill (3.51)

The additional factor $1/R^2$ accounts for the spherical divergence in the reflected beam. Putting Eq. (3.49) for θ_T, Eq. (3.36) for $\langle \psi^2 \rangle$ and $2\theta_w$ for θ , Eq. (3.50) becomes

$$I' = \frac{P_r \, s}{4\pi \, \sqrt{\pi} \, \langle \mu^2 \rangle \, R^3} \quad \exp \left[- \frac{v^2 s \, \sin^2\phi}{2 \, \sqrt{\pi} a^2 \, \langle \mu^2 \rangle \, R} \right] \quad (3.52)$$

This expression has the same functional form as Eq. (3.45). The numerical constant C_2 is identical and C_1 differs by a factor of 1/2. For future calculations we will use Eq. (3.45) - (3.47) since they are probably more accurate.

The expression for I can be considered as the product of an amplitude term and an angular distribution term. The amplitude term has a factor $1/R^2$ from spherical divergence, and a factor $s/R \, \langle \mu^2 \rangle$ from spreading of the beam. The angular distribution term has a maximum value of unity, and becomes very small if

$$\frac{v^2 \, s \, \sin^2 \phi}{2 \, \sqrt{\pi} \, a^2 \, \langle \mu^2 \rangle \, R} \gg 1 \hspace{2cm} (3.53)$$

Equation (3.53) is the condition for misalignment of the reflected beam and the receiving antenna and poor reception. When $\phi = 0°$, $180°$ condition Eq. (3.53) will not occur and the received signal will be detectable for all values of the parameters. This occurs when the direction of search and the wind direction are either

the same or opposite. From Eq. (3.53) we see that for fixed V, s, ϕ, and $\langle\mu^2\rangle$ there is some "blind range" R_o below which Eq. (3.53) may occur and signals may not be received at close range. If this "blind range" is less than the maximum range, R_{max}, of the probe, then a detectable signal will be received for $R_o < R < R_{max}$. From Eq. (3.46) we see that C_2 has the dimensions of a length and is directly proportional to the R_o mentioned above. C_2 is made smaller by decreasing V, decreasing s, or increasing $\langle\mu^2\rangle$.

From the above analysis, it appears that the most serious misalignment problems occur for small R. However, we must remember that the radar antenna has a finite diameter, D. From Eqs. (3.42) and (3.36), the reflected beam has an approximate radius

$$y_o = \sqrt{2}\, \pi^{1/4}\, \mu_{rms}\, R\, \sqrt{R/s} \qquad (3.54)$$

To receive a signal it is not necessary that the reflected beam fall on the center of the antenna but only that the beam fall on some part of the antenna. This condition may be stated as

$$\frac{D}{2} + \sqrt{2}\, \pi^{1/4}\, \mu_{rms}\, R\, \sqrt{R/s} \geq 2\, Vt \sin\phi$$

or

$$\frac{D}{R} + 2^{3/2}\, \pi^{1/4}\, \mu_{rms}\, \sqrt{\frac{R}{s}} \geq 4\, \frac{V}{a} \sin\phi \qquad (3.55)$$

For sufficiently small R, this condition is always satisfied. (It is also satisfied for sufficiently large R as was seen above.)

To obtain an estimate of the reflected intensity as a function of range we can make Eq. (3.46) dimensionless. For this purpose, let the normalized range variable be

$$X = \frac{R}{C_2}$$

and the normalized intensity variable be

$$Y = \frac{I}{P_r} \frac{C_2^3}{C_1}$$

Then substituting into Eq. (3.46)

$$Y = \frac{1}{X^3} \exp\left(-\frac{1}{X}\right) \tag{3.56}$$

This is plotted in Fig. 3.12.

In order to estimate expected values for intensity and range from Eq. (3.56) or Fig. 3.12, the following method can be applied. First choose (or measure) values for V, $\langle \mu^2 \rangle$, ϕ, and s thus giving C_1, C_2. The value of C_2 provides the conversion from X to R giving the graph a horizontal scale. The value of I calculated from

$$I = \frac{C_1}{C_2^3} P_r Y \tag{3.57}$$

-47-

is the <u>intensity</u> received at the radar antenna in terms of the <u>power</u> reflected from the acoustic wavefront. The value of P_r/P_i depends on the acoustic wave intensity and shape as discussed in Sec. 2. The dependence of acoustic wave intensity and shape on range, frequency, acoustic power radiated, and source geometry is discussed in Sec. 4.

The calculation of received power at any range takes place as follows:

1. Use assumed (or measured) values of V, $\langle\mu^2\rangle$, ϕ, s, and D to calculate C_1, C_2 and to determine the range of R for which $R < aD/(2V \sin \phi)$, i.e., for which the reflected beam falls on the antenna.

2. For $R < aD/2V \sin \phi$, the received intensity will be high provided the sound wave is strong enough $(R < R_{max})$

3. For $R > aD/(2V \sin \phi)$ continue as follows:

4. Find X from R by $X = R/C_2$

5. Find Y from X using Fig. 3.12

6. Find the acoustic wave intensity and shape at range R using the results of Sec. 4

7. Find P_r/P_i for reflection from the acoustic wave using the results of Sec. 2

8. Calculate I from Eq. (3.57) and knowledge of P_i

9. Power received = I x Area of radar antenna.

3.24 Off-Normal Reflection From a Train of Plane Shock Waves

As with a single shock wave, if a train of waves remain perfectly plane, there will be little or no off-normal reflected signal returning to the antenna when the angle between the radar beam and the normal to the acoustic wave exceeds 1/4 of the radar beamwidth. There will be a reflected signal if the wavefronts are sufficiently rough to have a part of their area normal to the radar beam. For the case of two wavefronts shown in Fig. 3.13 normal reflection occurs at points A and B' although not at A' and B. For the signals reflected at A and B' to interfere constructively, we must have

$$R_{B'} - R_A = \frac{m}{2} \lambda_e \qquad m = \text{integer}$$

Since $R_{B'} - R_A \approx \lambda_a \gg \lambda_e$, it should not be difficult to adjust λ_e so that (1) is satisfied. However, even though the radar frequency is adjusted to give optimum reflection from such areas back to the source, the fact that these areas exist at random locations over the region of the shock wave train illuminated by radar, they will be as a group incoherent in that direction. On the other hand, in the direction of specular reflection, all such irregularities will have coherence. It is apparent that a single shock wave front may be deformed sufficiently by irregularities in the atmosphere to direct a significant fraction of power back toward tne source by scattering. A train of waves however, is relatively insensitive to such irregularities and therefore reflection from such a wave train tends to be highly specular with very little energy directed back to the source when the waves are not normal to the radar beam. Thus a train of waves tend to support specular reflection in an inhomogeneous medium but cannot be made to improve reflection at an arbitrary angle by choice of the radar wavelength.
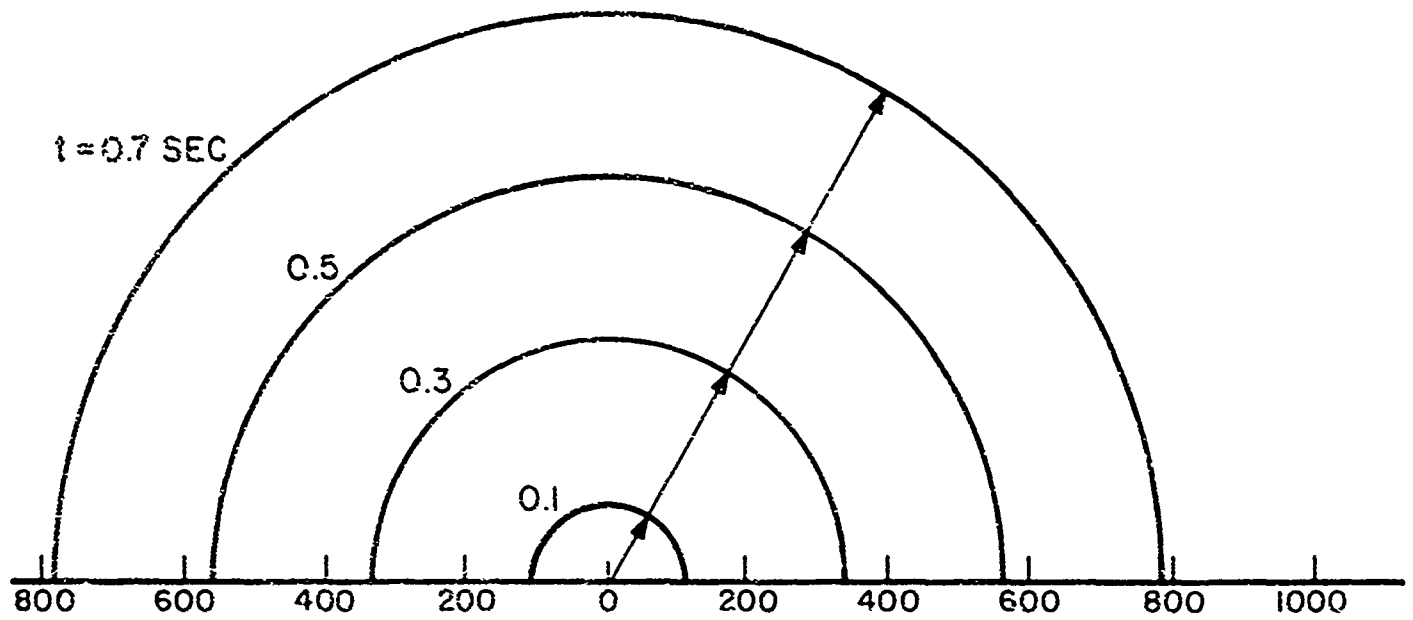
A. NO WIND
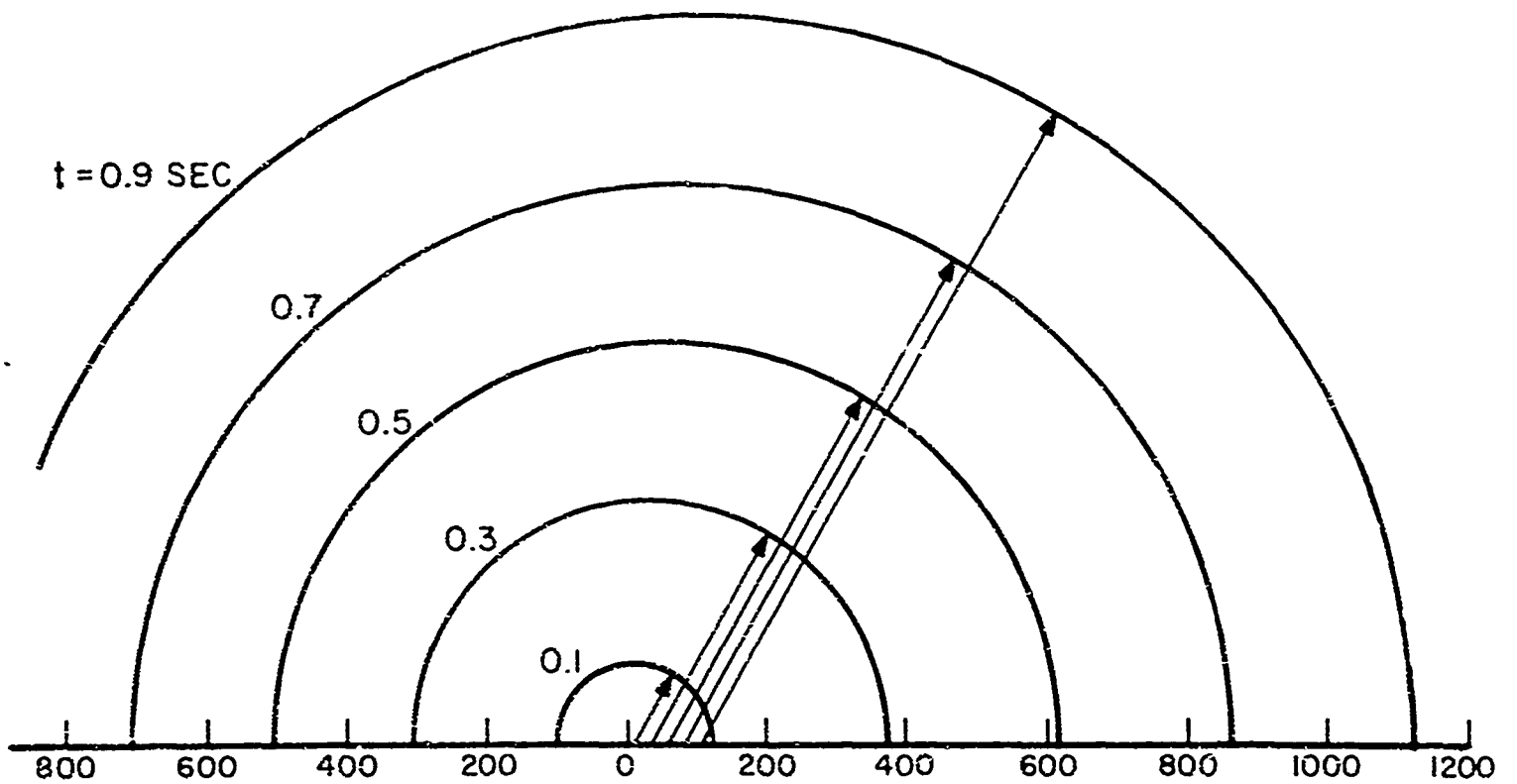
B. STEADY WIND OF 114 FT/SEC
(APPROX. 78 MPH; 0.1 a)

FIG. 3.1   WAVEFRONT SHAPES IN STEADY WIND
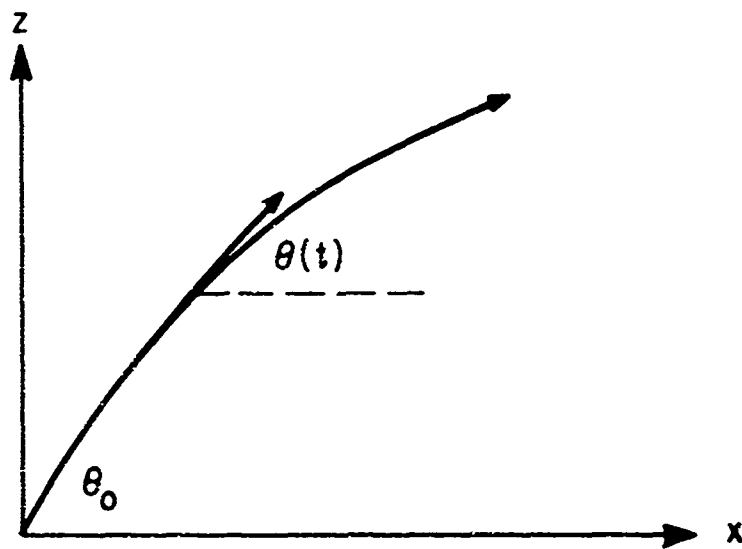
FIG. 3.2   PATH OF SOUND RAY

1200
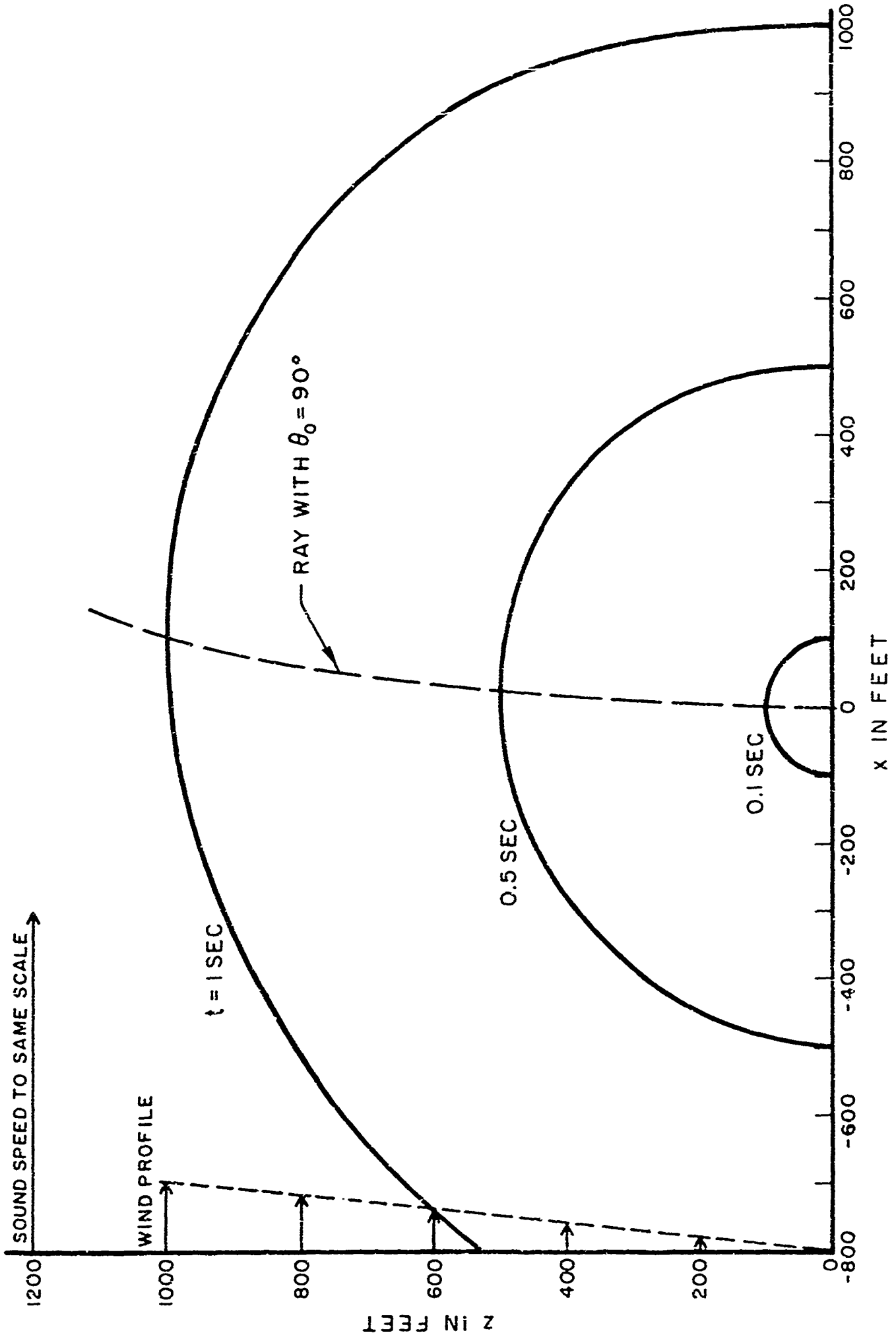
FIG. 3.3   ACOUSTICAL WAVEFRONT SHAPE AND SOUND RAY PATH IN CONSTANT WIND GRADIENT (0.2 FT/SEC)/FT
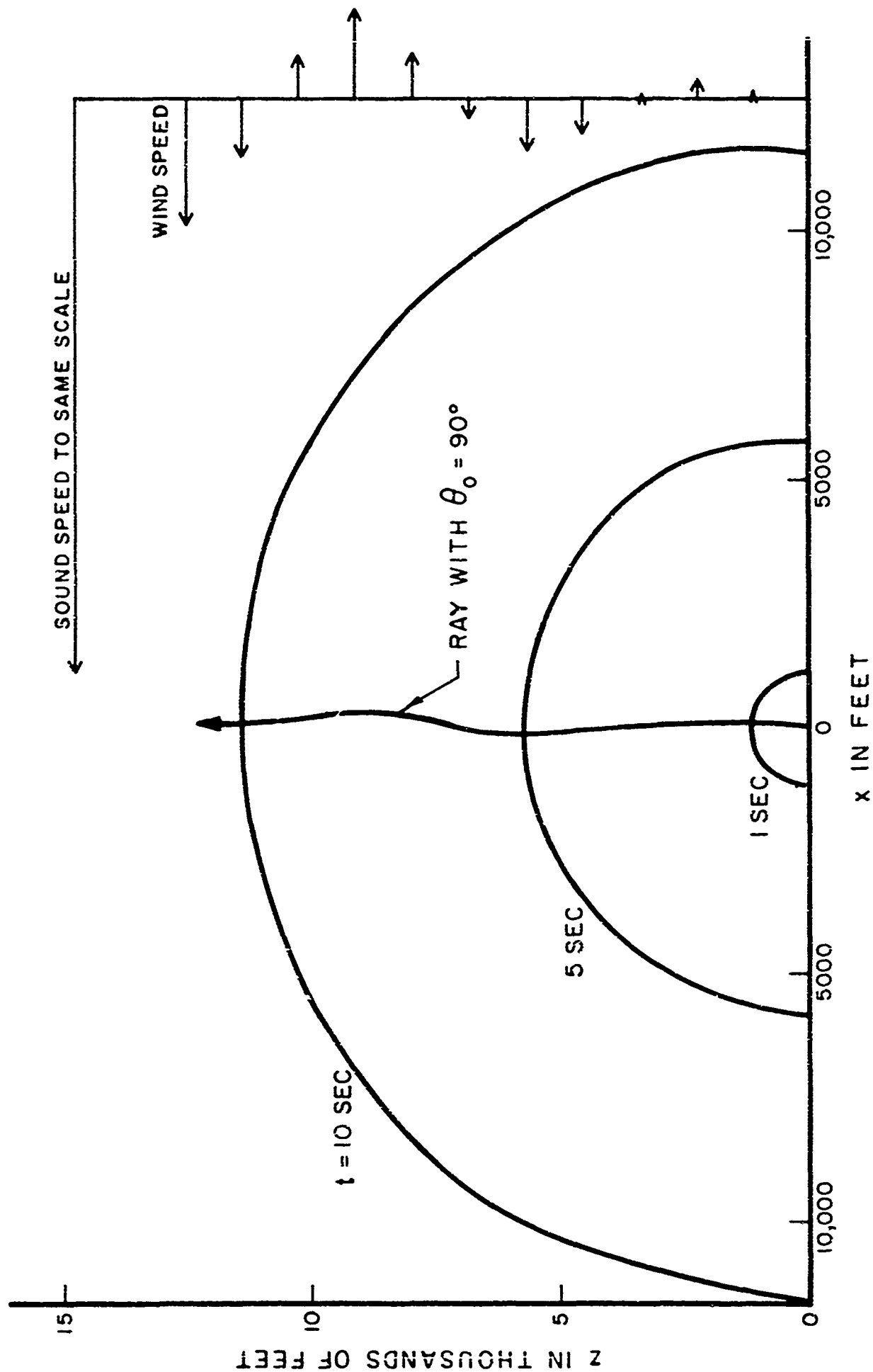
FIG. 3.4 ACOUSTIC WAVEFRONT SHAPE AND SOUND RAY PATH IN TURNING WIND
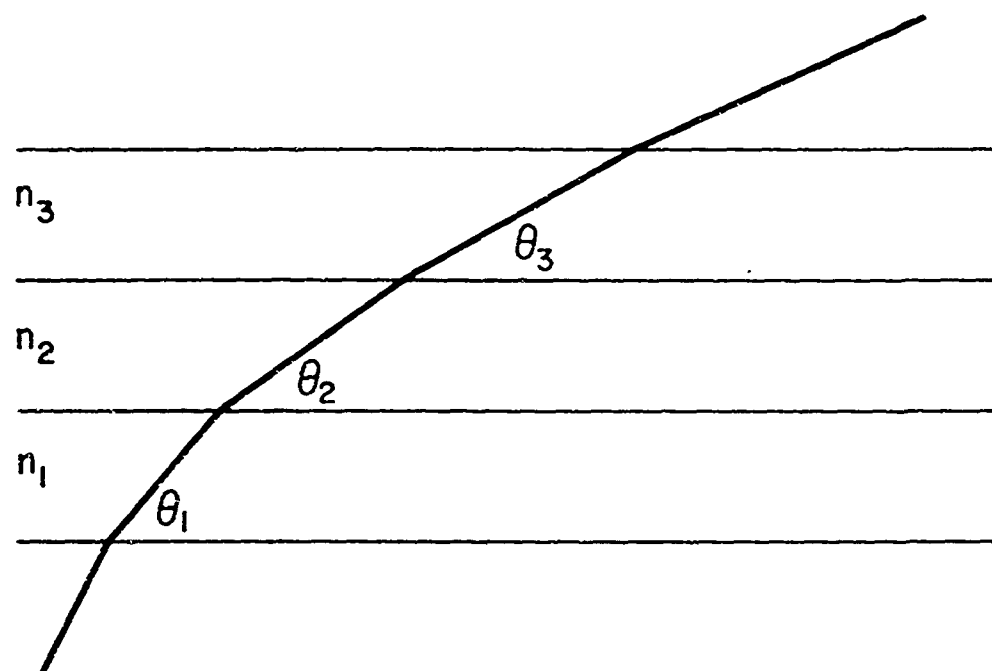
FIG. 3.5   SOUND RAY PATH IN LAYERED MEDIUM
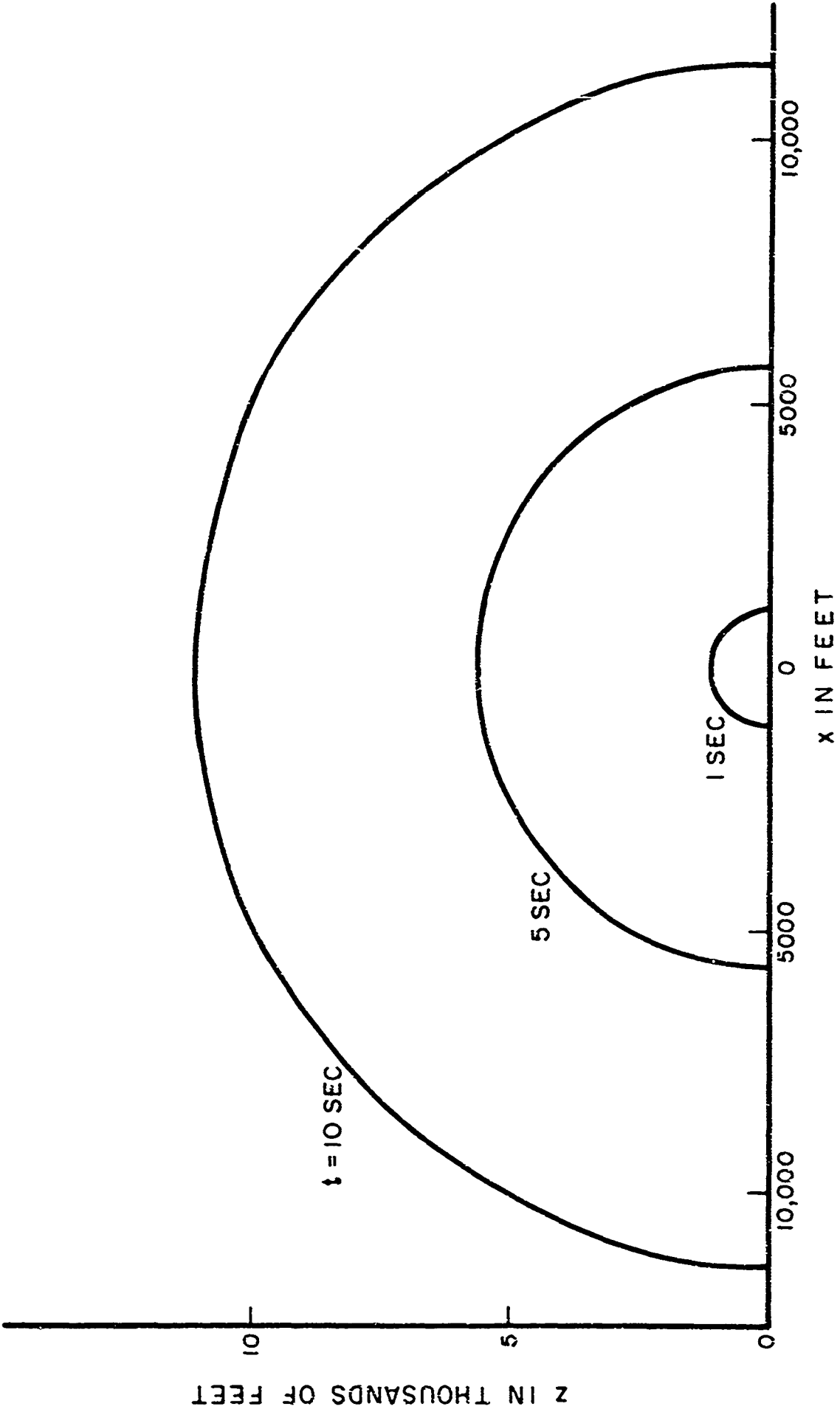
FIG. 3.6   ACOUSTIC WAVEFRONT SHAPE FOR CONSTANT TEMPERATURE
GRADIENT 1° C/400 FT
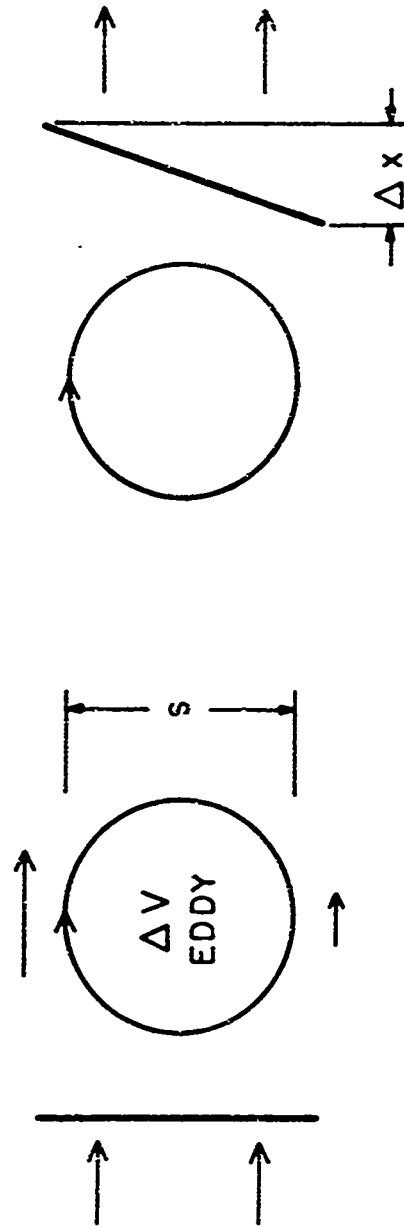
FIG. 3.7 WAVEFRONT DISTORTION BY TURBULENT EDDY
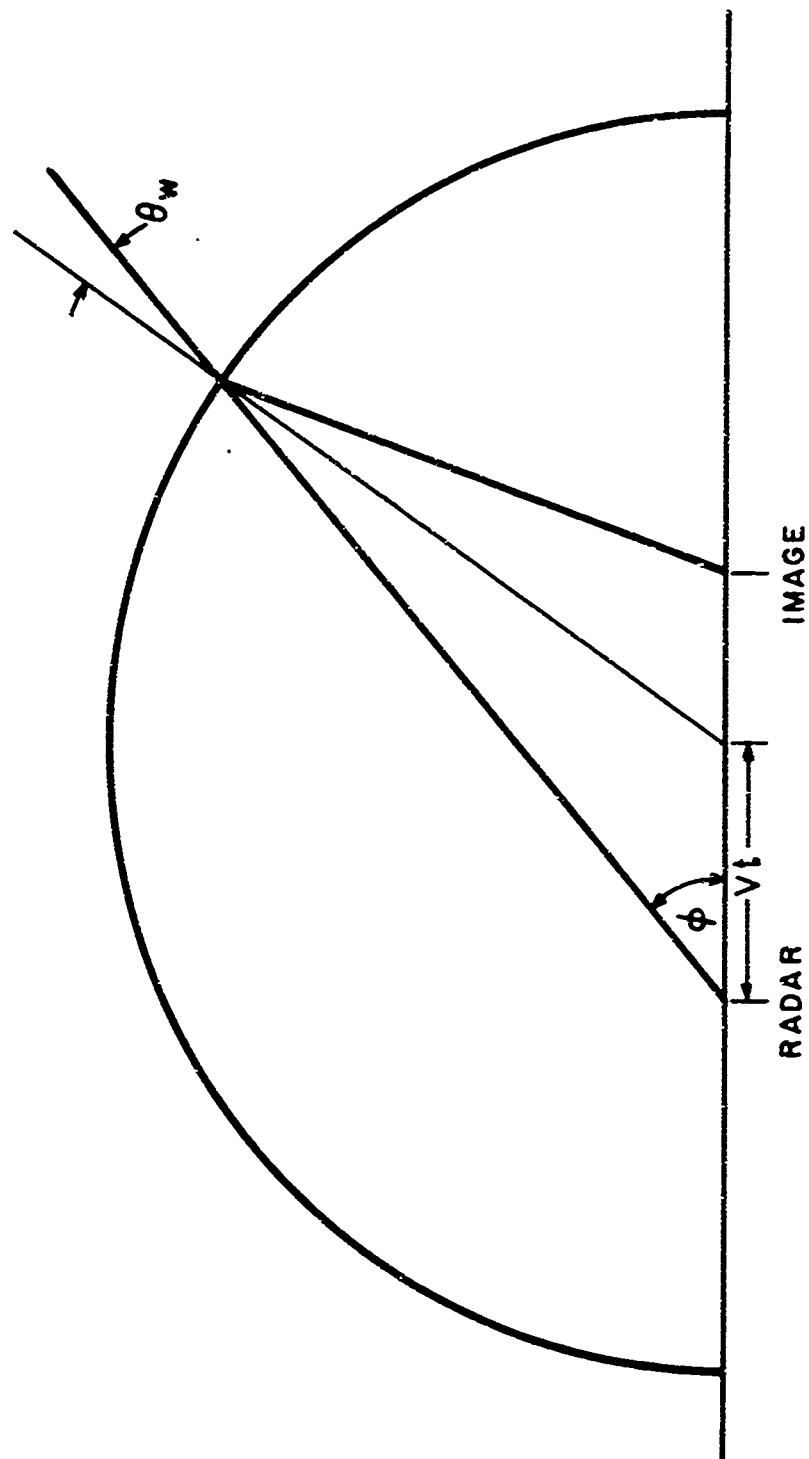
FIG. 3.8   RADAR RAY PATH IN STEADY WIND
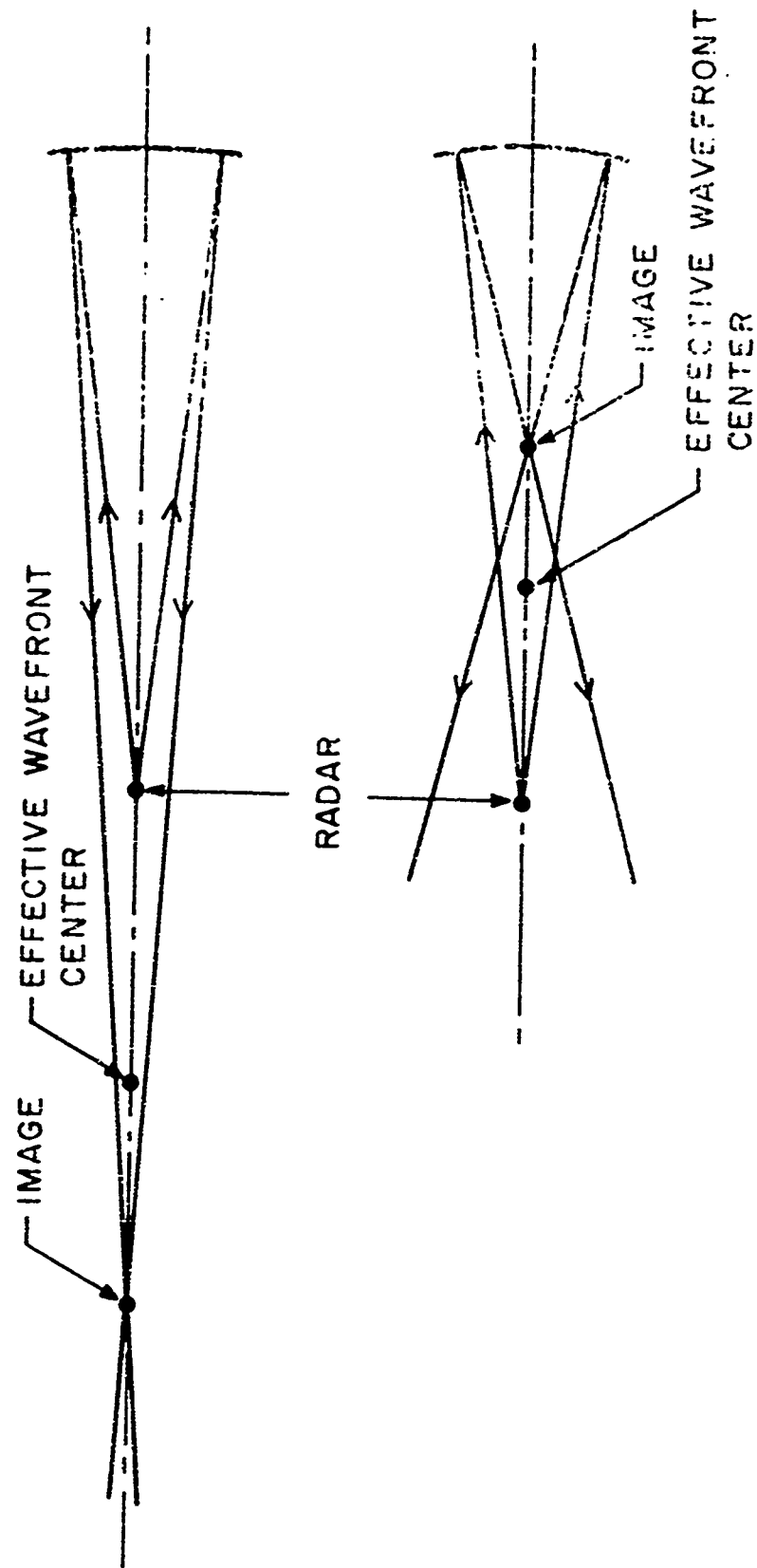
FIG. 3.9 RADAR REFLECTION FROM DEFORMED ACOUSTIC WAVEFRONTS
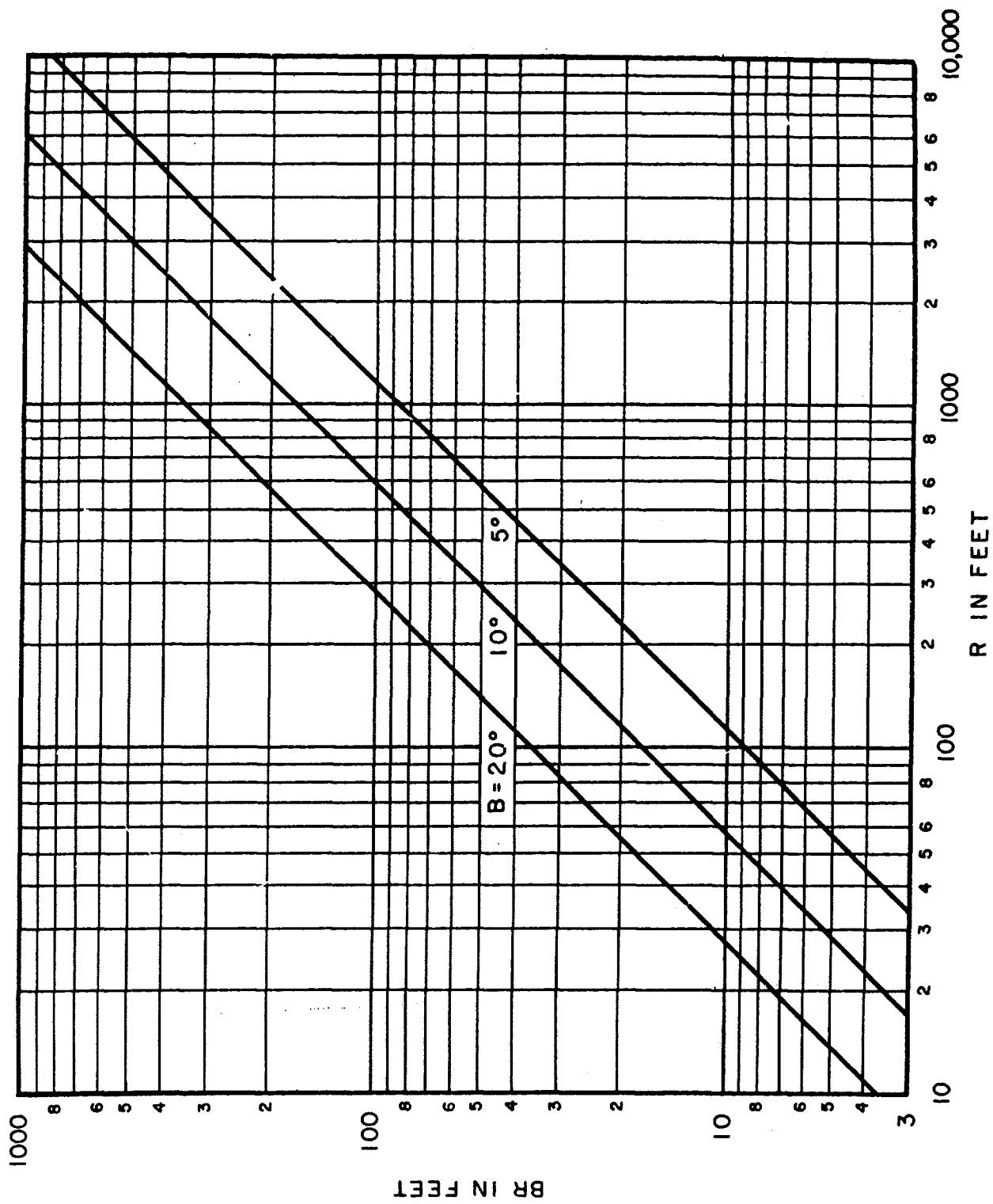
FIG. 3.10   DIAMETER OF ILLUMINATED PORTION OF WAVEFRONT VS. RANGE

ANTENNA

NORMAL

$2\theta_T$ $2\theta_W$

WAVEFRONT

FIG. 3.11   REFLECTION FROM ROUGH WAVEFRONT

$$X = \frac{R}{C_2}$$

$$Y = I\,\frac{C_2^3}{C_1}$$
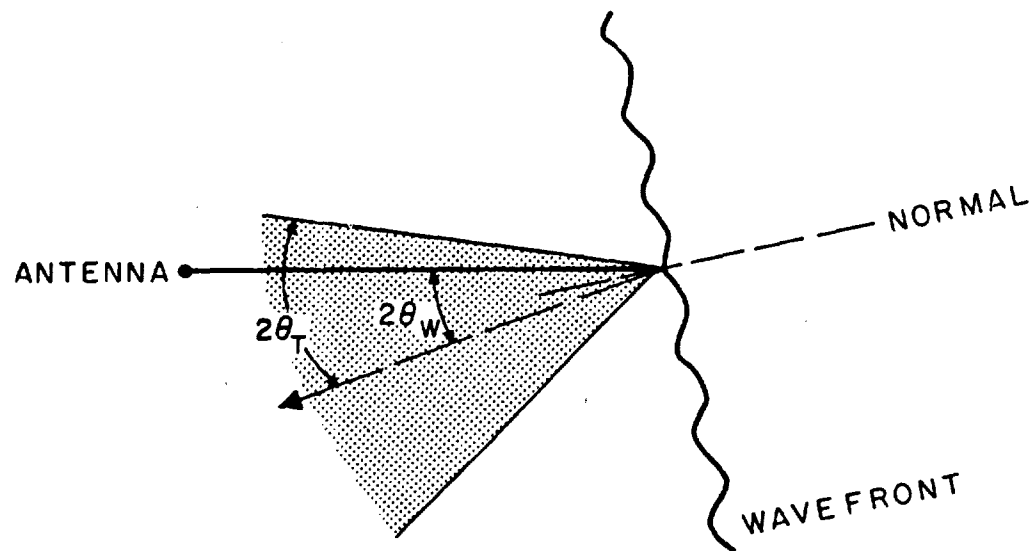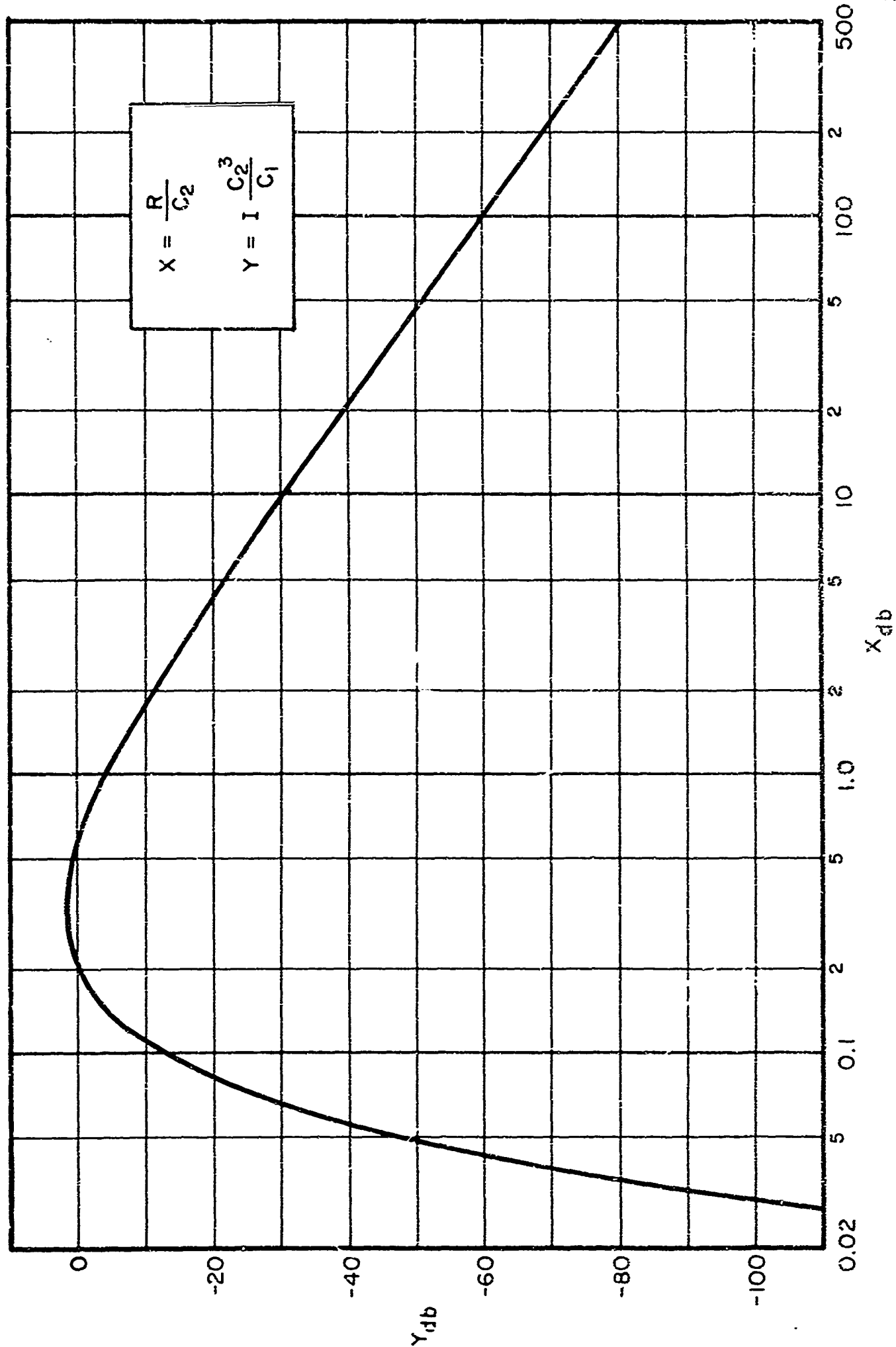
FIG. 3.12 NORMALIZED RECEIVED INTENSITY, Y VS. NORMALIZED RANGE, X
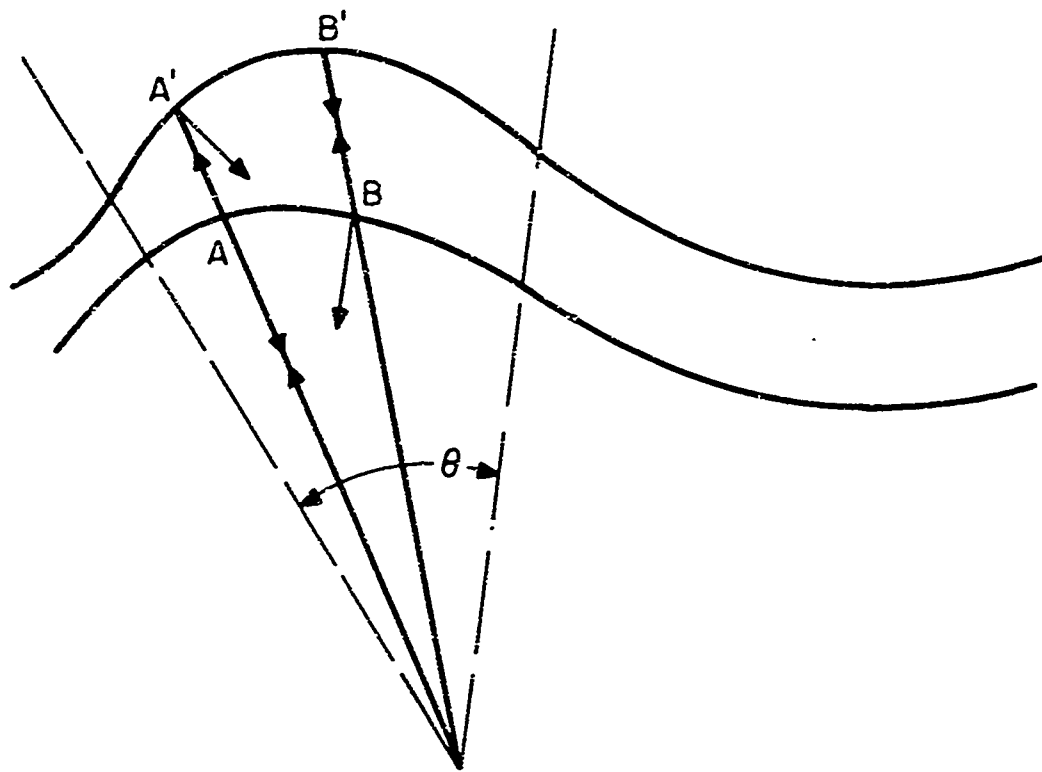
FIG. 3.13 REFLECTION FROM TWO WAVEFRONTS

4. SOUND PROPAGATION IN THE ATMOSPHERE

Sound in air is a longitudinal wave motion of the medium which propagates from its driving source at a speed determined by the physical characteristics of the medium. The directions of sound propagation away from the source are determined by the geometry of the source and its confinements. As the wave propagates through the air irregularities such as wind, wind shear, turbulence, temperature gradients etc., modify the local velocity of the sound causing significant alterations in the directions originally taken by the sound wave as it left the source.

As sound radiates it carries energy away from the source. The rate at which energy radiates from a source source is expressed in terms of power level PWL defined as

$$PWL = 10 \log W/W_{ref} \text{ db re } 10^{-13} \text{ watt} \tag{4.1}$$

where: W is the sound power radiated from the source and W_{ref} is a reference power unit conventionally taken as 10^{-13} watt.

The amount of power radiated per unit area normal to the direction of the wave propagation is the sound intensity expressed in db

$$IL = 10 \log I/I_{ref} \text{ db re } 10^{-16} \text{ watt/cm}^2 \tag{4.2}$$

For many purposes the pressure variations in a sound wave are of more direct concern than the intensity. In a free progressive wave the sound intensity and the rms sound pressure p in the wave are related by

$$I = \frac{p^2}{\rho a} \tag{4.3}$$

where ρ is the air density and a is the speed of sound.

The sound pressure level SPL is defined as

$$SPL = 20 \log \frac{P}{P_{ref}} \quad db \quad re \ 0.0002 \ \mu \ bar \tag{4.4}$$

The reference pressure is chosen to make the sound pressure level and the intensity level numerically equal for sinusoidal sound waves under conditions near room temperature and pressure.

Other pressure levels such as the peak pressure level and the peak to peak pressure level will be used subsequently in the following discussion. They will all employ the same reference pressure 0.0002 μ bar and so they will not be numerically equal to the intensity level of the sound wave.

As sound in air propagates away from a source it may undergo little change in amplitude and wave form or it may suffer a large decrease in amplitude and a radical change in its wave form depending upon the geometry of the source, the atmospheric attenuation characteristics, the sound frequency, and the amplitude of the sound wave.

4.1 Spherical Divergence

A sound source which is physically small compared with the wavelength of the sound acts as a point source and radiates uniformly in all directions. The sound intensity I at any distance r from such a source is therefore related to the total sound power, W, radiated by the equation

$$I = \frac{W}{4\pi r^2} \tag{4.5}$$

and the intensity level is

$$IL = PWL - 10 \log 4\pi r^2 \tag{4.6}$$

This same relation holds for any phy...cal spherical source which
radiates uniformly in all directions.

4.2 Directivity

A sound source which is comparable with or larger than a wavelength
does not radiate uniformly and is therefore said to be directive.
The directivity factor Q_θ for such a source is defined in any
direction θ as the ratio of the power radiated in that direction,
W_θ, to the average power, W_{avg}, radiated in all directions.

$$Q_\theta = W_\theta/W_{avg} \tag{4.7}$$

Near any real source it is generally not possible to specify a
directivity factor because the direction of energy flow is not
known. However, at large distances the energy flow is radial and
the sound intensity along any radius decreases inversely as the
square of the distance from the source. In this so-called far-field
the directivity factor in any direction can be determined from the
geometry of the source.

For the present purposes it is of importance to know the directivity
at a large distance along the axis of a plane piston radiator such
as a parabolic radar antenna or acoustic horn. The directivity for
such a radiator of diameter D is

$$Q = \left(\frac{\pi D}{\lambda} \right)^2 \tag{4.8}$$

This is the relation which is called antenna gain in radar
applications.[22]

The total beam width to the half power point for such a source at
large distances is given by[23/]

$$\theta = \frac{70\lambda}{D} \quad \text{in degrees} \tag{4.9}$$

In the near-field of a plane radiating surface the sound may radiate
nearly as a plane wave but edge effects cause small ripples in amp-
litude along the wave front and corresponding small undulations in
phase. From a practical standpoint, the near field of a plane
radiator acts like a plane wave field in most respects over an
area corresponding approximately to the area of the radiator. In
this near-field the average sound intensity remains substantially
constant along the axis. The division between the near-field and
the far-field is not sharp and indeed it does not have a unique
definition.

For the present purpose the end of the near-field will be defined
as the radius R_n for which the far-field equation gives a sound
intensity equal to the average intensity over the face of the
piston radiator.

The far-field intensity I_f at the end of the near-field R_n of a
circular piston of diameter D is given by

$$I_f = \frac{QW}{4\pi R_n^2}$$

the near-field intensity I_n is given by

$$I_n = \frac{4W}{\pi D^2}$$

Equating I_f and I_n and using Eq. (4.t. for Q gives

$$R_n = \frac{\pi D^2}{4\lambda} \tag{4.10}$$

Within the near-field the sound intensity exhibits a number of
maxima and minima determined by the source geometry and wavelength.
On the axis of a plane circular source the maxima all have a sub-
stantially constant value. This is illustrated in Fig. 4.1 for an
experimental source[24,25] 5 wavelengths in diameter. The average
sound intensity in the near-field is approximately 6 db below the
intensity peaks as indicated by the dashed horizontal line. The
calculated far-field sound intensity for this source is shown as
the dashed line having a slope of -6 db per distance doubled.
The intersection of these dashed curves determines the distance
R_n to the end of the near-field. At the end of the near-field
the measured sound intensity falls substantially 6 db per distance
doubled. Farther from the source atmospheric attenuation (dis-
cussed in Section 4.3) causes a more rapid decrease in the
intensity of the experimentally measured sound.

Directivity gain obviously increases with increase in the diameter
of the source relative to the radiated wavelength. Increase in
directivity has advantage from two major aspects:
(1) it decreases the main beam angle thus enabling a more
detailed searching pattern and (2) it permits the radiation
of increased intensities in the desired directions with a
given total radiated power.

For a radar signal, the amount of energy which can be transmitted by the main beam is limited only by the power capabilities of the source and by the degree to which side lobe radiation is suppressed. Thus the intensity of the main beam and therefore the total power incident upon a target which is small compared with the beam cross section can be increased directly as the cross section of the pencil beam is decreased, i.e., in proportion to the directivity.

For a sound wave, the advantages expected from an increase in directivity are modified by other factors not encountered with radar; these greatly affect and limit the extent to which a gain in performance is secured by increase in directivity. When a stationary and homogeneous medium exists around the source and when the sound waves do not carry much energy, the relations governing directivity are much the same as for radar waves. However, when the medium has a velocity as is the case of the real atmosphere with wind, the sound beam is swept down stream with the velocity of the wind. Although the wind may be slow, several feet per second compared with the speed of sound over 1000 ft/sec, the drift may be sufficient to throw a narrow beam seriously out of alignment with the radar beam and result in the need for introducing searching and tracking complications into the radar control system in order to follow the sound waves.

A much more stringent limitation upon the use of directivity arises from the nonlinear nature of air as a transmitting medium for sound. The air, in effect, will overload and will not

propagate sounds above a limiting intensity regardless of the
source power or the influence of directivity. This limitation
is more fully discussed in Section 4.4.

4.3 Atmospheric Absorption

A sound wave traveling through air undergoes a decrease in
intensity in addition to spherical divergence discussed above.
This additional decrease in intensity results from an absorption
of energy from the sound wave by heating the air or from dissipa-
tion of sound energy by scattering.

Absorption causes a decrease in intensity of the form

$$I = I_0\, e^{-mx} \tag{4.11}$$

where I and I_0 are intensities at x and $x = 0$ ft respectively

$\quad$ m is the attenuation coefficient in ft^{-1}

The attenuation constant a in db per ft is given by

$$a = 4.34\, m \quad \text{db/ft} \tag{4.12}$$

A normalized plot of attenuation in db for a plane wave is
presented in Figure 4.2. A similarly normalized plot for a
spherical wave is given in Fig. 4.3.

4.31 Classical Absorption

At audio frequencies minor losses occur as a result of classical
absorption including, 1) viscous losses, 2) heat conduction from
the warm regions of the pressure peaks to the cooler regions of

-56-

the pressure minima, 3) heat radiation between regions of different temperature and, 4) diffusion of molecules from the faster moving regions of the sound wave into slower moving regions.

All of these losses are insignificant in magnitude compared to molecular absorption at frequencies below 10 kc.[26]

4.32 Molecular Absorption

As sound vibrations pass through air containing small amounts of water vapor the molecules of water are set into vibration and absorb energy from the wave. The amount of absorption depends upon the sound frequency, the absolute humidity and the temperature in a complex way.[27]

1) At any chosen frequency f, a maximum absorption α_{max} occurs at a value of absolute humidity h_m which is independent of temperature

$$f = h_m^2 \qquad\qquad (4.13)$$

where f is in kc.

h_m is in gm/m^3
This relation is plotted in Fig. 4.4.

2) For any chosen frequency and humidity the ratio w of the molecular absorption α_{mol} to the maximum molecular absorption α_{max} is given theoretically in terms of the ratio of the absolute humidity h to h_m by the relation

$$w = \alpha_{mol}/\alpha_{max} = \frac{2}{(h/h_{max})^2 + (h_{max}/h)^2} \qquad (4.14)$$

the best experimental value for this relation is
plotted in Fig. 4.5. It should be noted that
the experimental values of absorption represented
by the curve in Fig. 4.5 are higher than those
predicted theoretically at high and at low values
of humidity but are in excellent agreement in the
region around h_m.

3) The value of α_{max} increases linearly with
   frequency as shown by the curves in Fig. 4.6
   for α_{max} vs. f, with temperature as a parameter.

4) The value of α_{mol} is obtained by multiplying
   the α_{max} obtained from Fig. 4.6 by the w
   obtained from Fig. 4.5.

Absolute humidity h can be determined conveniently from measured
relative humidity by use of Fig. 4.7.

4.33 Scattering

At low audible frequencies where molecular and classical absorption
both become very small, there is more attenuation of sound observed
experimentally in long range signaling than can be accounted for by
these processes. Some of this may result from a scattering of
sound by inhomogeneities in the atmosphere. Experimentally the
attenuation seems not to fall below approximately 0.001 db per
foot.

Such scattering has two effects of importance in relation to the
EMAC Probe. First, the scattering causes a withdrawal of energy
from the progressive sound beam and a resultant increase in atten-
uation by redirection of the sound energy. Second, it tends to
promote a broadening of the steep front of a shock wave by causing

-58-

slight variations in arrival time of wave contributions which have passed through slightly different paths of the inhomogeneous medium. Neither of these relations has received much theoretical or experimental study. The following discussion exposes the problem, presents plausible values related to some experimental observations, but indicates the need for experiemntal verification of results.

Inhomogeneities in the atmosphere cause variations in the speed of sound and thereby cause variations in the direction of propagation of the wavefront of any sound disturbances passing through these inhomogeneities. The effect of such variations in the wavefront is to cause a redirection of sound energy in a random manner from various points along any wavefront. It is possible to calculate the subsequent position of the wavefront and the shape of the shock wave by adding the contributions from all points on the wavefront during its entire path of travel from the source to the point in question substantially following the method of Section 3.14. Such an addition can be carried out only on a statistical basis because the inhomogeneities within the air are in themselves predictable only on a statistical basis. The net result is a reduction in the sound intensity at a distance by the direction of sound out of the direct path.

The inhomogeneities also tend to cause a broadening of the steep front of a shock wave but this broadening process is opposed by the finite amplitude distortion process discussed in Sec. 4.41. Whereas the broadening effect of turbulence is independent of the sound wave amplitude, the distortion effects tending to steepen the wave are directly proportional to the wave amplitude. Therefore, it is expected that turbulence will have little effect in broadening the wavefront if the wave has sufficient amplitude. However, when the amplitude drops below a level at which the

steepening and broadening effects are equal the wavefront will broaden rapidly. This amplitude is apparently dependent upon the magnitude of the turbulent velocities, the structure of the turbulence, the geometrical configuration of the wavefront, the initial form of the sound pulse, etc. A theoretical determination of shock wave structure as a func'.'on of all these variables would be very difficult and apparently has never been done. However, for use with the EMAC Probe, all that is required of a shock wave is that it be relatively thin compared with a radar wavelength, and that its level remain sufficiently high. A rough method for calculating level and shock front thickness is presented in Sec. 4.44 which gives the shock thickness produced by attenuation alone. Since these results are in good agreement with experimental measures of shock structure, it is fairly safe to assume that turbulence broadening is not the most important cause of shock thickening.

4.34 Precipitation and Fog

Suspended particles in the atmosphere produce acoustic losses by two mechanisms. First, there will be viscous dissipation and heat conduction near the suspended particles, and second, there are relaxation losses because the time lag between evaporation and condensation on the particles as the local pressure and temperature changes when the wave passes.

Experimental studies of sound attenuation in atmospheric precipitation and fog[26,28] show that these losses can be neglected. Attenuation in fog changes slowly with frequency and is below .3 db/1000 ft for frequencies less than 2 kc even in heavy fog. Absorption by water droplets exceeds molecular absorption at low frequencies (below about 300 cps) when both are small but at higher frequencies, absorption by droplets can be neglected compared with molecular absorption.

4.4 Nonlinear Sound Propagation

Sound waves of any shape or harmonic content tend to deform
toward the sawtoothed shape which is the stable wave form for
high amplitude sound. The leading edge of the stable wave is
a shock front whose thickness depends upon the amplitude of
the wave and the attenuation characteristics of the medium but
not upon the frequency of the fundamental component of the wave.

4.41 Wave Distortion

Finite amplitude distortion of this sort is important on two
accounts. First, energy is transferred from the fundamental
component into the higher harmonics; since these are more
rapidly attenuated than the fundamental, an excess attenuation
of the wave results which drains energy from the sound beam in
direct proportion to the magnitude of the pressure discontinuity
and the number of discontinuities per unit distance along the
sound beam. Second, the distortion of the sound wave creates
a sharp pressure discontinuity at its leading edge. This dis-
continuity provides the optimum condition for the reflection
of radar waves from a pressure variation of a given pressure
amplitude. This last fact is of utmost importance in the per-
formance of the sound wave as a reflector in the electromagnetic
acoustic probe.

There are two causes for the change in shape. The first relates
to the fact that sound consists of longitudinal vibrations and
as such the alternating particle velocity of the medium is
parallel to the direction of wave propagation. In such a wave
the maximum positive particle velocity corresponds in time and
space to the maximum excess pressure. The maximum negative

particle velocity corresponds to the minimum pressure of the
wave. Therefore, the pressure peaks and troughs of an acoustic
wave travel respectively with the velocity of sound plus and
minus the particle velocity. The second cause of finite ampli-
tude distortion is that an acoustic wave is adiabatic, i.e.,
the local temperature of the air increases as the pressure in-
creases. Since the speed of sound increases as the square root
of absolute temperature, the local wave velocity is greater
than average at pressure maxima and less at the minima. In a
normal gas the results of these two factors are additive causing
pressure maxima to overtake pressure minima and create a steep
pressure front at the leading edge of an acoustic wave.

As the wave front steepens, the energy of the wave is converted
from the fundamental and low harmonics into higher harmonic
components. The steepness of the wave front is limited by the
balance between the rate of transfer of energy into the higher
harmonics and the loss of energy from the higher harmonics by
means of attenuation which converts acoustic energy into heating
of the air through which the wave passes. The mechanism of the
absorption is unimportant. The magnitude of the absorption as
a function of frequency will determine the ultimate sharpness
of the shock front which is necessary to create the balance of
energy flow into the harmonics and from the harmonics into heat.
The lower the rate of absorption from each harmonic, the closer
the wavefront will approach a theoretical discontinuity and the
closer the amplitude of each harmonic will approach the theo-
retical absolute limit of $1/n$ compared with the amplitude of
the fundamental.

This action is shown dramatically in Fig. 4.8 by an assemblage of oscilloscope wave traces depicting the pressure as experienced by a microphone located in an intense 14 kc sound wave at several distances from a plane piston circular source for four sound output levels.

The traces in Fig. 4.8 have been adjusted all to the same height by increasing the gain in the oscilloscope so that the wave shapes could be compared directly. The widening of the trace at 200 cm for the lowest sound level is caused by circuit noise which becomes evident at the high gain setting since the display system uses a broadband circuit with no filtering.

It can be seen that at the lowest sound level (140 db rms averaged over the face of the source) the wave progresses with little observable distortion throughout the range of observation, 200 cm (approximately 90 wavelengths). At the highest level (155 db rms) although the wave is equally pure at the source, it distorts rapidly and becomes sawtoothed in a few wavelengths.

At the 155 db level the wave becomes noticeably sawtoothed at a distance of approximately 6 wavelengths whereas at 150 db the same amount of distortion requires approximately 20 wavelengths.

It is found theoretically and experimentally that, for geometrically similar sound fields, the amount of distortion obtained for any given sound intensity, is a function only of the distance from the source measured in wavelengths of the fundamental frequency of the sound radiated.

These considerations indicate that in order to obtain a maximum range with the EMAC system it is necessary to utilize a low frequency signal so as to reduce ordinary atmospheric attenuation and finite amplitude attenuation to an acceptable value for the chosen range. It is then necessary to increase the source power to the point where the acoustic wave will reach and maintain a sawtooth wave form in order to take advantage of the high reflectivity of the sharp pressure discontinuity at the leading edge of a finite amplitude wave. Mathematical relations governing the frequency and source power are discussed in the following section.

4.42 Finite Amplitude Limits

A high amplitude plane wave of stable form (i.e., sawtooth shape) will attenuate[29] in amplitude according to the relation

$$\frac{du}{u} = -\frac{(\gamma+1)\ udx}{a\lambda} \qquad (4.15)$$

where: u is the particle velocity amplitude

  x is the distance

  γ is the ratio of specific heats

  a is the velocity of sound

  λ is the sound wavelength

$$\frac{dp}{p} = -\frac{(\gamma+1)\ pdx}{\gamma\lambda P_o} \qquad (4.16)$$

where: P_o is atmospheric pressure

  p is excess sound pressure amplitude

For sound fields which are not plane the change in sound amplitude involves the divergence of the wave. A general treatment of non-plane fields has been considered by Rudnick in relation to the transmission of sound in horns of varying cross-section. If we consider a horn in which the area, S, of an equiphase surface of the wave depends upon the distance of propagation of the wave, then the area S at any distance x is given by:

$$Sg^2(x) = S_o \qquad (4.17)$$

where $S_r = S_o$ at $x = x_o$ and thus $g(x_o) = 1$.

Combining the relation for divergence and the attenuation from Equation (4.15)

$$\frac{du}{u} = \frac{dg}{g} - (\gamma+1)\frac{udx}{a\lambda} \qquad (4.18)$$

or from Equation (4.16)

$$\frac{dp}{p} = \frac{dg}{g} - \frac{(\gamma+1)pa\lambda}{\gamma\lambda P_o} \qquad (4.19)$$

Continuing now only with the equation for pressure and letting $p = vg$ where v is a new variable Eq (4.19) reduces to

$$\frac{dv}{v^2} = - \frac{(\gamma+1)gdx}{\gamma\lambda P_o} \qquad (4.20)$$

which can be integrated to give,

$$p = \frac{p_o \, g(x)}{1 + \frac{\gamma+1}{\gamma \lambda P_o} \, p_o \int_{x_o}^{x} g(x) dx} \qquad (4.21)$$

where p is the excess pressure amplitude in a sound wave at distance x from the source and p_o is the excess pressure amplitude at $x = x_o$.

From this equation it can be seen that there is a limit to the value of p at any distance x which cannot be exceeded regardless of the amplitude of p_o at the source and this value we shall call the limiting pressure p_ℓ

$$p_\ell = \frac{\gamma \lambda \, P_o \, g(x)}{(\gamma+1) \int_{x_o}^{x} g(x) dx} \qquad (4.22)$$

There are two cases of interest here for which the evaluation of p_ℓ is instructive. The first case is that of a plane wave. Although a truly plane wave cannot be generated and used in open space, its performance is descriptive of the process of finite amplitude limitation of the pressure in a sound wave as it progresses away from the source. The second case is that of a spherical wave. Here the limiting relation will be seen to involve an additional term modifying the limit for a plane wave in such a way that the two limits can be handled separately to advantage in real applications.

For a plane wave $g(x) = 1$

$$p_\ell = \frac{\gamma \lambda \, P_o}{(\gamma+1) \, (x-x_o)} \tag{4.23}$$

which indicates that the limiting pressure may be unlimited at
the source where $x = x_o$ but at any other distance this pressure
must decrease as $\frac{1}{(x - x_o)/\lambda}$ i.e., inversely as the distance
measured in wavelengths.

The limiting pressure is proportional to the atmospheric pressure
and for a normal atmosphere of 10^6 μbar (1 μbar $= 1$ dyne/cm^2) the
limiting pressure is

$$p_\ell = \frac{1.4 \times 10^6}{2.4} \left[\frac{\lambda}{(x - x_o)} \right] \tag{4.24}$$

$$p_\ell = .58 \times 10^6 \, \frac{1}{n} \tag{4.25}$$

where n is the number of wavelengths from the source. This
relation is indicated as the heavy solid line in Fig.(4.9) where
the reciprocal of p_ℓ is plotted against n.

When the excess pressure in the wave is not infinite at the source
but has some initial value p_2, the pressure at a distance n wave-
length from the source is given by

$$p = \frac{n_2 \, p_\ell}{p_2 + p_\ell} \tag{4.26}$$

which is seen to be represented in Fig. 4.9 by lines parallel
to that for an infinite shock at $x = x_o$ but intersecting the
$n = 0$ axis at values of $\frac{1}{p_2}$ corresponding to the sound pressure
radiated at the source.

Since this analysis assumes that the waves considered have reached,
or are generated with the stable sawtooth form, they remain saw-
toothed as they propagate.

Before proceeding to the spherical wave case it is helpful to
replot the results shown in Fig. 4.9 in a more conventional form
as shown in Fig. 4.10 where the sound pressure level is ex-
pressed in decibels against the log of the distance from the source
expressed in wavelengths. In this representation the limiting
pressure for an infinite shock at $n = 0$ is a straight line having
a negative slope of 6 db/distance doubled and passing through 189.3
db at a distance of one wavelength from the source corresponding
to Eq. (4.25). The curve representing the variation of pressure
level for a wave having a preassigned amplitude at the source will
be a curved line starting horizontally at the left with a value
approaching the assigned value at the source and approaching the
limiting pressure asymptotically toward the right.

It is interesting to note that the slope of the limiting pressure
curve as plotted in Fig. 4.10 for a plane wave is the same as
that for the sound pressure in a spherically diverging wave of
low amplitude. In the latter case the pressure amplitude falls off
as $1/r$ because of divergence but that process involves no loss of
energy. We may therefore expect a steeper slope when finite ampli-
tude losses are considered in a spherical field.

To determine the effect of finite amplitude limitation upon a spherical wave, return to Eq. (4.22); substitute r for x and $1/r$ for $g(x)$ representing the spherical divergence and then integrate.

This gives

$$p_\ell = \frac{\gamma\, P_0}{\gamma + 1} \quad \frac{1}{\frac{r}{\lambda} \log_e \frac{r}{r_0}} \tag{4.27}$$

where r is the distance from the center of divergence, r_0 is the distance from the center to the surface of the sound source. This equation, obtained by Laird[30] also using a somewhat different analysis is similar to that for a plane wave, but has the extra factor $\log_e r/r_0$ in the denominator. This factor becomes unity when $r/r_0 = e$ (i.e. $r/r_0 = 2.7$). A plot of this factor in decibels is given in Fig. (4.11). A plot of Eqs. (4.24) and (4.27) in Fig. (4.12) compares the limiting pressures for a plane and a spherical wave. The straight line is the limiting pressure for a plane wave starting at $r = 0$ and the curved line is the limiting pressure for a spherical wave having its center at $r = 0$ but starting from a spherical source whose radius is one wavelength. It is apparent that (as in Fig. 4.10) the amplitude of the plane wave is unlimited at $\frac{r}{\lambda} = 0$. The spherical wave is unlimited at the surface of the spherical source, $r = r_0$. The spherical wave and the plane wave have the same value of limiting pressure when the spherical wave has progressed to a radius 2.7 times the radius of the source.

The two curves of Fig. (4.12) are useful in combination because a simple translation of the spherical wave limit along the plane wave limit can be made to account for an arbitrary change in size

of the spherical source. For example, if the source radius is
2 λ instead of λ as assumed in Fig. 4.12 the spherical wave
limit may be translated to the right diagonally along the curve
for the plane wave limit until the source position corresponds
to 2 λ instead of λ. It will be seen that the two lines will
then cross at 5.4 wavelengths instead of 2.7

4.43 Applications to Experiment

As was noted in Section 4.2, real sources can seldom be considered
as strictly plane wave generators or as spherical wave generators.
A plane piston moving in a rigid baffle approximates a plane
source near its surface and a spherical source at large distances.
The dividing distance R_n between the near-field and far-field for
acoustic purposes was established in Section 4.2 as

$$R_n = \frac{\pi D^2}{4\lambda} \tag{4.10}$$

where D is the diameter of the piston source.

In applying the finite amplitude limits to real sources we may,
with good approximation, apply the plane wave limit to the
near-field and the spherical wave limit to the far-field by
matching the two limits at the distance R_n.

Experimental data taken with the same 14.5 kc piston source
described earlier in relation to Figs. 4.1 and 4.8 are compared
in Fig. 4.13 with the theoretical limits calculated for that
source. The upper four experimental curves in Fig. 4.13 corres-
pond to the four sound intensity levels shown in Fig. 4.8. There

is a 0 db difference because Fig. 4.8 refers to average intensity level in the near-field which is 6 db below the peak intensity level. It is seen at once that the sound pressure level measured 'the far-field behaves as it should for a spherically diverging field, i.e., a 6 db decrease per distance doubled for the lower sound levels recorded. However, when the sound level is raised at the source it is seen that the sound level in the farfield increases only so as to approach but not exceed the limiting pressure levels. At 100 wavelengths the sound at the highest level of operation is more than 8 db below the value expected if the finite amplitude limit were disregarded. Substantially no increase in level at this distance could be obtained by increasing the source power.

Even if the real source could be replaced by a theoretical plane source the plane wave limit would still limit the increase in sound level at large distances. The actual sound pressure would be a few db greater than for the spherical field but the total power loss would be very much greater.

It should be noted that the data shown in Fig. 4.13 apply to the fundamental component of the 14.5 kc signal. All harmonics were filtered out. The finite amplitude limits have therefore been drawn to indicate the rms level of the fundamental in a sawtooth wave having the peak amplitude indicated by the limits in Fig. 4.12. The relation between the two is

$$p_{rms} \text{ fundamental} = \frac{\sqrt{2}}{\pi} \, p_\ell \qquad (4.28)$$

$$SPL = 20 \log p_\ell - 7 \text{ db} \qquad (4.29)$$

-71-

The finite amplitude limits may be applied in the same way to the experiments of Midwest Research Institute. There, the frequency of 22 kc reflected from an 18" parabolic mirror gives an effective near-field distance of 34 ft.

First, however, we shall consider only the effects of molecular absorption as indicated in Fig. 4.14. If the total radiated power of 30 watts is assumed to be uniformly distributed over the beam area equal to the area of the reflector, the average SPL in the near-field will be 144 db as indicated by the horizontal line. The far-field SPL (neglecting absorption) will be represented by a line having a slope of 6 db passing through the point 144 db at 34 ft. Molecular absorption is accounted for by use of the curve 4.3 and setting 1 db absorption at a distance of 5 ft since the attenuation of the 22 kc signal is approximately 0.2 db per foot. The attenuated level in the far-field is represented by the light dashed curve. The attenuation expected in the near-field can be obtained similarly by use of curve 4.2. Blending these two attenuated curves gives the SPL expected from the source shown as the heavy solid curve. The one measured value of 140 db at 10 ft falls 2 db below the curve so constructed.

We now consider the effects of the finite amplitude limits on the MRI experiment. Figure 4.15 shows the near-field SPL as before, a horizontal line at 144 db. The wave is here assumed to be sinusoidal as generated. The plane wave limit for the near-field is presented as the rms limit which would be measured by a sound level meter for a sawtooth wave. It is related to p_ℓ

$$p_{\ell_{rms}} = \frac{1}{\sqrt{3}} p_\ell \text{ for a sawtooth wave.}$$

The $p_{\ell_{rms}}$ for the spherical wave limit for the far-field is matched at 34 feet. The expected p_{rms} for the sound wave is blended from its initial level to approach first the near-field limit then the far-field limit.

The experimentally measured sound pressure of 140 db at 10 ft is in almost exact agreement with the $p_{\ell_{rms}}$ and about 1 db higher than the expected value obtained by curve blending. It is seen that the p_{rms} expected at 93 ft is 105 db which is some 12 db lower than that which would be expected by considerling molecular absorption alone. This difference while large has even more importance when we consider means for extending the range of the EMAC Probe. By considering molecular absorption only, we might expect to be able to increase the sound level at any distance by increasing the source output. Figure 4.15 shows that increase in source power would make no increase in the sound level at distances beyond 10 feet.

Further consideration of the wave form of the sound indicates that harmonic content becomes significant beyond a distance of about 2 ft and energy is transferred from the fundamental to higher harmonics. The decrease in the level of the fundamental is indicated by the heavy dashed curve. It approaches a value

$$p_{rms} \text{ fundamental} = \frac{\sqrt{6}}{\pi} \, p_{rms} \text{ sawtooth}$$

which is 2.2 db lower than the level of the sawtooth.

When the sawtooth wave progresses to the distance at which the rate of decrease in level due to the finite amplitude limit is less than the rate of atmospheric absorption (primarily molecular)

-73-

the sound level will drop below the finite amplitude limit. The higher harmonics raise the level of the sawtooth wave above the fundamental. Therefore, we must apply a higher attenuation to the sawtooth and the attenuation of the fundamental to the fundamental itself. By this process it is seen that the sawtooth level is expected to approach the fundamental and the wave shape reverts to sinusoidal. This action is shown to take place beyond 60 ft for the 22 kc signal in Fig. 4.15.

From these discussions it is clear that no system using high frequency sound can produce useful signals much beyond two or three-hundred feet even with unlimited acoustic power at the source.

From these experimental results the serious nature of the finite amplitude limit is clearly apparent. In order to attain distances of several thousand feet it will be necessary to reduce the radiated sound frequency. Reducing the frequency will raise the finite amplitude limit in direct proportion to the increase in wavelength. Lowering the frequency will also decrease the rate of atmospheric absorption but this appears to be a secondary consideration.

In reducing the frequency we are faced with the fact that the increase in wavelength will affect the directivity of any chosen antenna and thereby affect the amount of power required at the source to create a given sound intensity on the axis of the radiator.

For a first cut we may look at a frequency near 1000 cps since this frequency will have a wavelength still short enough to serve as an effective reflector for useful radar wavelengths. Let us

choose the frequency 1140 since this will . $\approx \lambda = 1$ ft. We will
then choose arbitrarily a 10 ft diameter disk as a source. Then
the near-field R_n extends to 79 ft. Figure 4.10 shows that the
finite amplitude limit permits a level of 100 db in excess of
3000 ft. Applying the atmospheric attenuation of between .01 and
.001 db per ft indicates the sound wave amplitude would fall below
the finite amplitude limit at some distance between 300 and 3000 ft
as indicated by the shaded area. So it is obvious that a 1140 cps
signal can be maintained above 100 db to a distance of 1500 to
3000 ft.

If we assume the wave should become sawtoothed at least by a
distance of 100 ft then the average sound intensity in the near-
field should be approximately 145 db. This would require a sound
power level of $145 + 10 \log \frac{\pi D^2}{4} = 164$ db re 10^{-13} watt or approx-
imately 2.5 kw of acoustic power.

Any increase in acoustic power would not increase the range but
would serve only to cause the shockwave to be developed closer
to the source and cause more objectionable disturbance to equip-
ment and personnel.

This intensity would be extremely objectionable to personnel even
outside the main beam and even for relatively short bursts of the
acoustic signal.

Such a signal in short burst would retain the problem of matching
the radar and acoustic wavelength to give coherent reflections
from the several waves of the pulse.

It now appears that any acoustic signal involving a train of repeated waves which are commensurate with the longest usable radar wavelength will not be able to be projected much over 1000 ft and therefore will not serve for probing the atmospher at any useful range. We now therefore direct attention to the use of a single shock pulse as the only practical reflecting acoustic surface for long ranges.

4.44 Shock Wave Phenomena

A sound impulse may be considered to be made up of an infinite series of sine waves. If such an impulse is radiated from a plane piston source it will have a complicated directivity pattern. As an approximation we may consider this directivity pattern to be made up of the directivity patterns of all of the harmonic components of the impulse.

For the frequency components having wavelengths which are long compared to the diameter of the source the directivity pattern is essentially spherical. Only for wavelengths which are comparable with or shorter than the circumference of the source is there any practical gain in intensity along the axis due to directivity. As we have already found waves which are short compared with the diameter of the source (i.e., 1 ft long) will not have sufficient range. Therefore, let us consider generating a single sinusoidal half-wave pulse whose wavelength is equal to the diameter of the source, i.e., 10 ft or 114 cps for a 10 ft dish.

For this frequency and dish size the near-field extends to 8 ft and the plane wave finite amplitude limit (rms of a sawtooth) passes through 164.7 db at 100 ft. The plane wave and spherical

-76-

wave limit are assumed equal at 8 ft as shown in Fig. 4.17. In
order for the wave to be substantially sawtoothed at 100 ft the
average intensity in the near-field should be of the order of
175 db. A single pulse may tend to sharpen on its trailing edge
also thereby producing a double shock or N-wave which is not de-
sirable for the EMAC Probe system. To avoid such sharpening of
the trailing edge the intensity of the wave may be dropped approx-
imately 10 db; the wave would not be expected to sharpen signifi-
cantly for over 1000 ft. However, if the pulse generated contained
a fundamental of this lower magnitude and also contained higher
harmonics so phased that the wave had a steep leading edge and
gradual trailing edge as generated, the leading edge would sharpen
to a shock rapidly and the trailing edge would be expected never
to sharpen.

The higher harmonics included in the pulse for sharpening the
leading edge would have higher directivity than the fundamental
and would remain close to the center of the beam. Thus, these
harmonics, although more objectionable to personnel, would be
confined to the center of the acoustic beam.

The finite amplitude limits near the source would be those
applicable to the higher harmonics but at large distance would
be that applicable to the fundamental. A gradual transition
should occur as the wave progresses. This transition has not
been studied in detail and appears so complex that it should be
submitted to experimental test.

From these considerations it appears feasible to create a wave
which will become a shock wave within a few hundred feet from
the source and remain a sharp shock for a distance of the order
of 10,000 ft.

The thickness of a shock front theoretically should depend only
r   the amplitude of the overpressure not upon the frequency of
the fundamental. Calculations of the shock front thickness[31]
using the equations of motion for a steady state non-isentropic
transition across a shock indicate that it should be of the
order of 3 cm for a shock wave having a pressure amplitude of
the order of 100 db. This departs widely from the experimental
observations of shock fronts in air. Theoretical considerations
including the effects of molecular absorption have indicated
that the shock front should be about 15 cm thick at levels between
120 and 100 db. This is indicated indirectly by the curves of
Fig. 4.16 where the 1140 cps repeated shock wave begins to drop
below the finite amplitude pressure limit at between 120 and
100 db. In this region the shock front has grown to 1/2 wave-
length of the 1140 cps wave or approximately 15 cm. Experimental
evidence with N-waves of sonic booms bears out this conclusion.
Measurements[32] of several sonic booms are summarized in Table 4.1.

Boom No.	Amplitude of incident waves lb/sq ft	db	Rise time of steepest section	Corresponding Thickness
1	.5	122	.6 ms	.7'
2	.42	120	.9 ms	1.0'
3	apparently a ground wave; no shock front			
4	.75	126	.7 ms	.8'
5	.24	116	.5 ms	.6'
6	apparently a ground wave; no shock front			
7	.31	118	.6 ms	.7'
8	.42	120	.5 ms	.6'

Sonic booms 3 and 6 in Table 4.1 appeared to arrive in a nearly horizontal direction since there was no visible separation between the incident and reflected wave. The rise time was very long, several milliseconds, and included many shocklike ripples which are assumed to be due to the successive additions of components of the wave retarded by obstacles and inhomogeneities near the ground. Even for these waves the initiation of the rise was sharp.

A typical N-wave signature (Boom #7 from Table 4.1) is displayed as oscilloscope traces at two sweep rates differing by a factor of 10 in the photograph of Fig. 4.18. The leading edges of the incident and the ground reflected waves are clearly separated. For the incident wave the wavefront thickness is about 0.7 ft. It should be noted however, that in the fast trace the initiation of the pressure pulse forms a noticebly sharper corner than does the crest of the pressure pulse. The observed sharpness in Fig. 4.18 appears to be limited by the passband of the recording system which rolls off above 2,500 cps. Thus, the actual sharpness cannot be assessed from this figure. It seems likely, however, that the index variation accompanying such a sound shock most closely approximates an index variation with one sharp corner and one round corner.

For the purpose of radar reflection, the presence of one sharp corner significantly increases the reflection when the index of refraction variation occurs over a distance in excess of a radar wavelength as indicated in Fig. 2.3. Thus it is reasonable to look for a useful radar reflection from an acoustic shock wave even after the wave front has broadened beyond a wavelength of the radar wave. Again, this premise needs experimental verification.
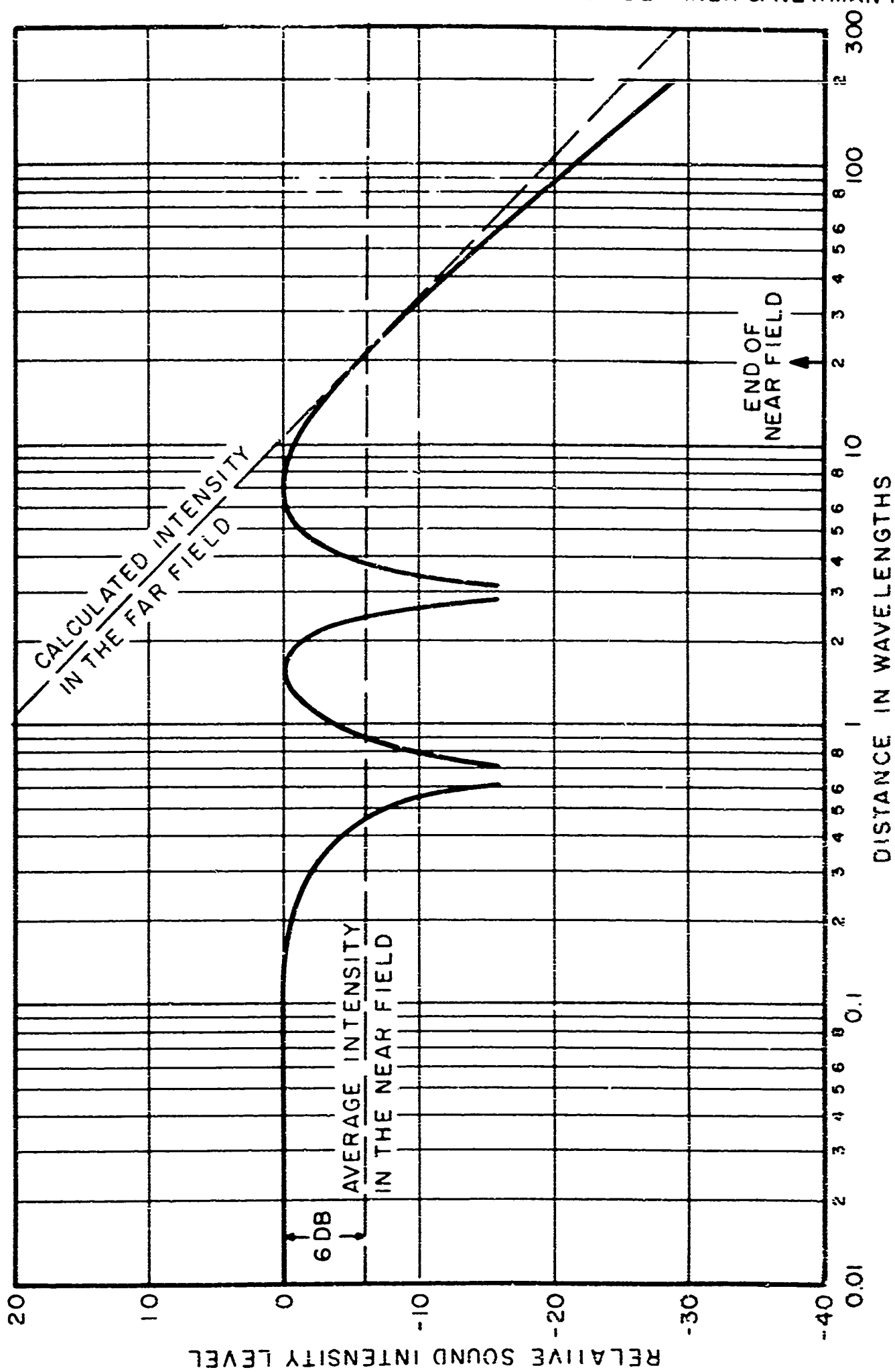
-79-

FIG. 4.1 EXPERIMENTAL VALUE OF SOUND PRESSURE LEVEL ON AXIS OF
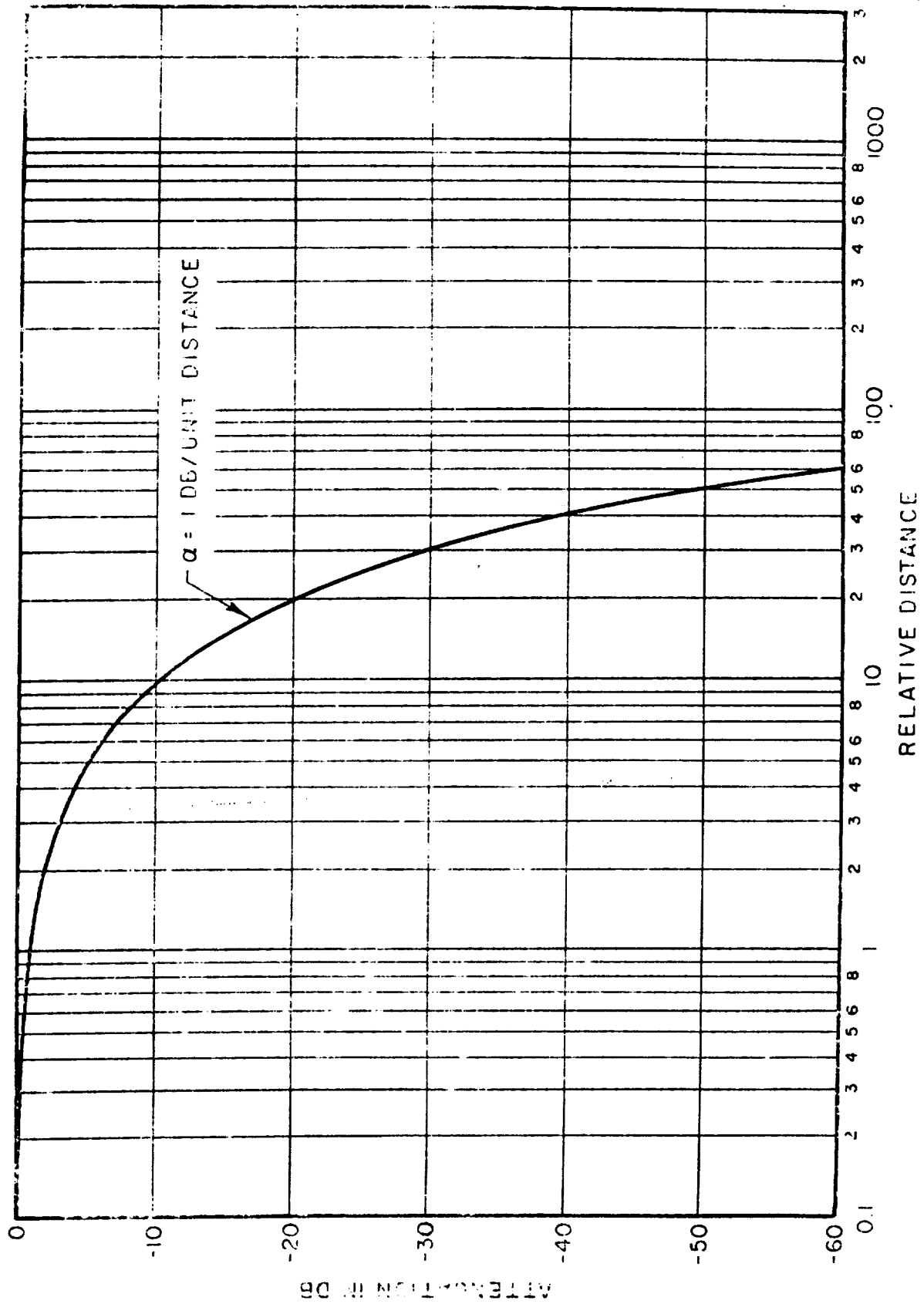PLANE PISTON SOURCE 5λ DIAMETER

DISTANCE IN WAVELENGTHS

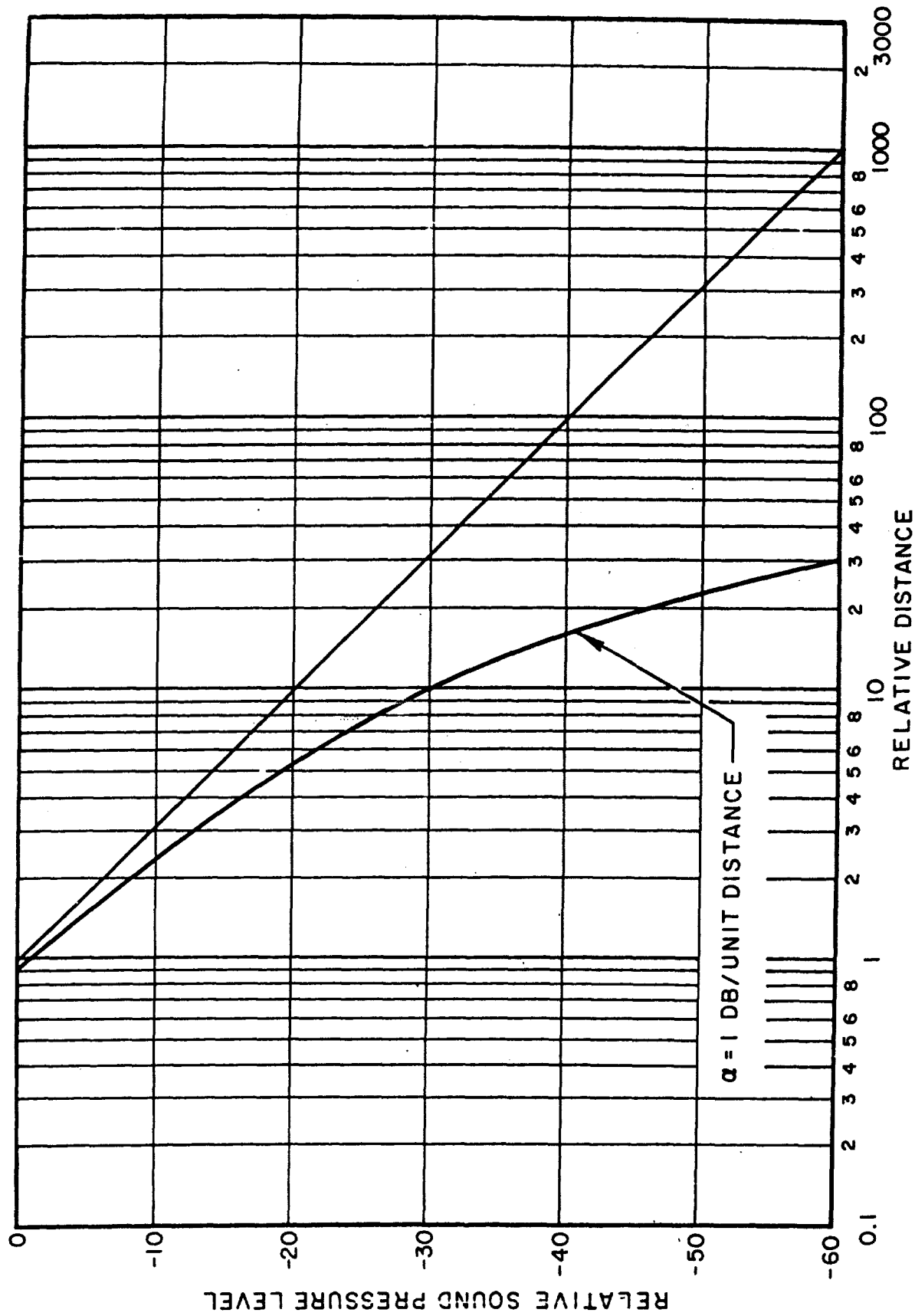RELATIVE SOUND INTENSITY LEVEL

CALCULATED INTENSITY IN THE FAR FIELD

AVERAGE INTENSITY IN THE NEAR FIELD

END OF NEAR FIELD

6 DB

$\alpha = 1$ DB/UNIT DISTANCE

RELATIVE DISTANCE

ATTENUATION IN DB

FIG. 42 . ATTENUATION FOR PLANE SOUND WAVE

FIG. 4.3 DIVERGENCE AND ATTENUATION FOR A SPHERICAL SOUND WAVE

RELATIVE DISTANCE

RELATIVE SOUND PRESSURE LEVEL
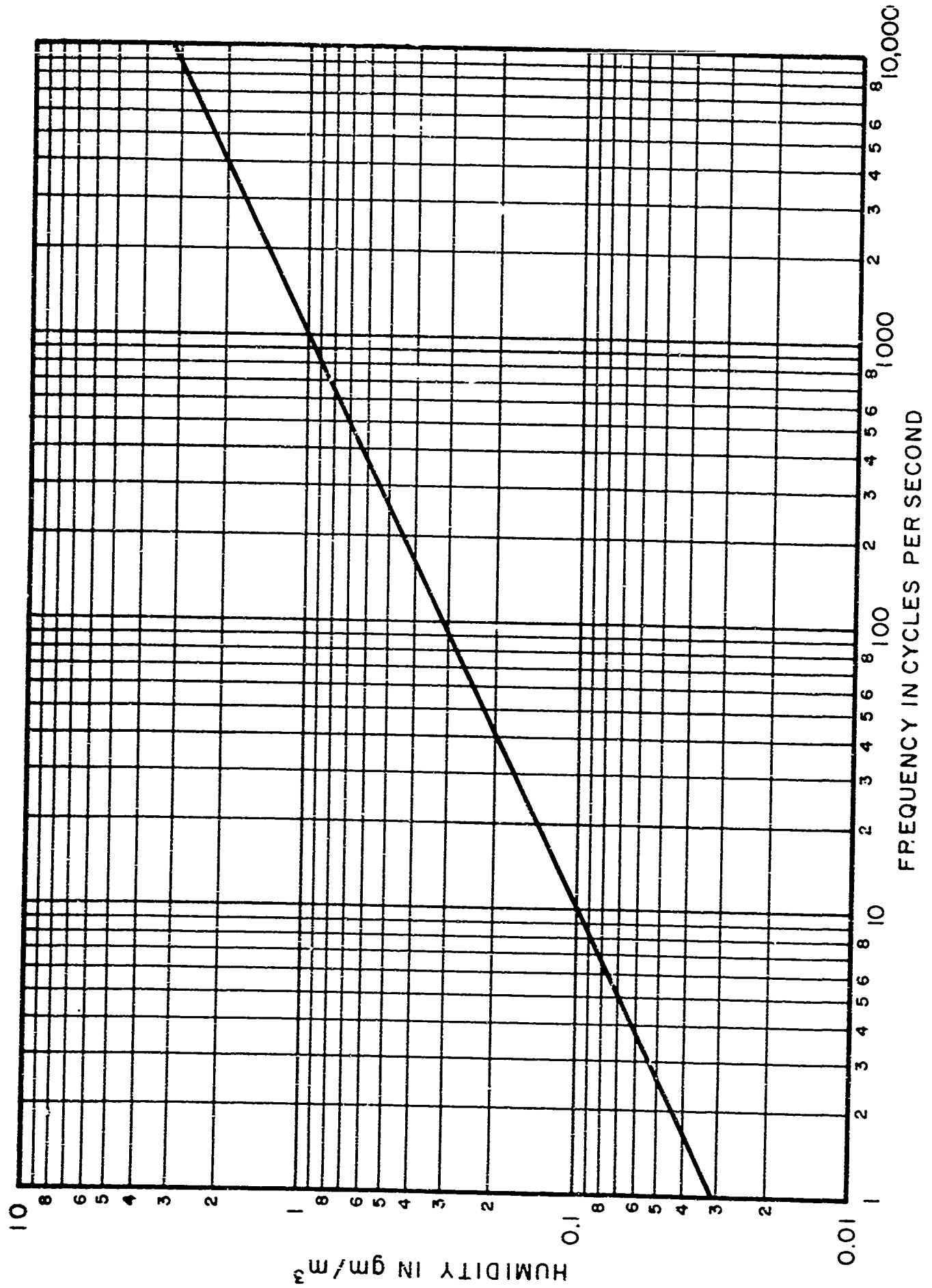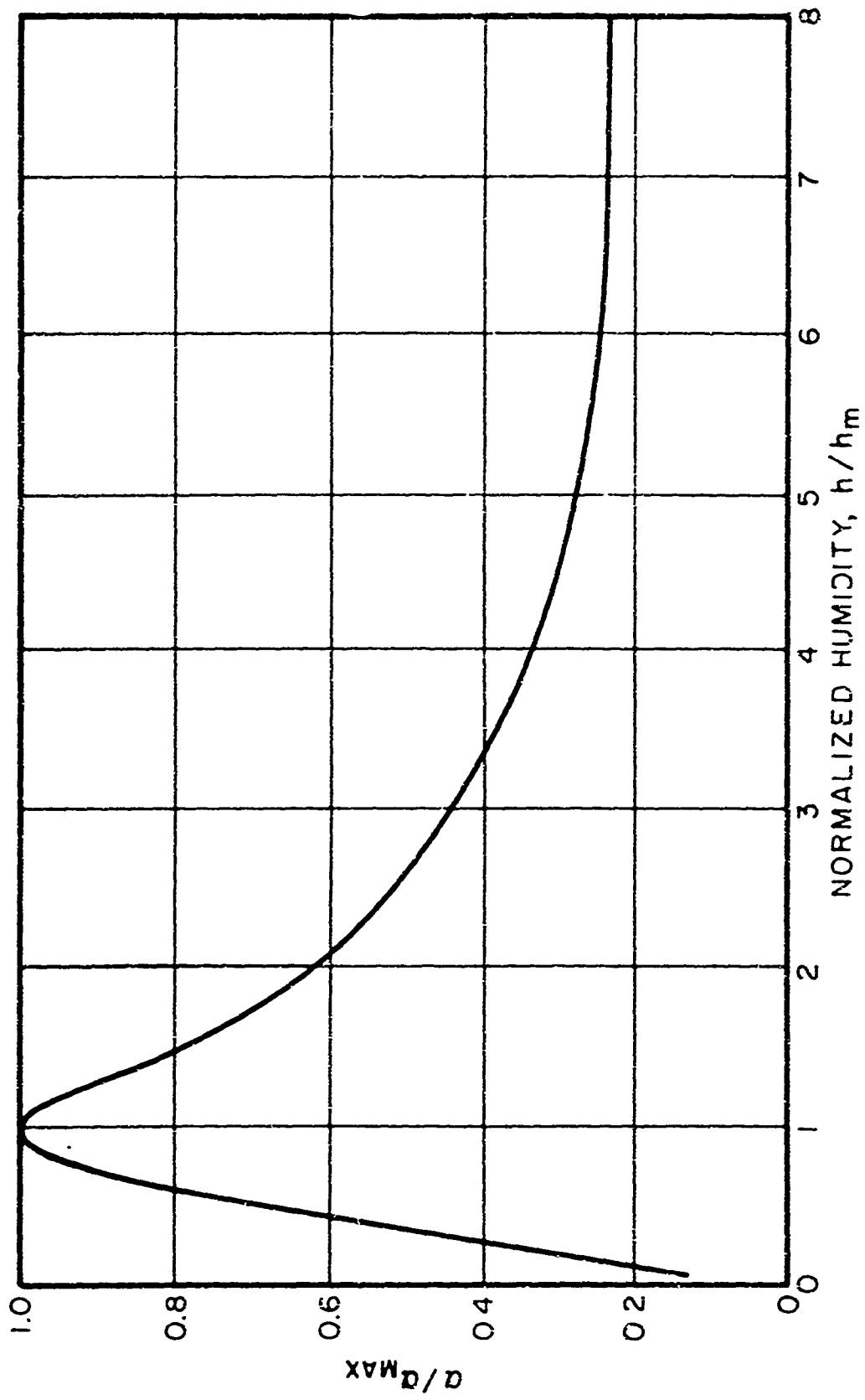
α = 1 DB/UNIT DISTANCE

FIG. 4.4   ABSOLUTE HUMIDITY FOR MAXIMUM MOLECULAR ABSORPTION
VS FREQUENCY

VS FREQUENCY

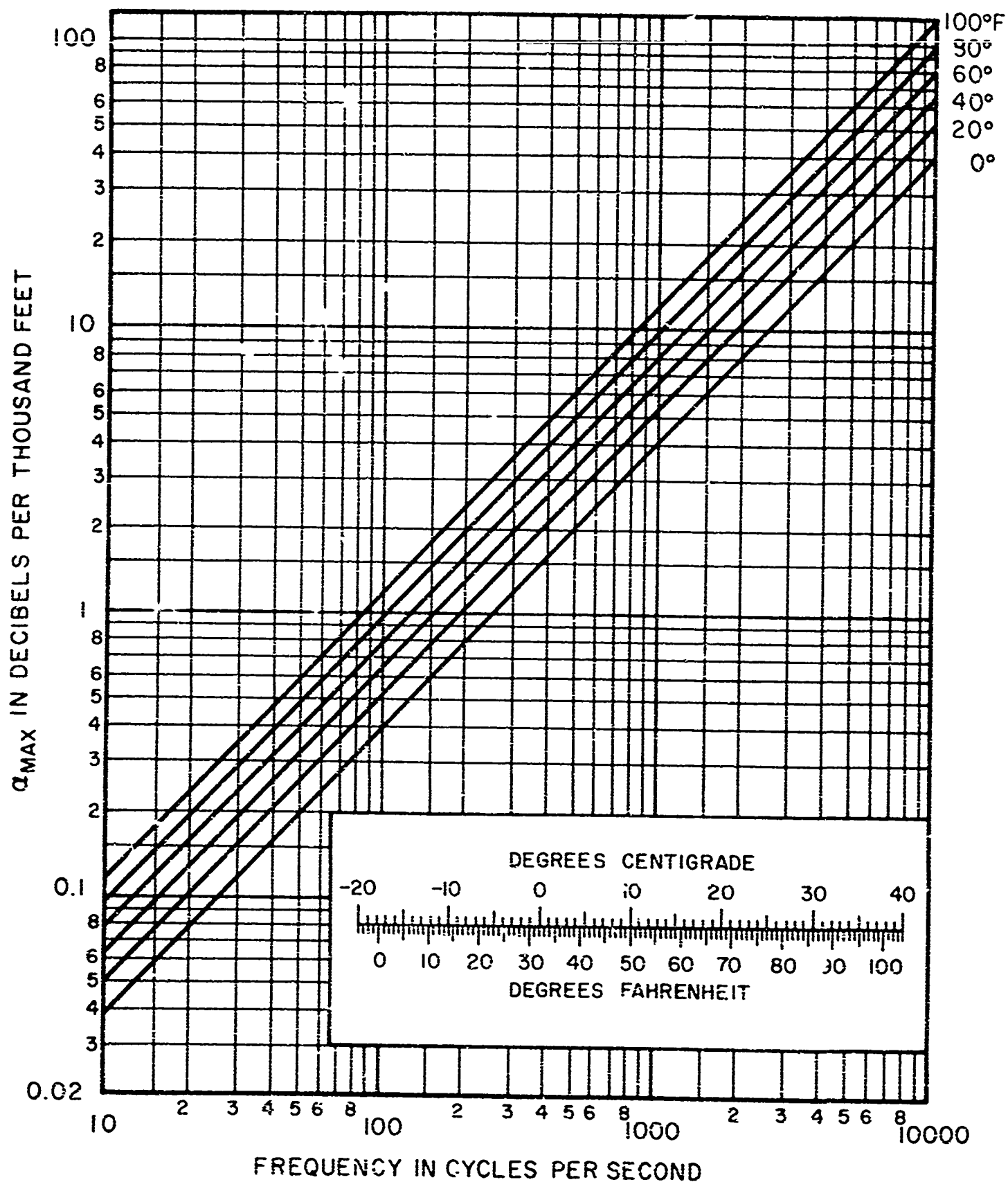FIG. 4.5   PLOT OF α/α_{MAX} VS. h/h_m (AFTER HARRIS)[33]

FIG.4.6   EXTENDED PLOT OF MAXIMUM MOLECULAR
ABSORPTION COEFFICIENT α_{MAX} VERSUS
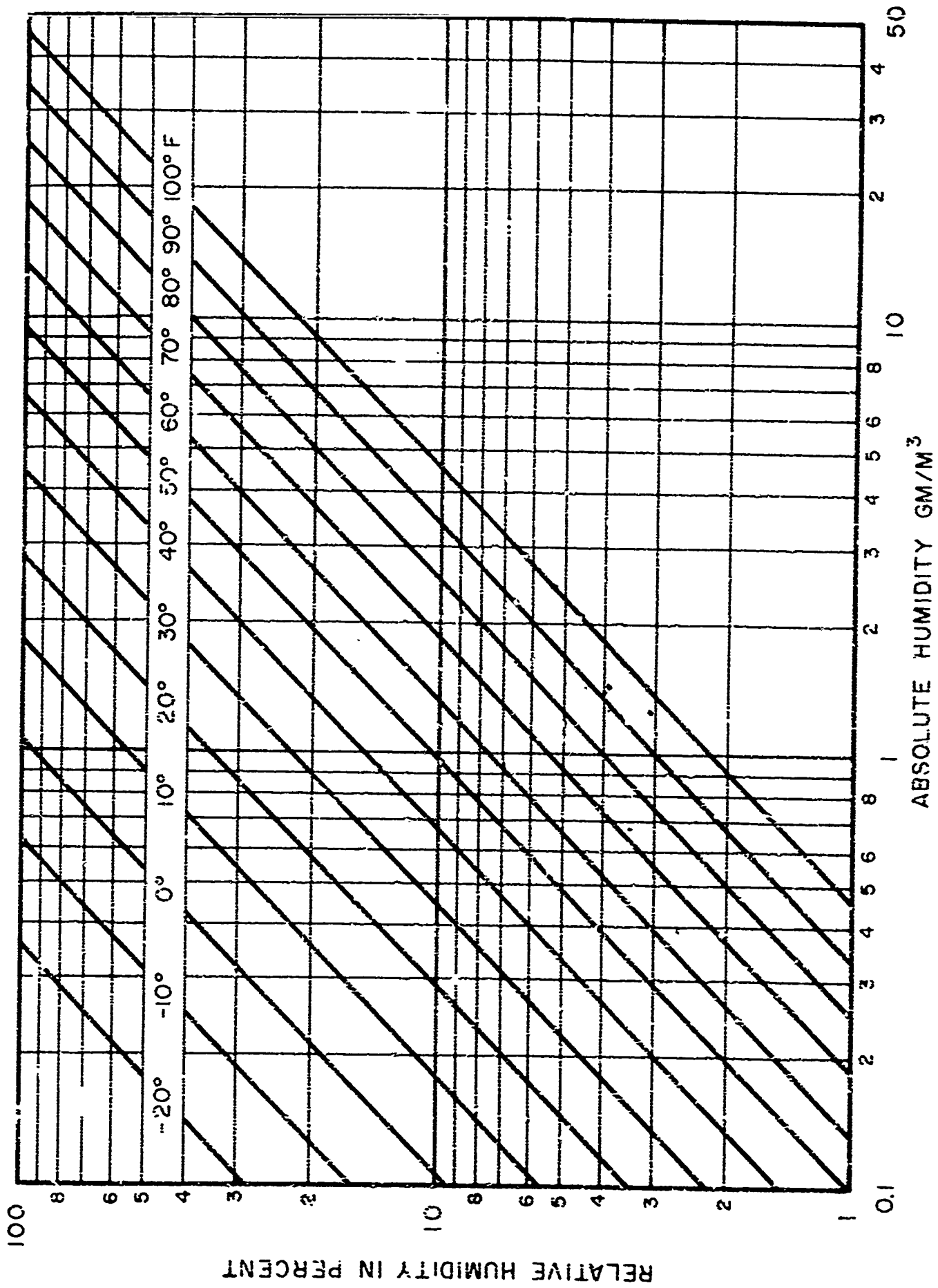FREQUENCY AT VARIOUS TEMPERATURES

FIG. 4.7 CHART FOR CONVERTING UNITS OF HUMIDITY

TIME AXIS FOR TRACES
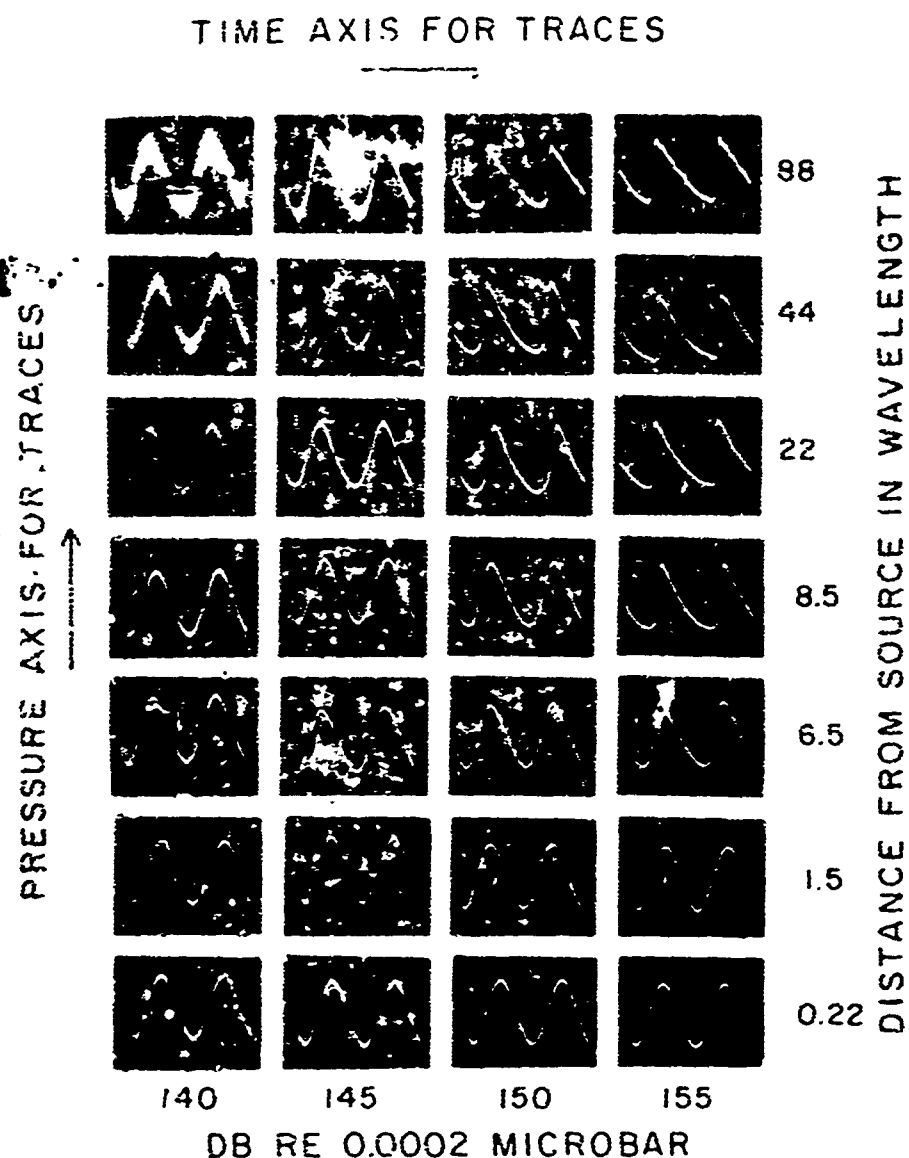
FIG. 4.8 SOUND PRESSURE LEVEL IN AIR AVERAGED
OVER THE FACE OF A PLANE CIRCULAR
RADIATOR, 5 WAVELENGTH IN DIAMETER,
IN A BAFFLE (DIA. 4.8", FREQUENCY 14.6 KC)
SYSTEM GAIN ADJUSTED TO GIVE EQUAL
TRACE HEIGHT
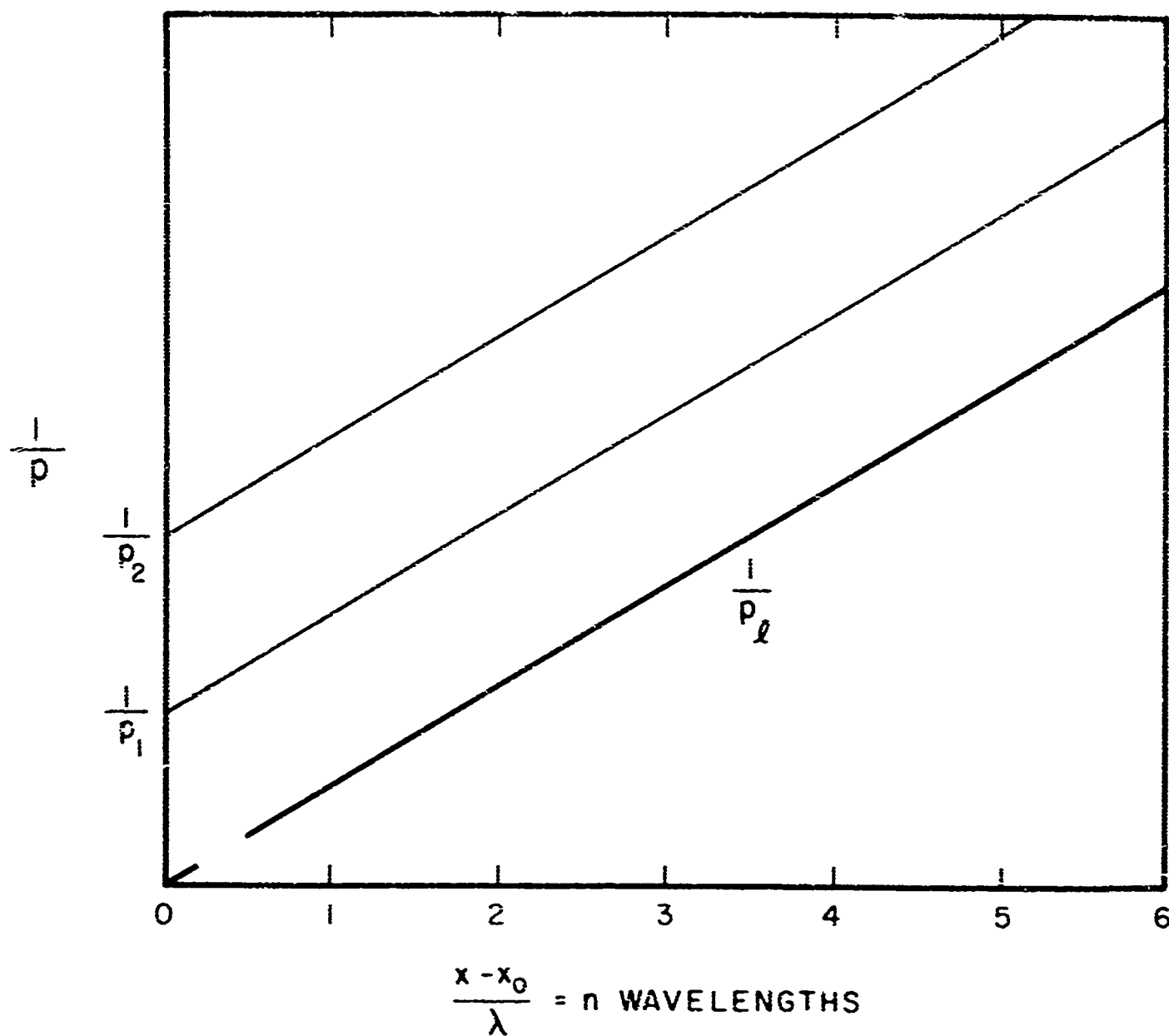
FIG. 4.9   RECIPROCAL PRESSURE IN A SAWTOOTH
ACOUSTIC WAVE VS. DISTANCE IN WAVE-
LENGTHS
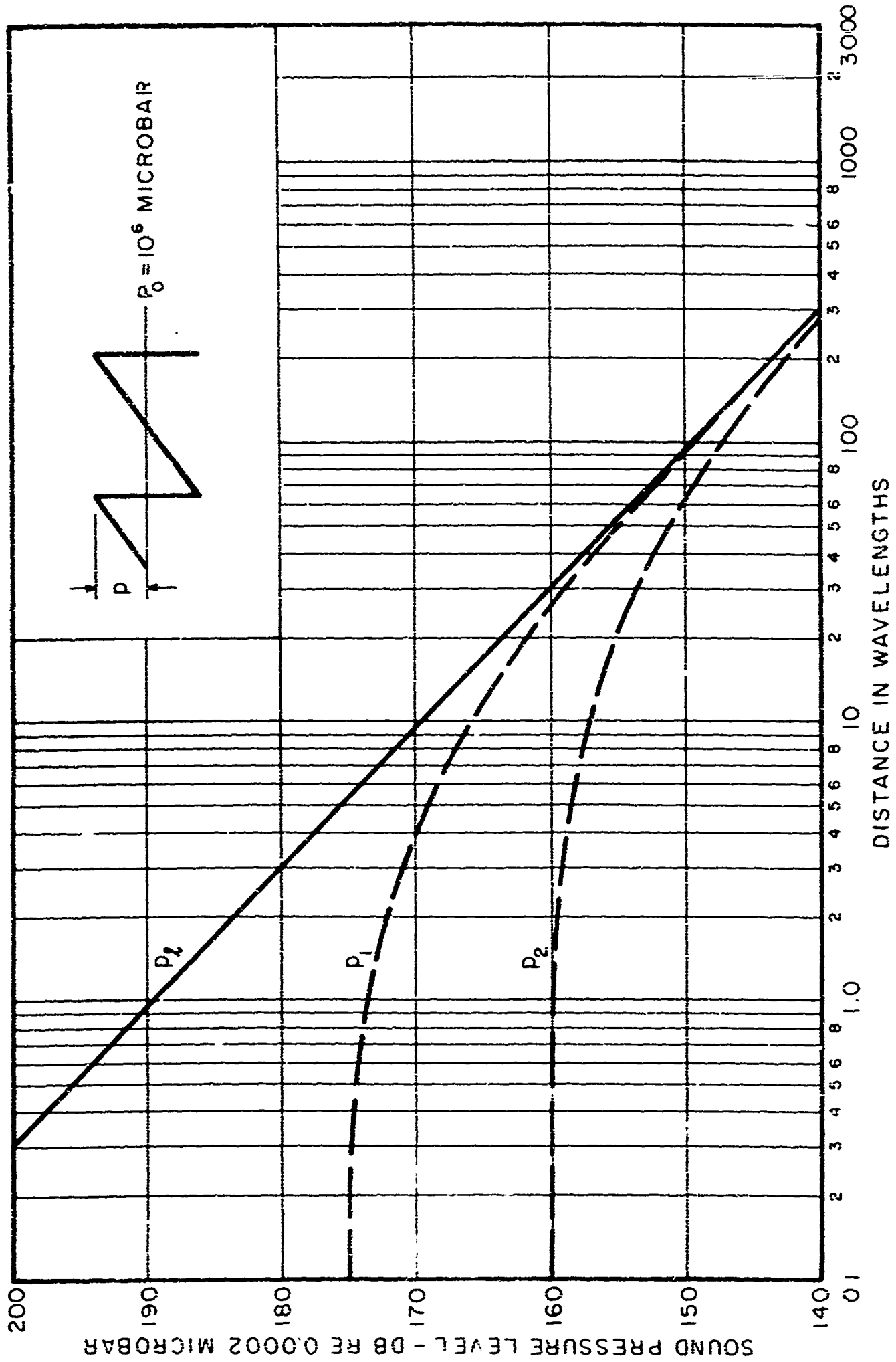
FIG. 4.10 PLOT OF SPL FOR THE LIMITING PRESSURE p_ℓ FOR A PLANE WAVE AND THE CALCULATED PRESSURE FOR TWO PLANE WAVES HAVING PRESSURES p_1 AND p_2 AT THE SOURCE
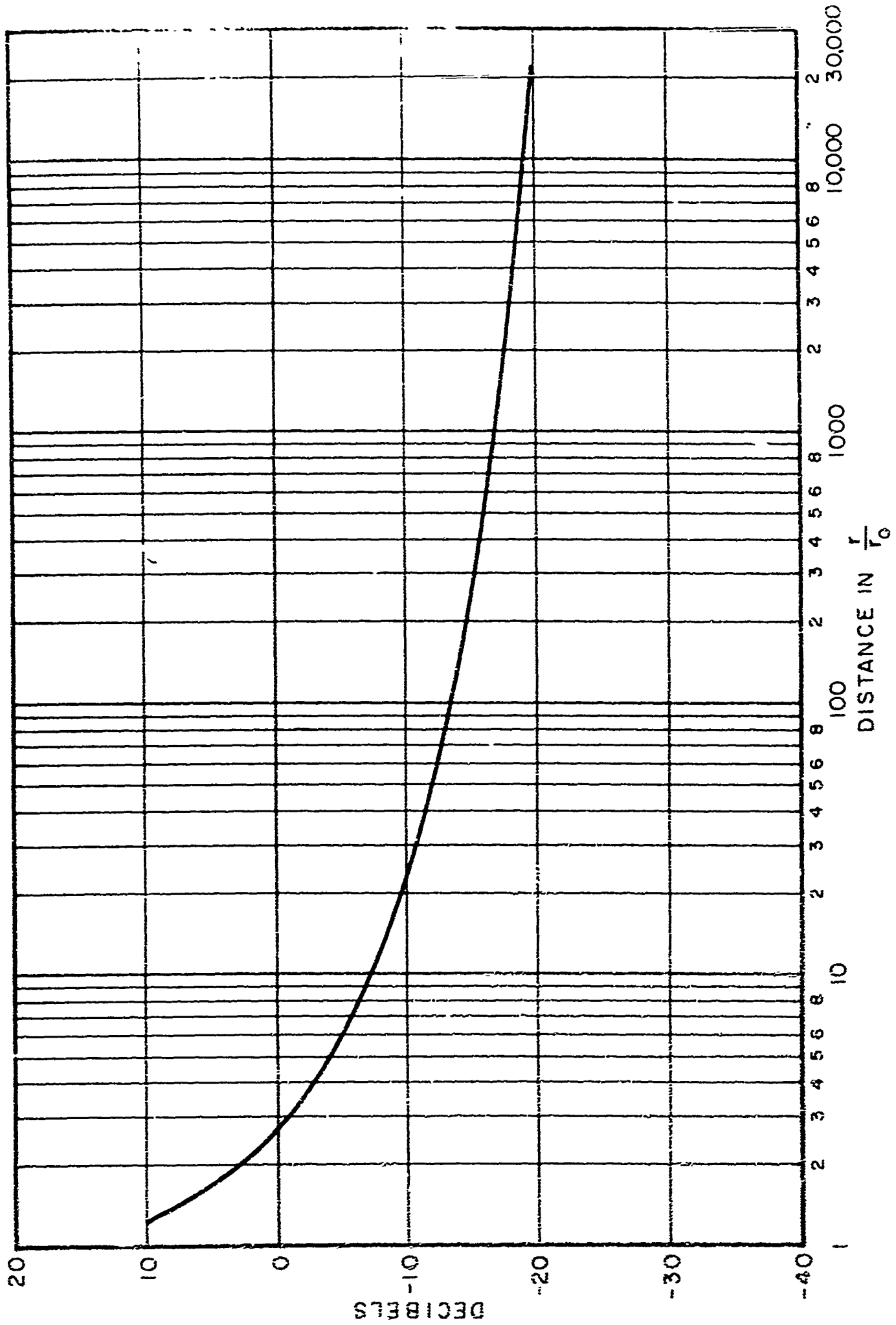
FIG. 4.11 PLOT OF 10 LOG $\left(\dfrac{1}{LOG_e \left(\frac{r}{r_0} \right)} \right)$
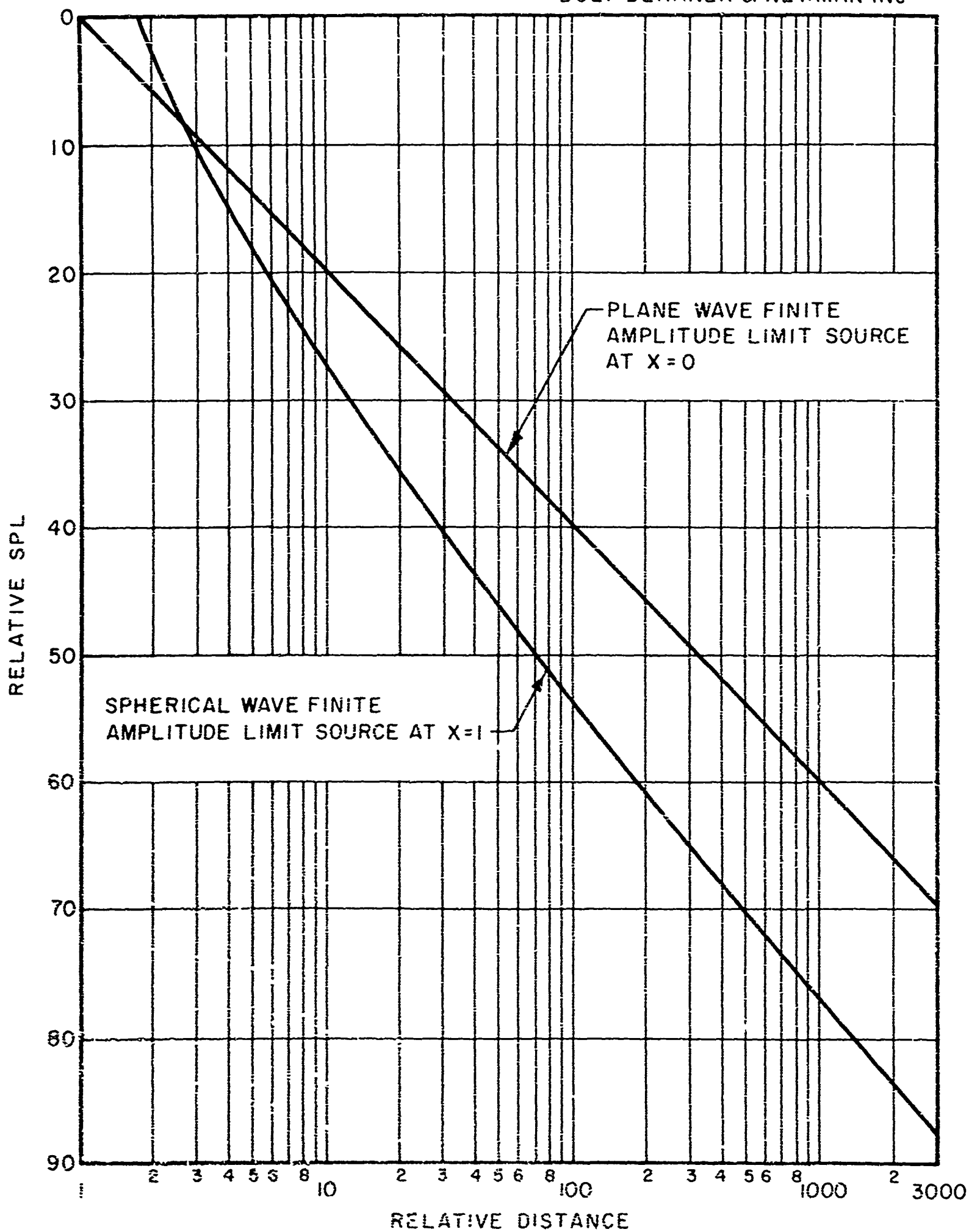
FIG. 4.12   PLANE AND SPHERICAL WAVE FINITE AMPLITUDE LIMITS

DISTANCE FROM SOURCE IN WAVELENGTHS
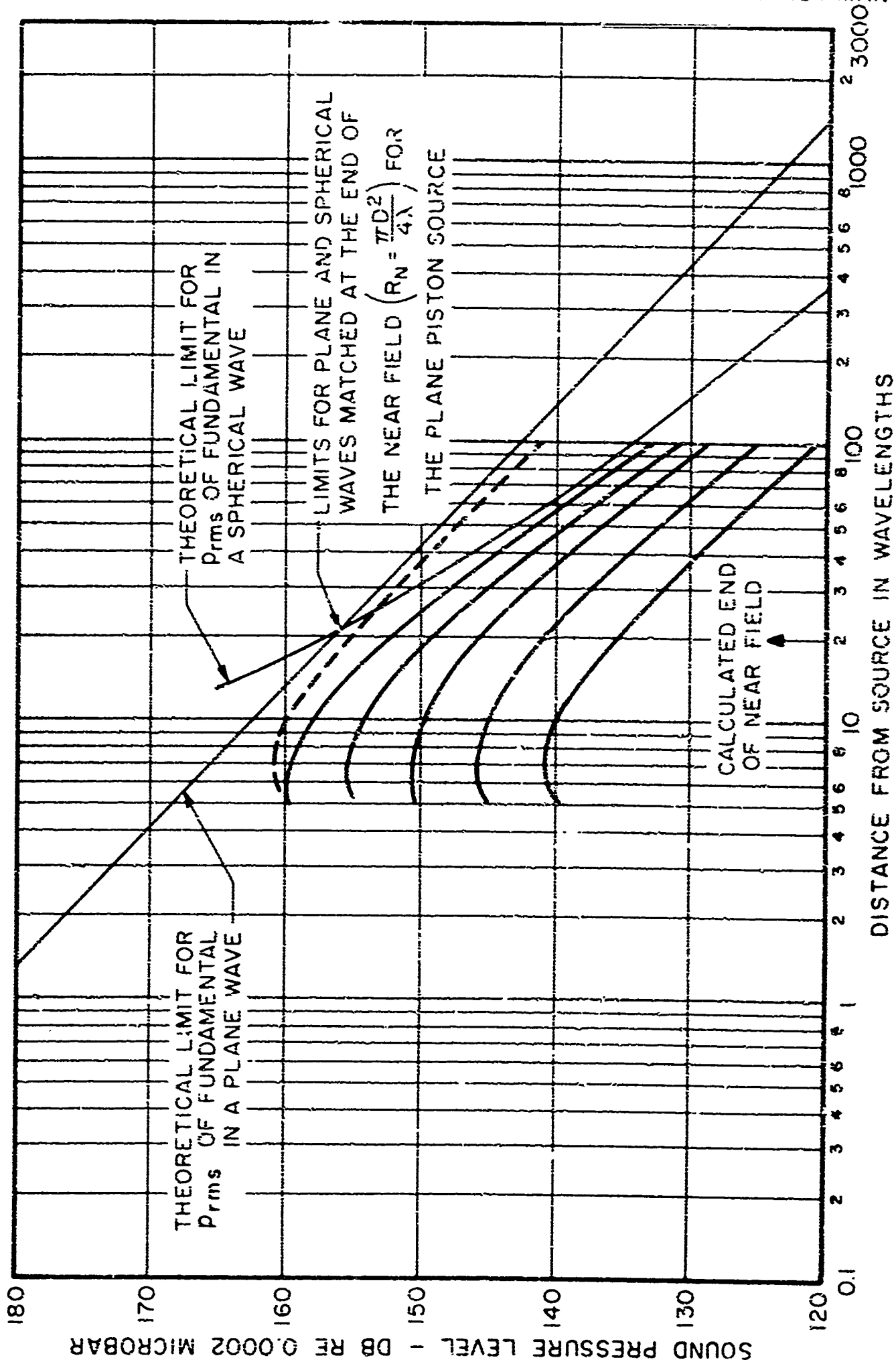
FIG. 4.13 EXPERIMENTAL VALUES OF SOUND PRESSURE LEVEL IN THE FAR FIELD OF A PLANE PISTON SOURCE
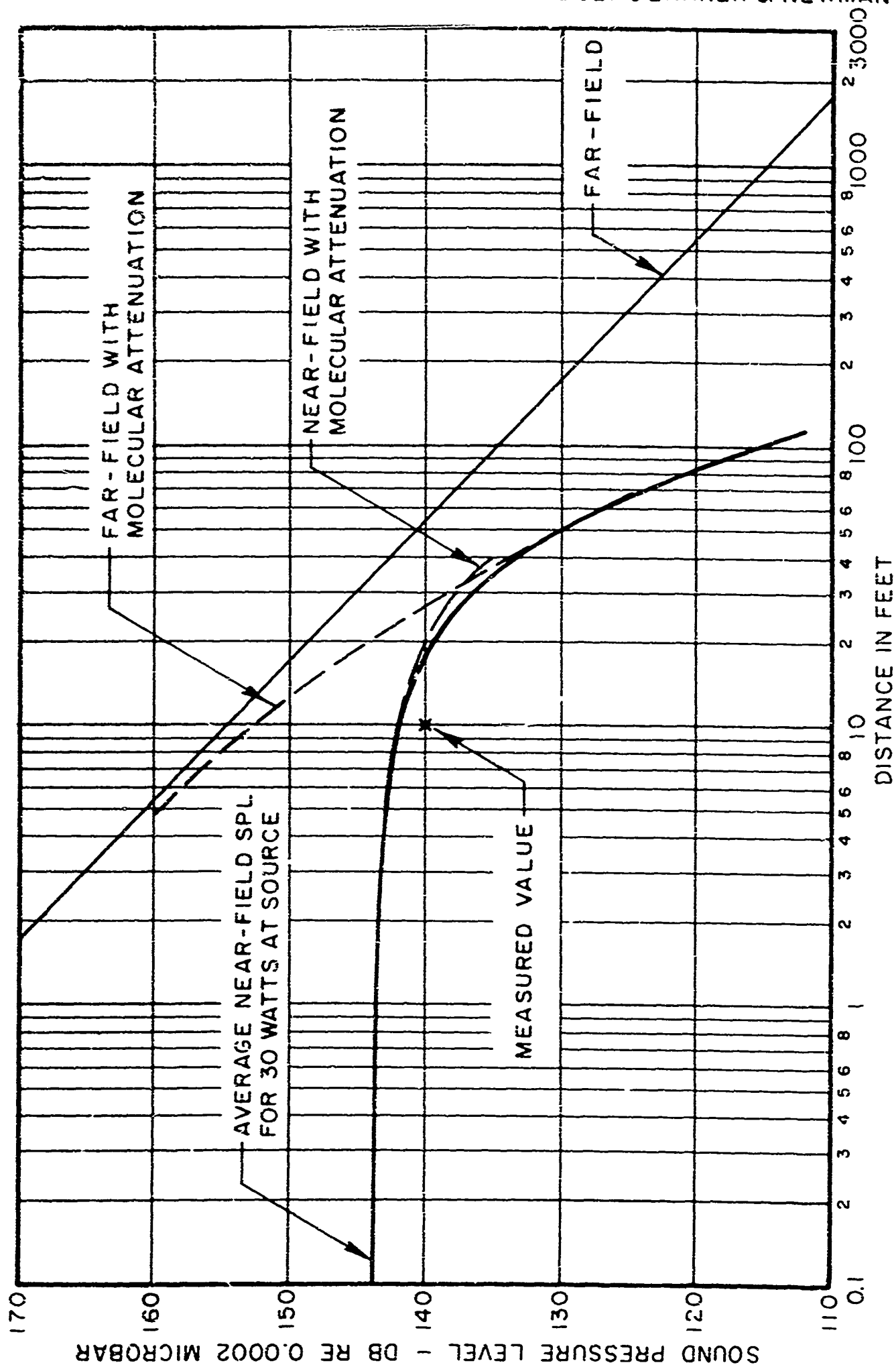
FIG. 4.14 SOUND PRESSURE LEVEL EXPECTED WITH MIDWEST RESEARCH SOUND SOURCE
CONSIDERING MOLECULAR ABSORPTION NEGLECTING FINITE AMPLITUDE LIMITS
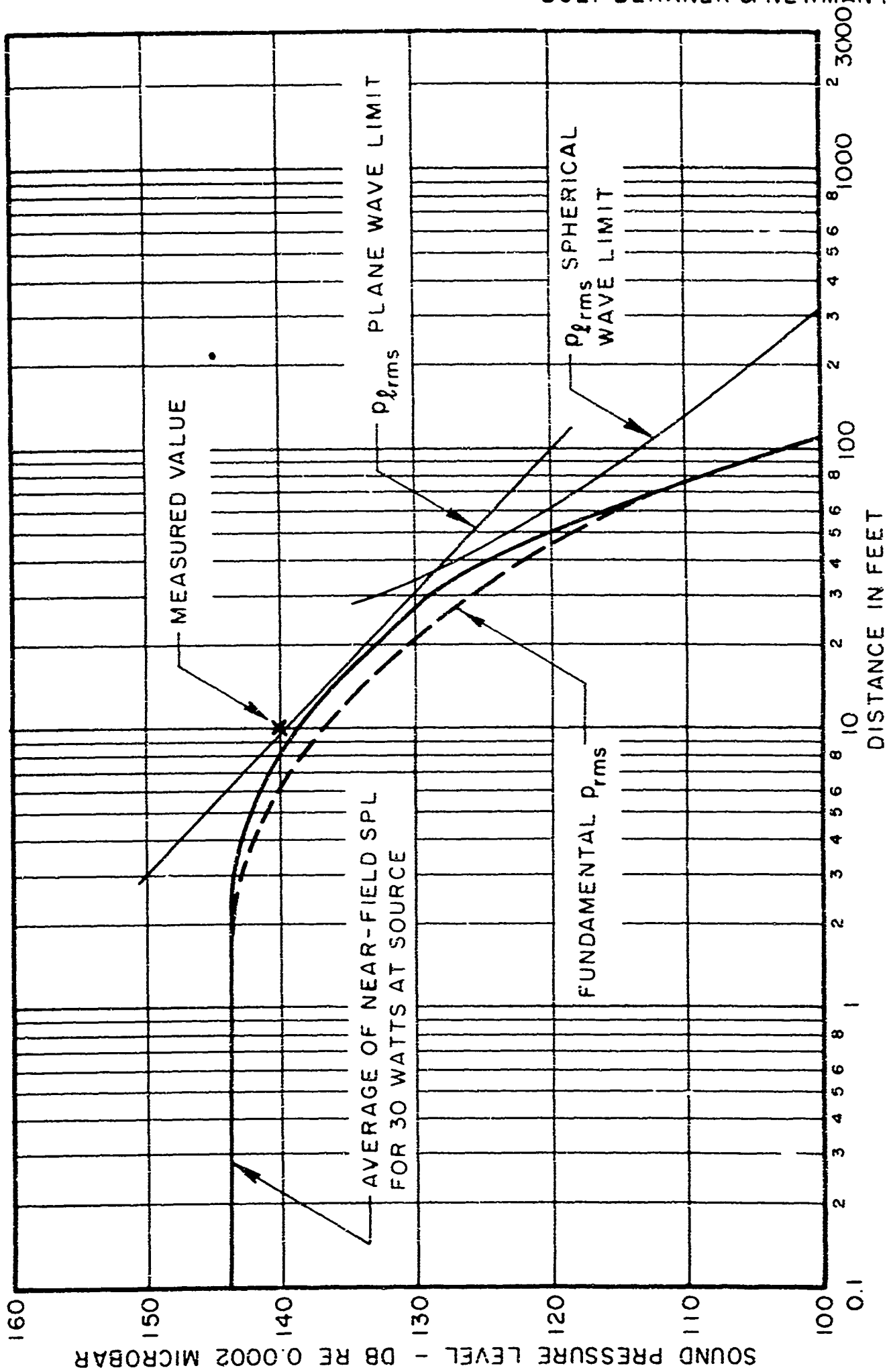
FIG. 4.15   SOUND PRESSURE LEVELS EXPECTED WITH MIDWEST RESEARCH SOUND SOURCE
CONSIDERING BOTH FINITE AMPLITUDE LIMITS AND MOLECULAR ABSORPTION
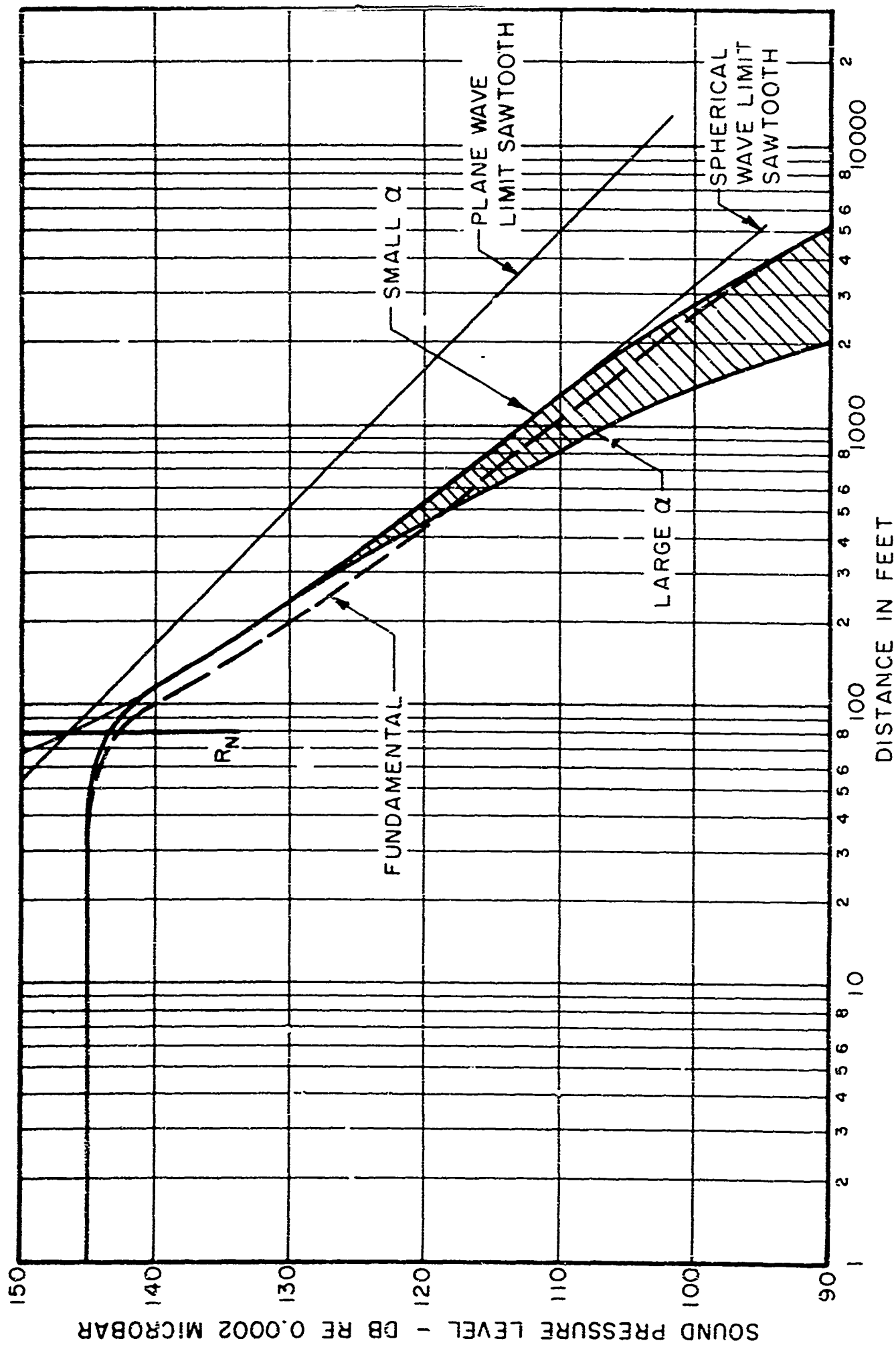
FIG. 4.16 SOUND PRESSURE LEVEL FOR 1140 CPS SIGNAL RADIATED FROM 10 FT. DIAMETER SOURCE WITH AVERAGE SPL OF 145 DB NEAR SOURCE
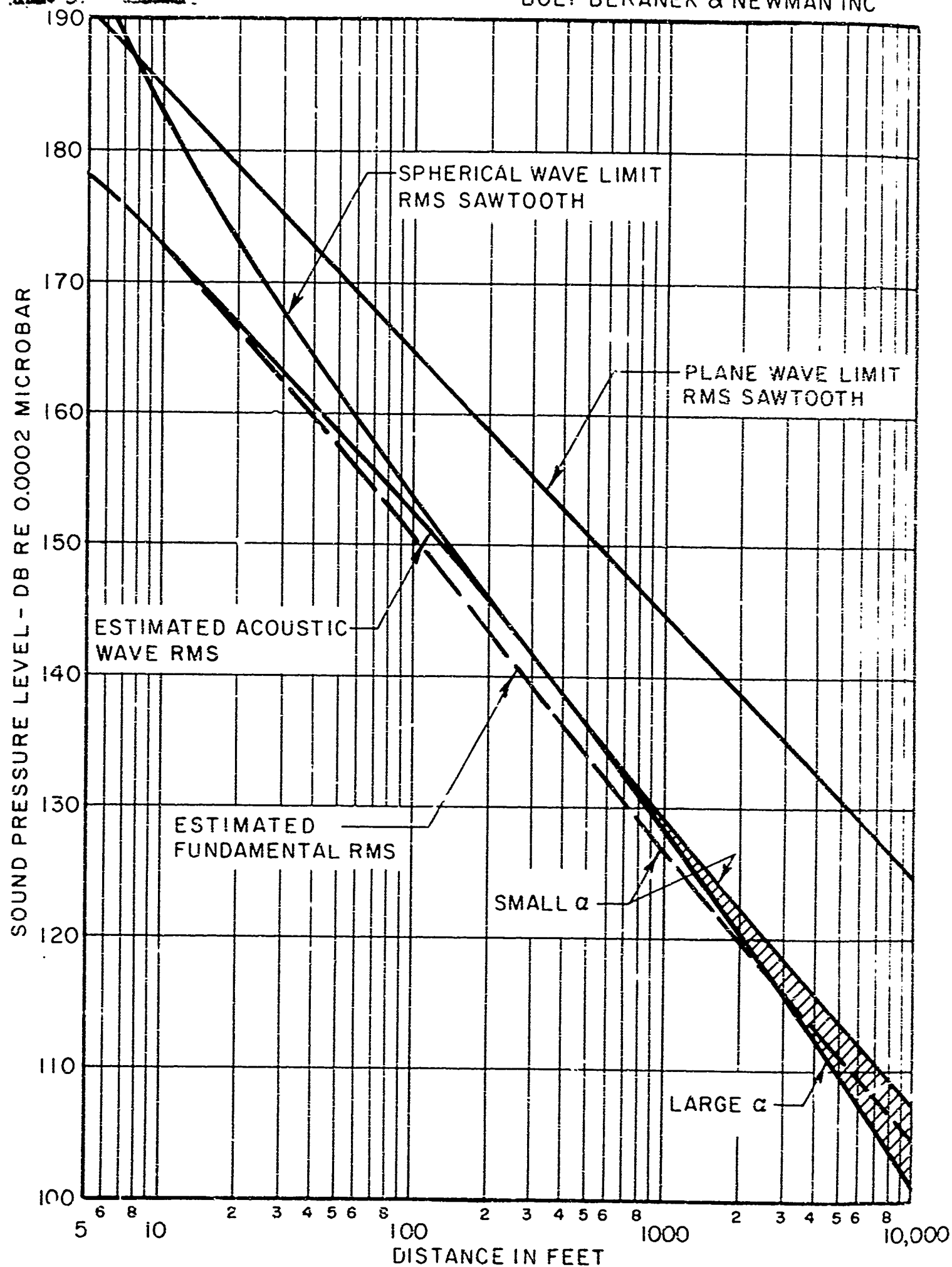
FIG. 4.17   SOUND PRESSURE LEVEL FOR 114 CPS SIGNAL RADIATED FROM 10' DIA. SOURCE WITH AVERAGE SPL OF 175 DB NEAR SOURCE
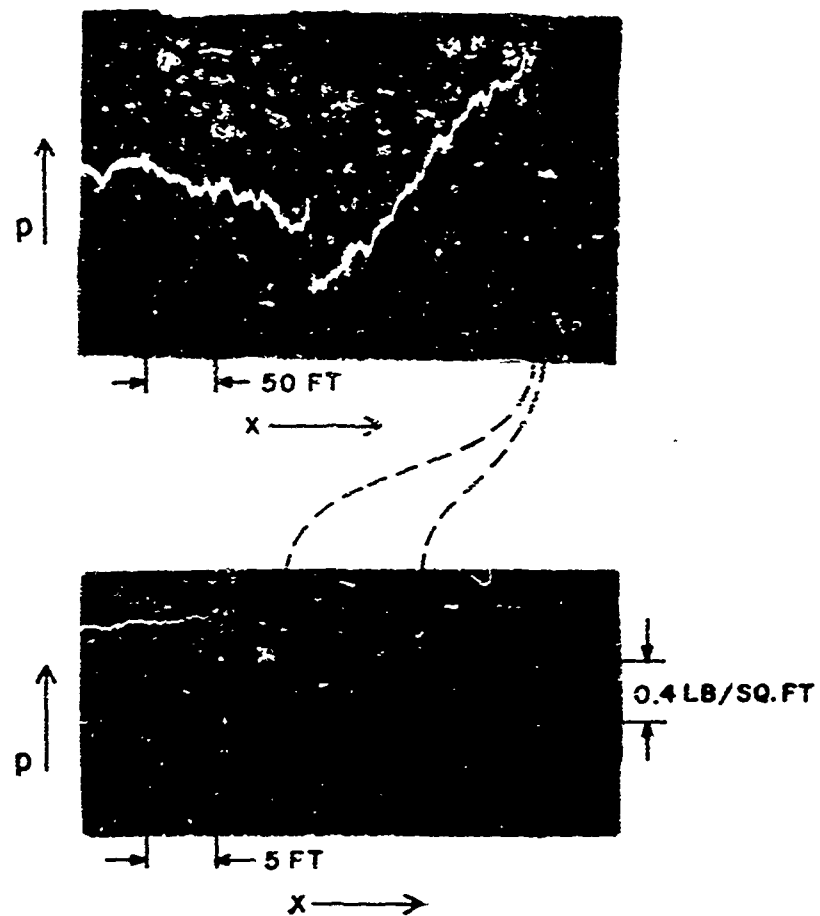
FIG. 4.18   OSCILLOSCOPE TRACE OF
SONIC BOOM SIGNATURE
BOOM NO.7 (TABLE 4.1)

5. SOURCE CHARACTERISTICS FOR MAXIMUM RANGE

5.1 Acoustic Source

A sound source must provide sufficient shock intensity to travel several thousand feet in order to be useful. The source should be somewhat directive in order to conserve source power out more important it should be directive in order to avoid hazards to operating personnel and minimize annoyance in surrounding communities.

It now appears that an ideal pulse at the source should have a rise time which is of the order of a few milliseconds so that there will be a minimum of the high frequency sound components. The high frequency components are undesirable at the source because they are more hazardous and more annoying than the very low frequency components.

It appears that the pulse should have a long decay time for two reasons: (1) a long decay time implies a large amount of energy in the single pulse, (2) the long decay time, returning to atmospheric pressure without the creation of a negative pressure, will prevent the creation of a negative shock. Thus, such an acoustic wave can avoid the variable interference effects expected in radar reflections from the sonic boom N-waves.

The source need not and should not produce a shock wave near the radar installation but should rely upon finite amplitude distortion to create the shock at a distance somewhere in the region between 100 and 1000 ft frcm the source. Such a design would minimize hazard and annoyance and maximize the conservation of energy in the wave. The decay of the trailing edge of the pulse will not create a shock wave at any range if the decay is sufficiently gradual.

To form a ... between 100 and 1000 feet from the source, the intensity level near the source must exceed a critical value determined by the initial pulse shape. The source power level will be determined by this intensity level, the source size and its directivity. On the other hand the sound intensity level outside the main beam must not be high enough to cause personnel hazard or annoyance. As mentioned in Sec. 4.44 the high frequency components of the sound pulse will be much more directive than the low frequency components. These high frequency components which are more annoying can be confined to a fairly narrow beam and can be directed away from the populated areas. The design of an acoustic source with these desired characteristics will require future study.

The intensity and directivity of the sound field near the source will of course be greatly influenced by the size of the sound source itself. If the EMAC system is to be mobile, the source and radar antenna both probably will be restricted to units of the order of 10 ft in diameter. Such a source will give some appreciable directivity for a 100 cps wave, Q will be of the order of 10. For the higher frequency components needed to sharpen the leading edge, the source will be more highly directive, Q is about 1000 for 1000 cps. Since the amount of power needed in the harmonics is small compared with that in the fundamental, and since the source is more directive for these components the amount of sound which spreads away from the center of the main beam is relatively small for the high harmonics and should therefore cause only a minor and perhaps negligible problem as regards personnel exposure especially since the pulses are of short duration and spaced at relatively long intervals.

For a longer range installation where the sound source and radar
antennas may be permanently located, larger source areas may be
utilized with the added advantage of greater directivity at the
chosen frequency or with the possibility of reducing the fundamen-
tal frequency component of individual pulses.

The personnel hazard for pulses is much less than that for contin-
uous tones. No experimental results are at hand for the effects
of low frequency pulses but extrapolation of data from 100 cps
indicates a probable increase in permissible exposure levels for
pulses repeating at 10 cps or less would be of the order of 20 db
or more.

The personnel hazard for low frequency pulses should be subjected
to experimental study. Some work is planned at BBN in this area
and equipment is available for controlled experiments at the
present time. It may be advantageous to augment this work by
experiments directed specifically toward evaluating the effects
of an EMAC source once a more definite specification of the system
has been developed.

5.2 Electromagnetic Source

As opposed to the situation of the acoustic source, there is no
fundamental limit to the intensity which can be propagated in
the radar beam (at least within the range of power capabilities
currently available). Thus, the radar power can and should be
increased as necessary to utilize the full range for which the
acoustic signal is above the background noise, but need not be
increased further. Some existing radar systems seem adequate
for this purpose. The most important parameter of the radar
system for maximizing the range of the EMAC Probe is the radar
wavelength. As discussed in Sec. 2.2 the power reflection

coefficient from a dielectric variation is sensitive to the ratio
of the radar wavelength to the thickness of the dielectric varia-
tion. To have an adequate reflection the radar wavelength must
be comparable with or smaller than the shock thickness. The shock
becomes thicker as it propagates and thus the range of the probe
is limited substantially at the distance where the wave front
thickness equals the radar wavelength. There exist Doppler radars
such as the FPS-7 and FPS-20 having a wavelength of about 23 cm
which is sufficiently long to provide adequate reflections from
shock waves with sound pressure levels of the order of 120 or 130 db
re 0.0002 microbar.

Other parameters of the electromagnetic source have less effect on
range and can be varied within fairly wide limits. The beam width
can be decreased to give greater detail and higher intensity or
can be increased to cover a larger area. The duty cycle and search-
ing sequence can be modified depending on the meteorological condi-
tions and atmospheric parameters of interest.

Since the overall power loss will be very high it will be necessary
to use such techniques as coherent integration and parametric ampli-
fication to obtain maximum range. It is estimated that, under the
most favorable conditions, an overall power loss of 239 db can be
permitted between the transmitted and received signal at the limit
of detectability for a system such as the FPS-7 or FPS-20. Using
this information and the method given at the end of Sec. 3 an estimate
of the maximum range of an EMAC Probe system can be made. Such
calculations will be given for a variety of atmospheric conditions
in Sec. 6.7.

6. ACCURACY OF MEASUREMENT OF ATMOSPHERIC PARAMETERS

6.1 Wind Speed in Direction of Search

The local speed of propagation of the acoustic wavefront is the vector sum of the sound speed and wind speed $\bar{a}(\bar{r},t) + \bar{V}(\bar{r},t)$. The measured Doppler shift indicates the radial component of this speed. Thus,

$$f - f_o = \frac{2}{c} (a_r + V_r) \approx \frac{2a_o}{c} \quad , \tag{6.1}$$

where

$$
\begin{aligned}
f &= \text{frequency of returned signal} \\
f_o &= \text{frequency of radiated signal} \\
c &= \text{speed of light} \\
a_r, (V_r) &= \text{radial component of sound (wind) speed} \\
a_o &= \text{sound speed at source}
\end{aligned}
$$

The relations between the several variables can be seen in Fig. 6.1. We find

$$a_r = a \cos \beta \quad \text{and}$$

$$\beta \approx \sin \beta = \frac{Vt \sin \phi}{at} = \frac{V \sin \phi}{a} \tag{6.2}$$

Also

$$V_r = V \cos \phi \quad \text{so that}$$

$$a_r + V_r = a + V \cos \phi - \frac{V}{a} V \sin^2 \phi \quad , \tag{6.3}$$

where ϕ = angle between V and radial direction. The V cos ϕ term dominates the $\frac{V}{a}$ V $\sin^2\phi$ term except for $\phi \approx 90^\circ$ where the direction of search is perpendicular to the wind direction. If the wind were uniform at all points, the Doppler shift vs ϕ curve would have the form shown in Fig. 6.2

In this case, the magnitude and direction of V could be determined from the shape of the curve. However, if the wind is not uniform, Eq. (6.3) must be used. Unless the wind is very strong and $\phi \approx 90^\circ$, only the V cos ϕ term is needed. Even in that case, the maximum error in V would be 10% and this could be reduced by applying the correction term. The error in the Doppler shift from changes in the direction of propagation is thus fairly small. The shift also depends on the magnitude of the sound speed which is related to the local temperature, T, by

$$a = \sqrt{\gamma RT}$$

where $\gamma = C_p/C_v$, R = gas constant.

If T deviates from the temperature at the source, T_o, then there is a change in $f-f_o$ given by

$$\frac{2}{c}(a-a_o) = \frac{2}{c} a_o \frac{T-T_o}{2T_o} \quad .$$

This change in sound speed due to a temperature change would appear the same as a change in the radial wind speed. The value of Δa corresponding to various ΔT's is shown in Table 3.1, Sec. 3.

Since temperature varies primarily with height, these corrections will enter as the altitude of the test region is increased. If the probe is pointed vertically, it will measure the change of temperature with altitude and the vertical component of the wind, V_z. Since V_z is almost always less than 5'/sec, a vertically pointing probe can measure T as a function of altitude to within about 3°. If V_z is known roughly, then T as a function of height can be found much more accurately. Knowledge of the temperature at a specified altitude can then be used in computing horizontal components of the wind at the corresponding altitude as discussed in Sec. 6.2. A horizontal wind which is uniform in direction is a good assumption when considering altitudes which are high compared with influencing obstacles on the ground. This assumption will be used in computing the wind components.

6.2 Wind Direction

Complete determination of the wind direction requires a determination of three components of the wind velocity. In practice, the vertical component, V_z, is much smaller than the other two and can be neglected. Under some atmospheric conditions the vertical component is far from negligible but in such cases the vertical component is confined to rather local areas and examination of these areas in relation to surroundings can yield vertical velocity calibration data.

6.21 Single Probe Methods

If the wind is assumed to vary slowly with distance and time, then measurement of the radial wind in two directions can give information on two components of the wind. Consider the following measurements made on two nearby regions at low elevations as shown in Fig. 6.3.

assuming the wind has the same components V_x, V_y, V_z at (1) and (2), we may measure the Doppler shift at (1) and (2). If the temperature is the same at the two locations then the Doppler shifts give directly the radial wind velocities, $V_{r(1)}$, $V_{r(2)}$. From Fig. 6.3 these can be seen to be

$$V_{r(1)} = V_x \cos \theta \sin \frac{\phi}{2} + V_y \cos \theta \cos \frac{\phi}{2} + V_z \sin \theta$$

$$(6.4)$$

$$V_{r(2)} = -V_x \cos \theta \sin \frac{\phi}{2} + V_y \cos \theta \cos \frac{\phi}{2} + V_z \sin \theta$$

where θ and ϕ are defined in Fig. 6.3

The term $V_z \sin \theta$ can be dropped since both V_z and θ are small. $\cos \theta$ can be set equal to one giving

$$V_{r(1)} = V_x \sin \frac{\phi}{2} + V_y \cos \frac{\phi}{2}$$

$$(6.4')$$

$$V_{r(2)} = -V_x \sin \frac{\phi}{2} + V_y \cos \frac{\phi}{2} \ .$$

Solving Eq. (6.4') gives

$$V_x = \frac{V_{r(1)} - V_{r(2)}}{2 \sin \frac{\phi}{2}} \qquad V_y = \frac{V_{r(1)} + V_{r(2)}}{2 \cos \frac{\phi}{2}} \ .$$

The error inherent in this method can be seen by considering that there is an uncertainty δ in each radial velocity measurement. Then

$$\text{Error } (V_x) = \frac{\delta}{\sin \phi/2} \qquad \text{Error } (V_y) = \frac{\delta}{\cos \phi/2} \qquad (6.5)$$

This is graphed in Fig. 6.4.

For ϕ very small, V_x can be determined very poorly as would be expected since both probings are essentially measuring V_y. Increasing ϕ increases the accuracy of wind direction measurements, but decreases the probability that the wind and temperature are the same at both points of probing. Adding additional regions of measurement can provide more information on T and V to reduce the uncertainty as these parameters change from one point to the next.

6.22 Multiple Probe Methods

This method uses several probes to sample one region rather than one probe to sample several regions. The wind components are obtained in the same manner as with one probe. The advantage of this method over the single probe method is that it is not affected by spatial variations of wind and temperature. However, it does not seem that this advantage compensates for the additional complexity and cost required to erect and coordinate two or more probe systems. Various techniques of this type are discussed in the MRI Reports.[9]

6.3 Turbulence

6.31 Detection and Intensity

One effect of turbulence on the acoustic wavefront will be to cause some parts to move faster or slower than others. Thus, different parts of the wavefront will have different Doppler shifts.

If all parts of the wavefront had the same speed relative to the radar, the returned signal would have a single frequency and

would give a definite Doppler shift. However, if this is not
the case, the returned signal will have a spread of frequencies.
The Doppler shift is measured by comparing the phase difference
between transmitted and received signals as a function of time.
This phase difference will have a form similar to that shown in
Fig. 6.5.

The frequency spectrum of this curve then can provide information
on velocities and turbulence. A possible frequency spectrum is
shown in Fig. 6.6.

The location of the maximum gives the mean radial velocity while
the width of the maximum gives the rms fluctuation in radial
velocity. These fluctuations result from wind and temperature
inhomogeneities and are related as follows:

$$\frac{\Delta f}{f_0} = \frac{2}{c} \left[\Delta V_r + \Delta a_r \right] \approx \frac{2}{c} \left[\Delta V_r + \frac{\Delta T}{2T_0} a_0 \right] \approx \frac{2a_0}{c} \mu_{rms} \qquad (6.6)$$

where ΔV, ΔT = amplitude of velocity, temperature fluctuations
throughout the reflecting region, and μ is defined in Eq. (3.30).

6.32 Localization

The measurement of Δf determines the largest variation in radial
velocity occurring in the echoing region of the wavefront. It
would be very difficult to localize the turbulence to a smaller
region than this. It may be expedient, however, to use more than
one radar frequency in order to be able to obtain extended range
with the lower frequency and fine definition of close wind struc-
ture with the short radar waves.

6.33 Structural Definition

There are several ways that the scale of the turbulence can be
measured. The simplest method uses the fact that the width of
the echoing region increases with range and is fairly well known.
The Δf for each region measures the full intensity of turbulence
with a scale smaller than the region but only part of the inten-
sity of larger scale turbulence. If the intensity of turbulence
is plotted against the size of the echoing region, a curve like
Fig. 6.7 is obtained.

Since there is no increase in turbulence intensity above $L = L_{max}$,
the maximum scale of the turbulence is L_{max}. It will be much more
difficult to determine the minimum scale of the turbulence. One
possible method uses the results of Sec. 3. The reflected power
at large ranges decreases as SPL/R^3 because of spherical divergence
and beam spreading. However, if the wavefront is rough on the scale
of the radar wavelength, the radar reflection will be almost iso-
tropic and the beam will not spread with increasing R. In this
case the reflected power will decrease as SPL/R^2. In this case,
the existence of turbulence having a scale comparable with λ_e can
be determined.

The scale of the turbulence discussed above relates to the size of
individual turbulent fluctuations or eddies and does not necessarily
relate to the size of a turbulent region. The size of a turbulent
region must be determined in a different manner. If the turbulent
intensity is known for all echoing regions within a large volume,
contour lines of equal intensity can be drawn which will show the
size and shape of regions of strong turbulence. This method will
work well for turbulent volumes larger than several echoing regions.
Smaller patches of turbulence might be localized by using measure-
ments from overlapping echoing regions but since these regions do

not have sharp boundaries, the precision of this method will require experimental evaluation.

6.4 Possibility of Differentiation Between Inhomogeneities of Various Kinds

As seen in Eq. (6.6) temperature and wind fluctuations affect the Doppler shift if the same manner. Observations in the atmosphere show that these fluctuations are of the same order of magnitude.

While it will be very difficult to distinguish between temperature and wind fluctuation experimentally, this will not be a major problem. Variations in wind and temperature are related theoretically through the equations of atmospheric dynamics. Thus, experimental knowledge of Δf can provide information on both ΔV and ΔT. The accuracy of this method will probably have to be determined experimentally.

6.5 Temperature Discontinuities

Temperature discontinuities or sharp temperature gradients will reflect both sound and radar and can be detected in several ways. Consider the discontinuity shown in Fig. 6.8. At points A, B, C, where the discontinuity is perpendicular to the radar beam, the radar signal will be reflected and will return to the probe. This signal will not have a Doppler shift near $\frac{2a_0}{c}$ and may be difficult to detect. Sound reflected all along the discontinuity will return to the probe but will not give much information on the shape of the discontinuity. It may also be masked by sound reflected from other objects. The reflected radar and sound waves will give the information that there is a discontinuity which can be investigated with standard EMAC probe techniques. The transmitted sound wave will be speeded up (if $T_2 > T_1$) and this will appear as an

...nce in the Doppler shift whose location and magnitude can
...e measured. This will suffice to determine the location and
...plitude of the temperature discontinuity.

6.6 Humidity Changes

Humidity changes serve to alter the attenuation coefficient of
the sound waves and the dielectric constant of the air. A change
in attenuation coefficient will considerably alter the range of
the EMAC Probe. Since changes in the wind alter the range in
some directions more than others while humidity changes alter the
range in all directions, a change in the average range probably
corresponds to a humidity change and can be used to detect and
measure these changes.

Changes in the dielectric constant of air affect the returned
signal much less than does a change in attenuation coefficient
and will not be very useful for humidity measurements.

Changes in liquid water content should be examined by means of
humidity and water vapor absorption of sound.

6.7 Maximum Range of EMAC Probe

The maximum range of the probe depends on the characteristics of
the acoustic system, the radar system, and the atmosphere. We can
control the characteristics of the acoustic and radar system but
cannot control those of the atmosphere. In this section we will
choose some operating parameters for the EMAC Probe system and
calculate the maximum range under several atmospheric conditions.

The radar system will be characterized by a radar wavelength of
23 cm., a radar antenna diameter of 10', and a maximum permitted

difference of 239 db between transmitted and received power
as discussed in Section 5.2.

The output of the acoustic system will be chosen as a single
pulse but will be considered to propagate as an acoustic signal
with a fundamental frequency of 114 cps and a SPL near the source
of 175 db. A sound source, 10' in diameter is assumed as a plane
circular radiator. This sound field is discussed in Section 4.44
and shown in Fig. 4.17.

The atmospheric parameters for which we will take several values
are the steady transverse wind speed component (V sin ϕ), and the
turbulent wind speed (ΔV). The fractional radar power reflected
at any range is found by using Figs. 4.17, 2.7, and 2.3 in com-
bination. The received power is then found using the method of
Section 3, page 48. We will assume a turbulence scale of s =
100'. The maximum range is found by equating the received power
level to the radiated power level minus 239 db.

The maximum range for given values of V sin ϕ and ΔV varies with
the amount of atmospheric attenuation the sound signal encounters.
This attenuation may vary by a factor of 10 at any given frequency
depending upon temperature and humidity as detailed in Section 4.3.
Values for the maximum range calculated for several values of V
sin ϕ and ΔV are presented in Table 6.1a and 6.1b. Table 6.1a
represents conditions of low atmospheric attenuation and Table
6.1b represents conditions of high atmospheric attenuation.

ΔV / V sin $\dot{\phi}$	0	1'/sec	10'/sec
0	50,000'	15,000'	10,000'
10'/sec	500'	10,000'	10,000'
100'/sec	50'	50'	9,000'

Table 6.1a

ΔV / V sin ϕ	0	1'/sec	10'/sec
0	20,000'	5,000'	4,000'
10'/sec	500'	3,000'	4,000'
100'/sec	50'	50'	3,000'

Table 6.1b

It is apparent that where a transverse wind occurs there is need
for turbulence in order that a usable amount of the reflected
radar signal be returned to the radar antenna. Without such
turbulence, specular reflection directs the main signal away
from the antenna. Fortunately, where high winds exist, turbu-
lence is usually encountered and in general the turbulence will
be of greater magnitude when the wind velocities are high. Cer-
tainly large turbulence will exist in regions where there are
large wind gradients which are probably the regions of greatest
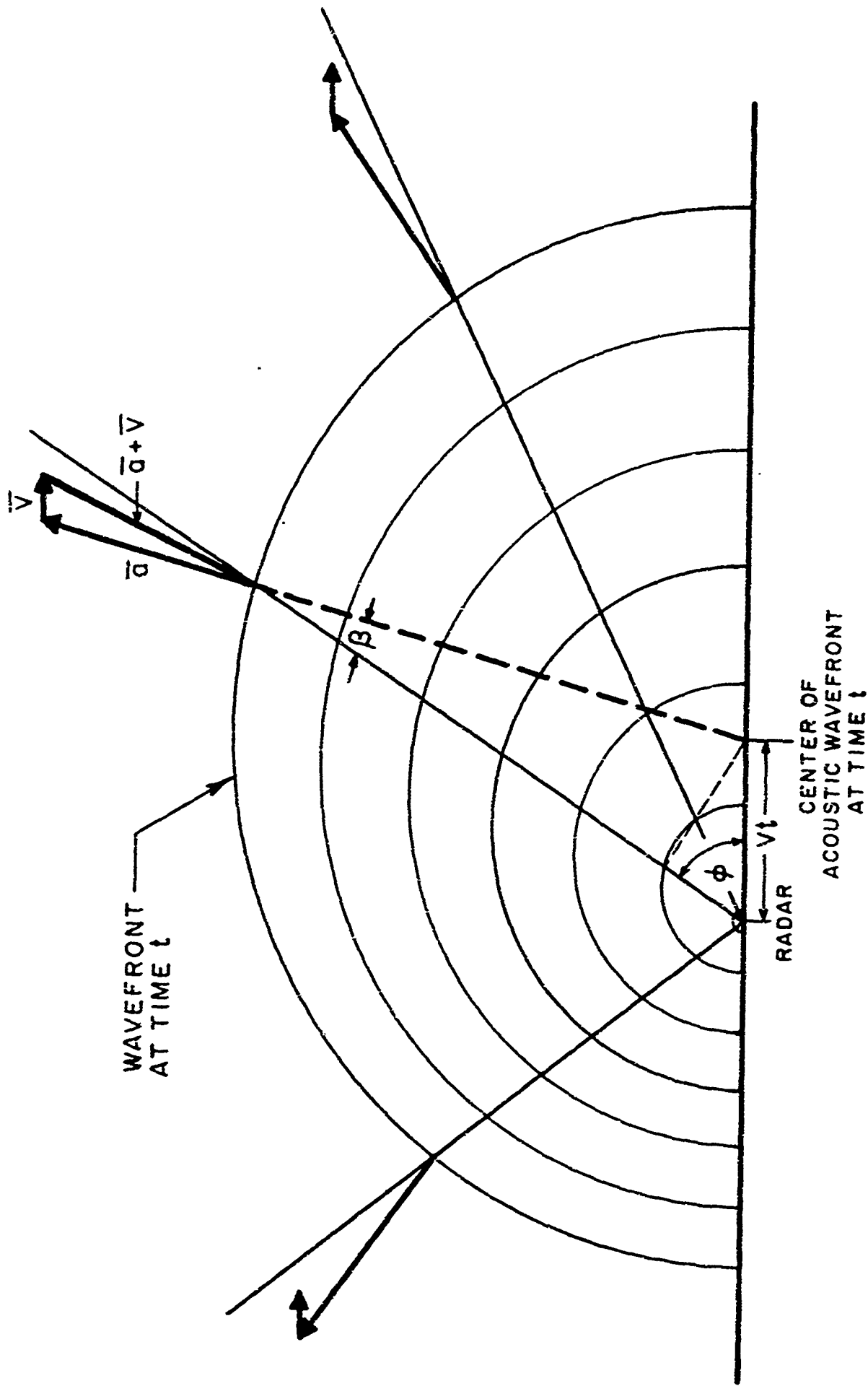interest.

FIG. 6.1 FIGURE FOR FINDING COMPONENT OF
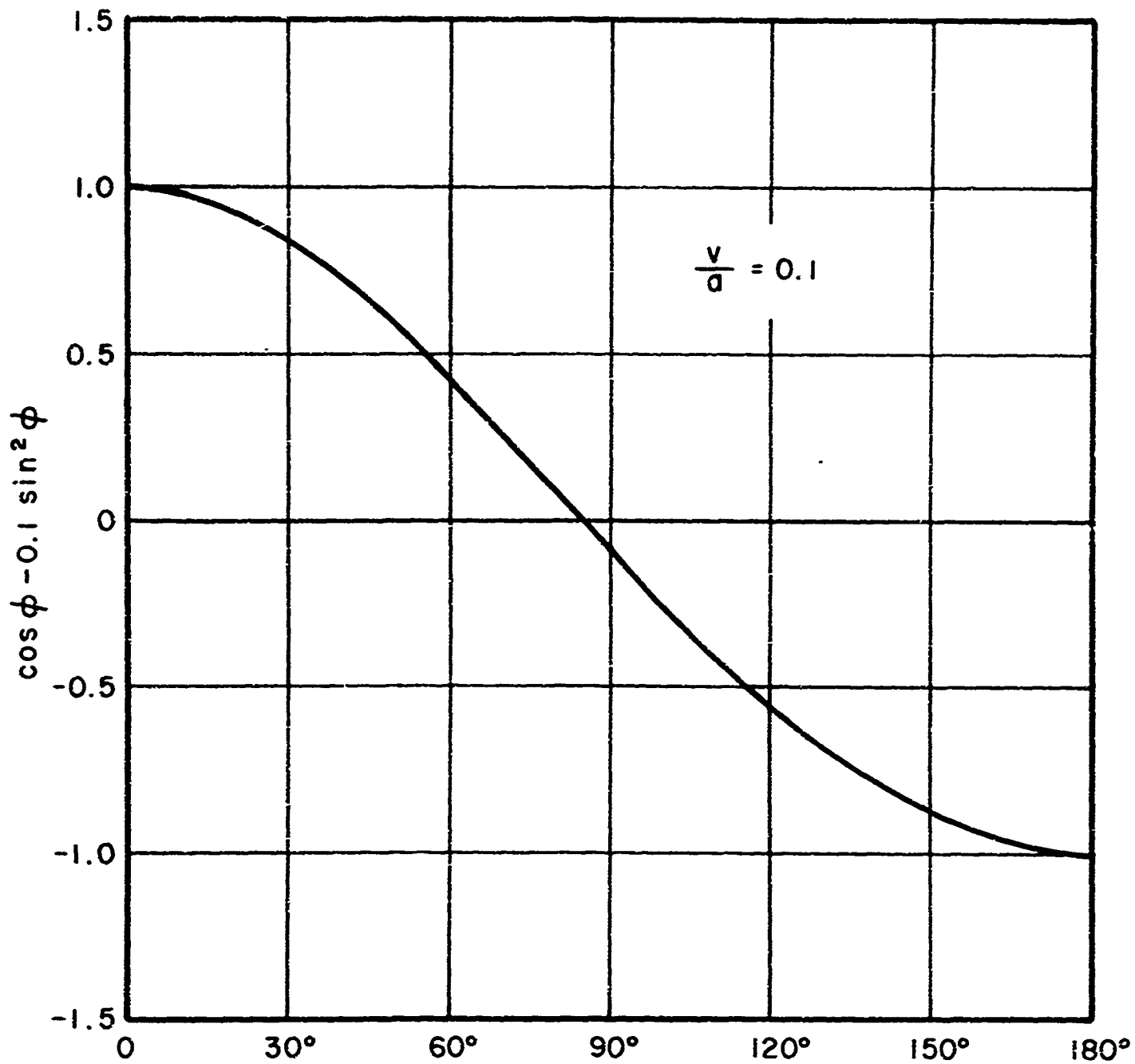ACOUSTIC VELOCITY ALONG RADAR RAY

FIG. 6.2 FUNCTION $\left[\cos\phi - \frac{v}{a}\sin^2\phi\right]$ VS. ϕ, $0 < \frac{v}{a} \lesssim 0.1$
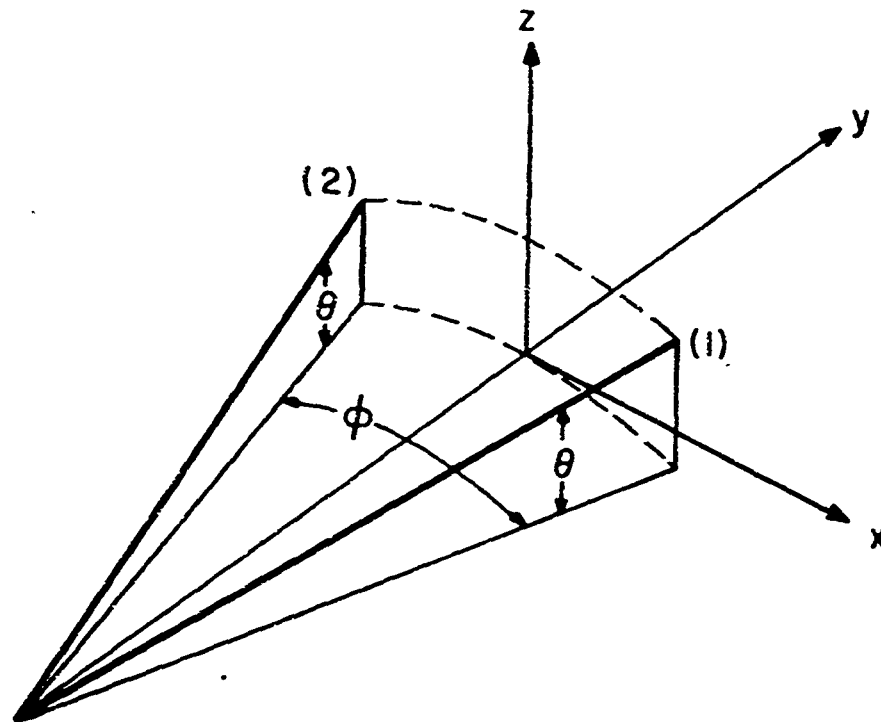
FIG. 6.3 MEASUREMENT OF HORIZONTAL WIND
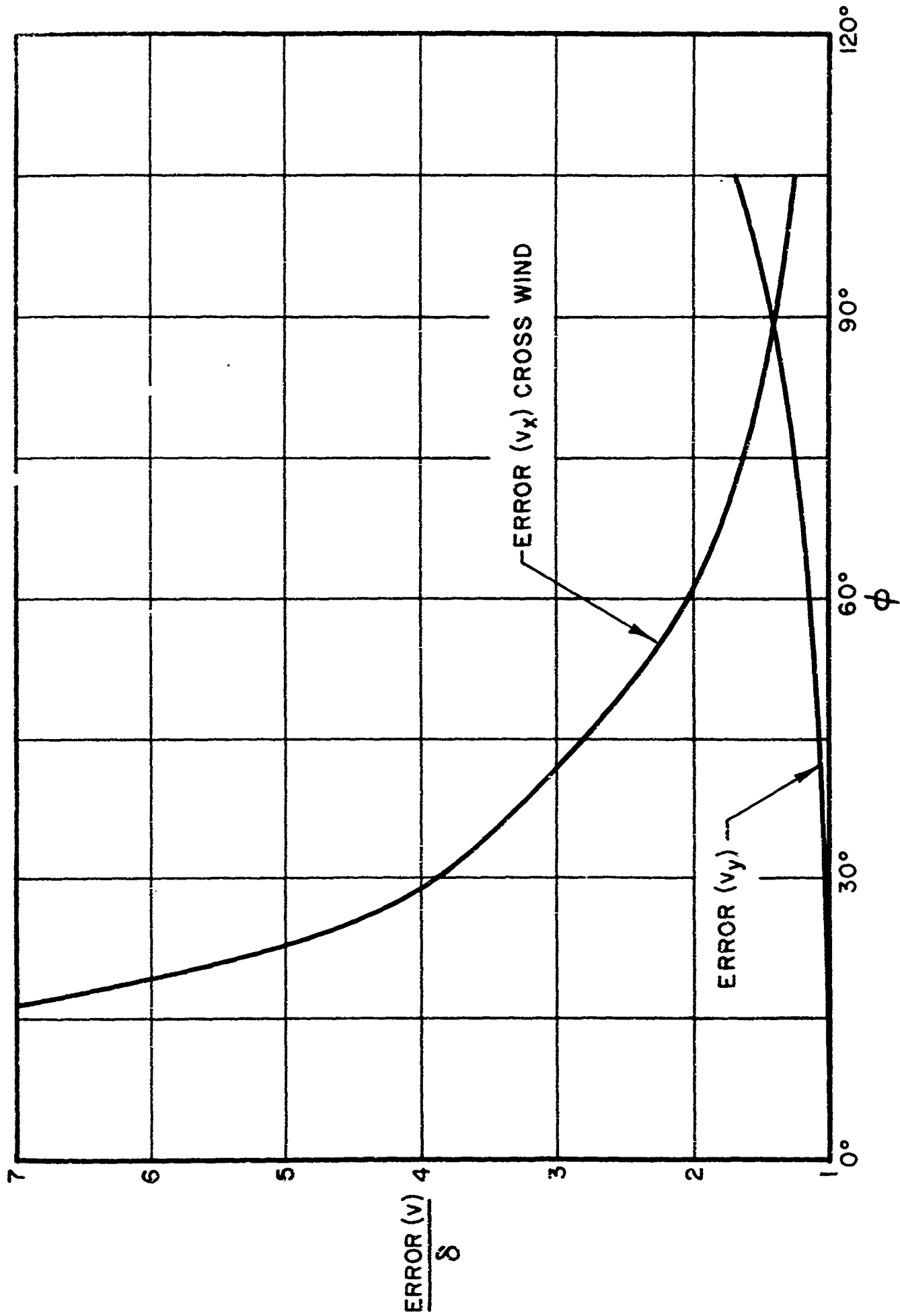COMPONENTS WITH SINGLE PROBE

FIG. 6.4 RELATIVE ERROR IN HORIZONTAL WIND COMPONENTS VS.
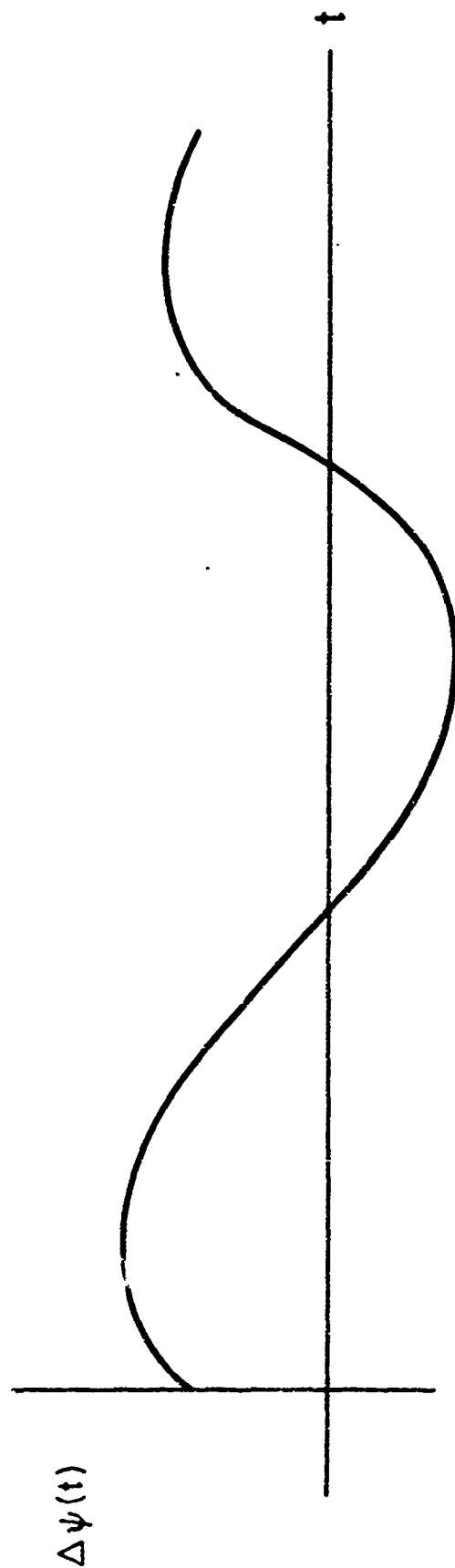ANGLE BETWEEN PROBING DIRECTIONS

FIG. 6.5 POSSIBLE CURVE FOR PHASE DIFFERENCE BETWEEN
TRANSMITTED AND RECEIVED RADAR SIGNAL AS
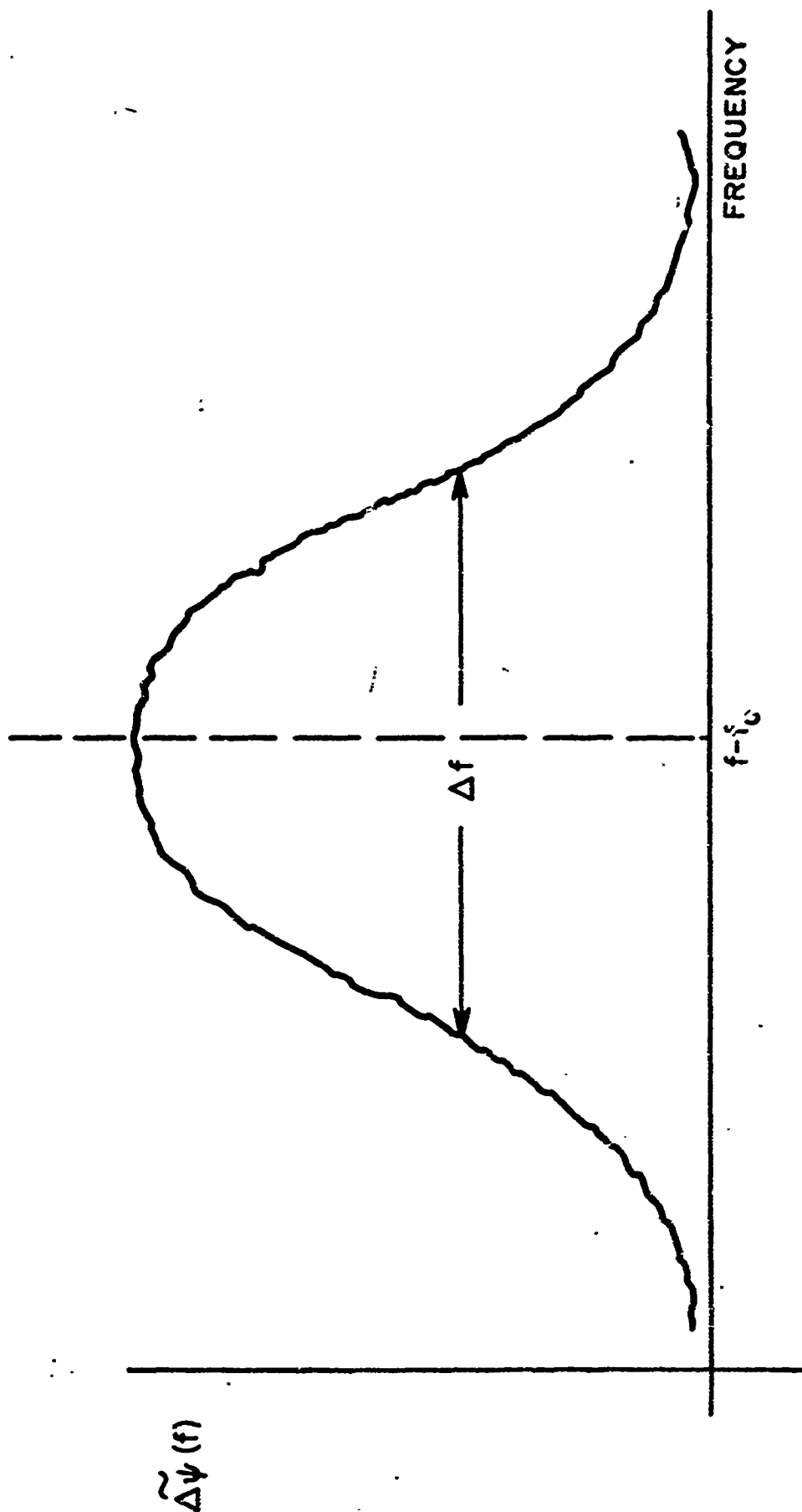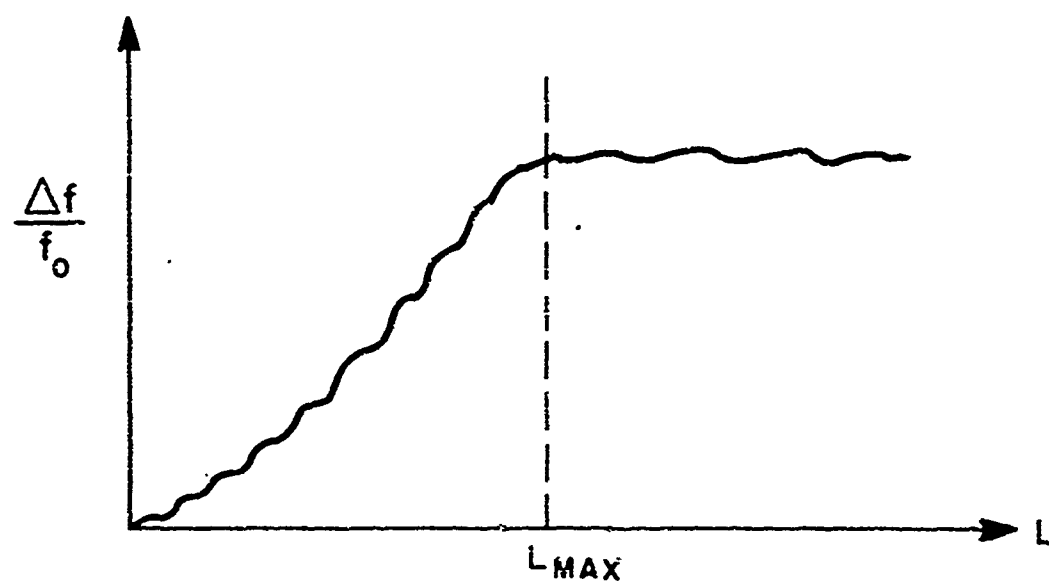FUNCTION OF TIME

FIG. 6.6 POSSIBLE FREQUENCY SPECTRUM OF DOPPLER SHIFT

L = DIAMETER OF ECHOING REGION

FIG. 6.7   SPREAD IN DOPPLER SHIFT VS.
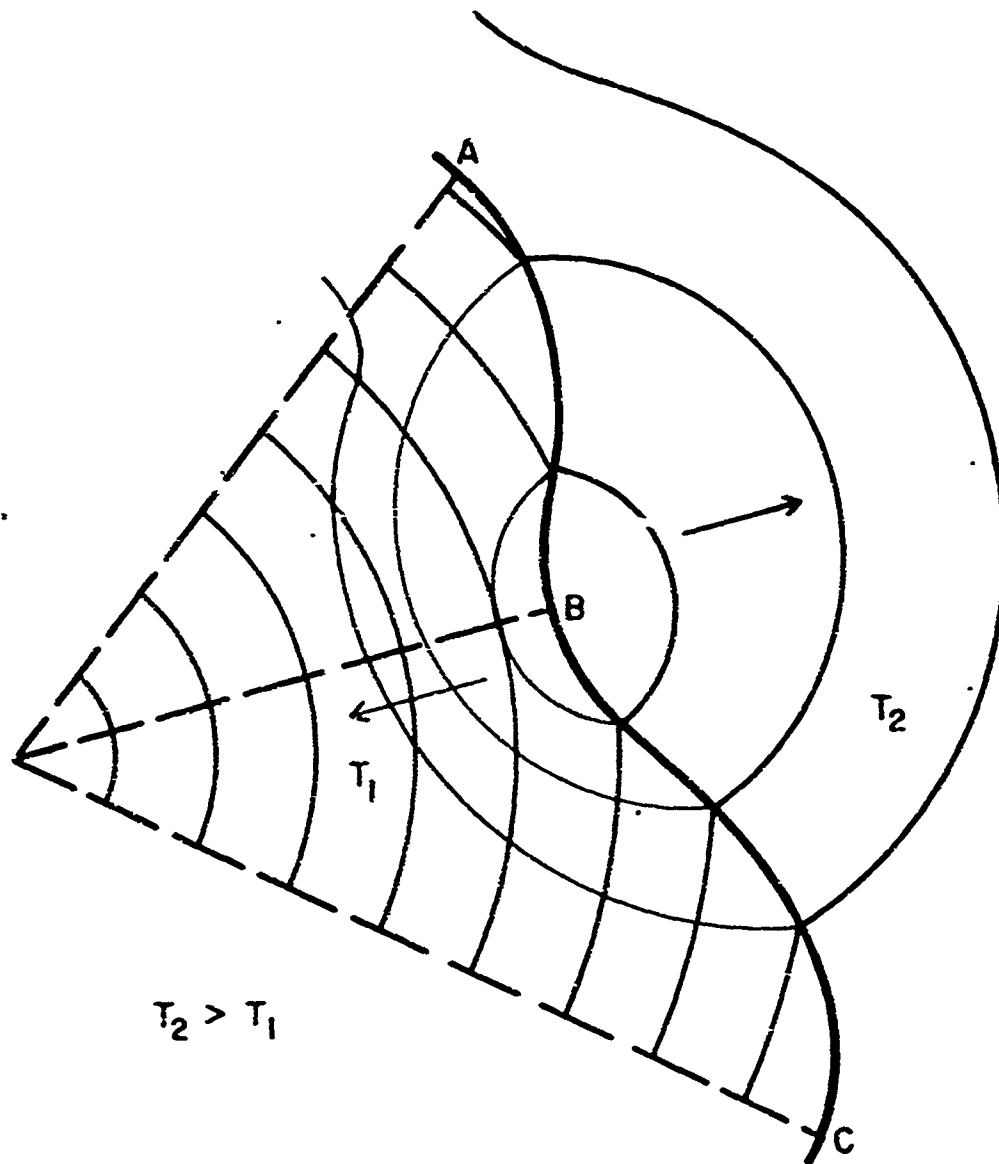DIAMETER OF ECHOING REGION

FIG. 6.8   SOUND AND RADAR REFLECTION
            FROM TEMPERATURE DISCONTINUITY

7. PRELIMINARY EXPERIMENTAL SYSTEM

Four phases of experimental and developmental study are proposed
which may be undertaken in succession: (I) An experimental study
of radar reflection from sonic booms using suitable existing
Doppler radar installations. (II) An experimental study of a
number of simple, impulsive sound sources and a theoretical
design study for optimizing the most favorable one as an EMAC
component. (III) Construction and acoustical test of the sound
source designed in Phase II. (IV) An experimental study using
the source of Phase III in conjunction with a suitable radar
system. This phase is intended to demonstrate the practical
range and weather limitations to a first approximation and to
reveal the nature of the more important refinements which should
be incorporated into a working EMAC System.

Phase I

Phase I is designed to demonstrate the feasibility of obtaining
usable Doppler radar returns from snock waves in air.

It is suggested that a suitable radar system be operated so as to
provide substantially normal incidence upon the ground reflected
sonic boom produced by an aircraft passing directly overhead as
indicated schematically in Fig. 7.1. There is the possibility
of obtaining radar reflections from ground-reflected boom and
also from the high altitude boom, however, these reflections will
be easily separated because of range differences. There is also
the problem of double reflections from the two shock fronts of
the sonic boom N-wave. The reflections from the bow and tail
waves will be added and probably will not be resolvable because
they are generally separated only by a distance of the order of
100 ft. This addition will involve variable amounts of phase
cancellation depending upon the exact distance between the two

.ks of the N-wave. Thus, the returned signals may vary widely
in amplitude because of this interference phenomenon. At some
ranges, however, (because the distance between the shock fronts
is continually expanding) the two signals should add in phase
and give four times the reflected power of a single shock. At
these ranges the velocity of the wave should be determinable by
Doppler techniques. The variation in intensity which is antici-
pated by this interference process should prove valuable in
determining the lower limit of sensitivity of the system.

Study of the returns from both the ground reflection and the
high altitude booms should provide a measure of the diminution
of radar reflection with height and with two related sound
intensities at the same height.

The actual experiment which is contemplated is the observations
of sonic booms created by supersonic aircraft provided by the
Air Force. As an example it might be possible to use one or
both of the two radar stations at North and South Truro on Cape
Cod for such observations. It is anticipated that the FPS-7
and the FPS-6 systems at the ADC installation at North Truro,
and the FPS-20 and FPS-6 systems at the Mitre Corp. installa-
tion at South Truro could be operated by experienced government
personnel under the direction of the Air Force and suitable
recordings made which can be correlated in time direction and range.

Acoustic measurements would be made simultaneously. These measure-
ments would be made near the ground at two or three positions
along the ground zero flight path to establish the value of the
shock over-pressure and provide a detailed analysis of N-wave
signature. Several shocks should be observed at various times

during the day in order to determine as far as practicable the
effects of weather upon the shock wave and upon the observable
radar reflection.

Phase II

II is designed to utilize the results of Phase I in a
tical study of sources of controlled shock waves which
be adapted to an EMAC Probe ground installation.

air looms although readily available for the initial experiments
in Phase I obviously have serious limitations as a tool for weather
vation. Their expense is prohibitive, their direction of
travel is not optimized with respect to the radar, and the charac-
teristics of an N-wave are probably not ideal because of the double
shock and the resulting uncontrolled interference between the two
reflected pulses.

Several sound sources should be investigated including:

1. Yachting cannon
2. Dynamite
3. Mild explosives
4. Internal combustion devices
5. Compressed air discharge

The last of these appears, at the outset, to offer the greatest
promise because of the much closer control of the significant
parameters such as over-pressure, volume change, rise time, decay
time, and discharge products.

Specifically a theoretical study program should be undertaken to
determine in detail the control parameters of such a source and
to determine the necessary power and physical dimensions which

will optimize the useful range. As a starting point for this
theoretical analysis acoustic measurements should be made of the
shock wave signatures of a limited number of simple impulsive
sources near the ground.

Phase III

Phase III is directed toward the production of an experimental
sound source applicable for use in conjunction with a suitable
radar installation. This phase depends largely upon the outcome
of Phases I and II.

The cost of the source obviously will depend upon its mode of
operation and final size as determined by Phase II. It is
expected that a usable source could be constructed from the
developments of Phases I and II which could be tested for its acous-
tic characteristics by ground measurements on an open range such
as Bedford or Logan Airport. Ground measurements of the acoustic
pulse should be made over distances, hopefully up to one mile
from the source depending upon the clear range which can be made
available.

The operating parameters of the source should be varied by steps
during these experimental measurements in order to obtain optimum
values for pulse shaping and for maximizing range. Such tests
might involve a few weeks of performance in order to cover a
range of operating parameters and to encounter at least a moderate
amount of variation in atmospheric conditions. The acoustic source
parameters should also be adjusted to minimize personnel hazard
and annoyance without reducing the range significantly.

Phase IV

Phase IV is intended to demonstrate the joint operation of a suitable radar system and the sound source developed under Phase III.

The sound source developed under Phase III should be operated with a suitable radar system. Measurements of the acoustic signal along the ground should be made simultaneously with some of the near-horizontal radar observations.

Measurements of acoustic wave signatures at elevated heights by means of balloon-supported microphones should also be conducted for some of the non-horizontal sound projections. Measurements at heights beyond those for which cable connections are practical might also be considered with radio-link systems.
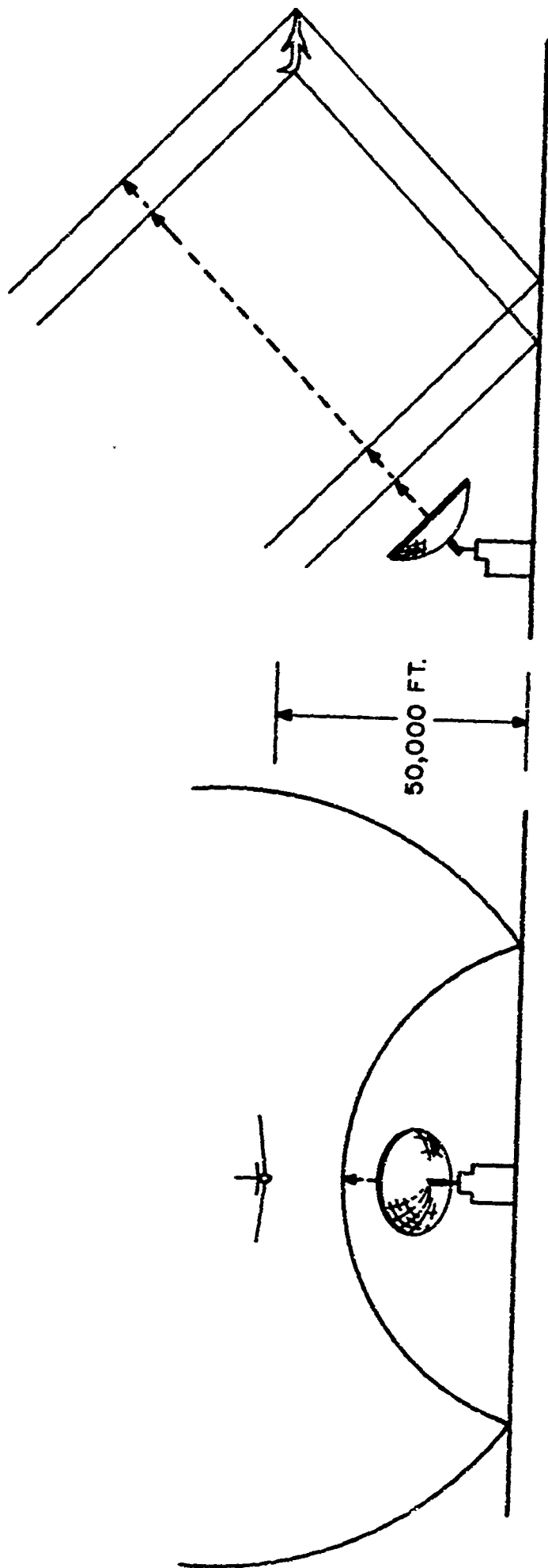
FIG. 7.1   SCHEMATIC VIEWS OF THE PROPOSED SYSTEM
FOR RADAR DETECTION OF A SONIC BOOM

50,000 FT.

8. CONCLUSIONS

1. The use of a high frequency acoustic beam is the major limiting factor in the range of the EMAC Probe system.

2. For long range, 10,000 ft or more, the acoustic signal should have a frequency of less than 500 cps.

3. The use of a long wave train for obtaining reinforcement of the radar reflection involves serious problems which outweigh its advantages.

a) Such a long train will require coherent matching between the radar wavelengths and the sound wavelengths wherever the reflection is to be reinforced by this process. Therefore, as the wave passes through areas where the ground velocity of the wave is altered the radar frequency must be altered simultaneously. Circuitry to enable such frequency tracking is complex and valuable radar search time will be used in order to provide a wavelength matching adjustment.

b) In turbulent and inhomogeneous areas, sound wavelength will vary and may be expected to change within the length of the wave train, thereby restricting the length of the useful beam.

c) If the acoustic wavelength is increased by reducing the acoustic frequency as necessary for long range propagation, the radar wave will require a corresponding increase, and the radar beam can no longer be maintained as narrow as is necessary for detailed probing with any practical size of radar antenna.

d) At the low frequencies required for long range transmission, the length of a wave train itself would preclude detailed probing of small regions of interest.

4. As an alternative for the multiple wave train, the use of a single shock wave front as a radar reflection surface has many advantages.

a) The single shock provides a thin reflection surface which is well defined and thereby provides the best or possibly optimum condition for the radar reflection.

b) More power can be carried by a single shock than can be carried by a train of sound waves. A shock wave can be launched as a portion of a sine wave and thereby result in little annoyance to personnel in the vicinity of the launching site, even though the sound pressure may be extremely high near the source.

c) The single sinusoidal pulse can be made as long as is consistent with the requirements for directing the sound in desired directions while shading critical areas that may be affected by the intense sounds. The single pulse, though generated nearly sinusoidal in shape will deform and become a shock wave as the wave progresses provided only that its initial amplitude is sufficiently high. The single shock will remain sharp for a distance approximately n times as far as a train of n shock waves having the same length as a single shock.

d) When the sound wave surface is carried down stream by the wind the specular reflection of the radar from the sound surface will be directed away from the radar antenna. Turbulence and homogeneities in the air will serve to roughen the spherical wave front surface and cause scattering of the radar beam. The effectiveness of this scattering mechanism for returning radar power to the antenna is far greater for a single shock wave than for a train of waves since the latter would have inherent coherence in the direction of the specular reflection and would cause a high retension of reflected energy in that direction even with scattering irregularities.

5. A sound source for developing single shock pulses appears to be relatively simple. A chamber which can be filled with air and opened explosively should be tried as the actual source. This might be placed at the focus of the parabolic reflector in order to obtain the advantage of directivity.

6. The propagation of a single acoustic pulse through the air should be studied by a simple experiment. The proposed experiment should include as a minimum the generation of an explosive signal having high energy at frequencies as low as 100 cps and this pulse should be tracked with Doppler radar to determine the magnitude of the signal and the potential range using for example a 400 megacycle signal and perhaps also a higher frequency for comparison purposes. It would be desirable simultaneously to make acoustic measurements of the wave along the ground at elevations as high as practicable as a check upon the theoretical analysis which is presented in this report.

7.   It is important that the radar wavelength be larger than the thickness of the acoustic shock wave front for good reflection. A preliminary experiment should be carried out using sonic booms to determine the practical thickness of shock fronts with small values of overpressure for a range of atmospheric conditions. These experiments should include simultaneous observation of the amount of radar reflected from the measured booms. Such experiments should materially aid in the evaluation of the requirements of an acoustic source for an EMAC Probe system.

REFERENCES

1. Atlas, David, "Radar Detection of the Sea Breeze,"
   J. of Meteorol., 17, No. 3, pp. 244-258, June 1960.

2. Atlas, David, "Possible Key to the Dilemma of Meteorological
   'Angel' Echoes," J. of Meteorol., 17, No. 2, pp 95-103,
   April, 1960.

3. Atlas, David, "Radar Studies of 'Angels'", Session IV,
   Radar Studies of Meteorological "Angel" Echoes, J. of
   Atmos. and Terres. Physics, 15, pp. 262-287, 1959.

4. Atlas, David, "Meteorological 'Angel' Echoes," J. of Meteorol.,
   16, No. 1, pp. 6-11, 1959.

5. Atlas, David, "Indirect Probing Techniques," BULL. of the
   Am. Meteorol. Soc., 43, No. 9, pp. 457-466, 1962.

6. U. S. Pat. No. 2,539,593, 2,823,365; patents issued to
   Robert H. Rines, a member of the staff of Bolt Beranek
   and Newman Inc.

7. Smith, P. L., Jr., "Remote Measurement of Wind Velocity
   by the Electromagnetic Acoustic Probe," I. System Analysis,
   Conf. Proc. 5th Nat. Conv. on Military Electronics, Wash.,
   D. C., Midwest Research Institute, Report No. 419, pp. 48-53,
   1961.

8. Fetter, R. W., "Remote Measurement of Wind Velocity by the
   Electromagnetic Acoustic Probe," II. Experimental System,
   Conf. Proc., 5th Nat. Conv. on Military Electronics, Wash.,
   D. C., Midwest Research Institute, Report No. 420,
   pp. 54-59, 1961.

9. Fetter, R. W., P. L. Smith, Jr., B. L. Jones, H. F. Schick,
   and R. M. Stewart, Jr., "Investigation of Techniques for
   Remote Measurement of Atmospheric Wind Fields," Phase II:
   Analysis, Report No. 2, Midwest Research Institute,
   Oct. 1961 - Feb. 1962.

10. Fetter, R. W., P. L. Smith Jr., and B. L. Jones,
    "Investigation of Techniques for Remote Measurement of
    Atmospheric Wind Fields," Phase III: Design of Experiments,
    Report No. 3, Midwest Research Institute, Feb. 1962 -
    June 1962.

11. Kerr, Donald E., Ed., _Propagation of Short Radio Waves_, Radiation Lab. Series, Vol. 13, McGraw-Hill Book Co., Inc., Appendix B., 1951.

12. Friend, Albert W., "Theory and Practice of Tropospheric Sounding by Radar," Proc. Inst. Radio Engr., pp. 116-137, 1949.

13. Jones, B. L. and P. C. Patton, _IRE Trans. on Antennas and Propagation_, AP-8, pp. 418-423, 1960.

14. Harris, C., _Handbook of Noise Control_, McGraw Hill Book Co., Inc., Chap. 3, 1951.

15. Ref. 11, pg. 46.

16. Chernov, L. A., _Wave Propagation in a Random Medium_, English Edition, McGraw Hill Book Co., 1960.

17. Golitsyn, G. S., A. S. Gurvicn and V. I. Tatarskii, "Investigation of the Frequency Spectra of Amplitude and Phase Difference Fluctuations of Sound Waves in a Turbulent Atmosphere," Soviet Acoustics, $\underline{6}$, No. 2, pp. 185-194, 1960.

18. Ref. 16, pg. 85.

19. Ref. 16, pp. 84-107.

20. Silver, Samuel, Ed., _Microwave Antenna Theory and Design_, Radiation Lab. Series, Vol. 12, McGraw-Hill Book Co., Inc. p. 188, 1949.

21. Ref. 16, pp. 125-146.

22. Ridenour, Louis N., Ed., _Radar System Engineering_, Radiation Lab. Series, Vol. 1, McGraw-Hill Book Co., Inc., p. 20,. 1947.

23. Ref. 22, pg. 271.

24. "Atmospheric Physics and Sound Propagation," prepared at the Dept. of Phys., The Penn. State Univ., under Signal Corps Contract W-36-D39-SC-32001, Sept. 1, 1950.

25. Allen, C. H., "Finite Amplitude Distortion," thesis, Dept. of Phys., The Penn. State Univ., 1950.

26. Nyborg, W. L. and D. Mintzer, "Review of Sound Propagation in the Lower Atmosphere," WADC Tech. Report 54-602, May, 1955.

27. Ref. 26, pp. 19-22.

28. "Investigation of Acoustic Signaling Over Water in Fog," BBN Final Report Phase 2, USCG Contract No. Tcg-40854, CG-43, 458-A, p. 64, Jan. 1960.

29. Rudnick, I., "On the Attenuation of High Amplitude Waves of Stable Form Propagated in Horns," J. Acoust. Soc. Am., 30, 339, 1958.

30. Laird, Donald T., "Spherical Sound Waves of Finite Amplitude," thesis, The Penn. State Univ., 1955.

31. Becker, R., "Shockwave and Detonation," Zeit. für Phys. 8, pp. 321-362, 1921.

32. Pearsons, Karl S., BBN Quarterly Progress Report No. 5, Contract No. NASr-58, July 1962-Oct. 1962.

33. Harris, C. M., "Absorption of Sound in Air in the Audio-Frequency Range," J. Acoust. Soc. Am., 35, 11, 1963.